



Search for anomalies in vector-boson fusion production of the Higgs boson in $H(\rightarrow \gamma\gamma)jj$ events using 164 fb^{-1} of pp collision data collected at $\sqrt{s} = 13.6 \text{ TeV}$ with the ATLAS detector

The ATLAS Collaboration

This article details two studies of Higgs boson properties using the vector-boson fusion production mode and the $\gamma\gamma jj$ final state. Both efforts are based on a data sample corresponding to 164 fb^{-1} of $\sqrt{s} = 13.6 \text{ TeV}$ proton–proton collisions recorded by the ATLAS experiment at the Large Hadron Collider. The first study employs matrix element-based optimal observables to constrain CP-odd couplings beyond the Standard Model within the Standard Model Effective Field Theory framework, expressed in the Warsaw basis. The second study exploits angular distributions to probe the Higgs boson’s couplings to longitudinally and transversely polarised W and Z bosons in the production of the Higgs boson. To maximise the sensitivity, the constraints of the CP-odd couplings are combined with those from a previous analysis performed in $\gamma\gamma jj$ events in a data sample of proton–proton collisions at $\sqrt{s} = 13 \text{ TeV}$, corresponding to an integrated luminosity of 140 fb^{-1} . A significant improvement with respect to the previous analysis is achieved through the implementation of a new neural network-based classification algorithm. All measurements are in agreement with the Standard Model prediction of a CP-even Higgs boson with the expected relative coupling strengths to longitudinally and transversely polarised vector bosons.

Contents

1	Introduction	2
2	Theoretical framework and analysis methodology	4
2.1	CP Violation in the EFT Framework	4
2.2	Polarisation-dependent coupling-strength scale factors	5
2.3	CP- and polarisation-dependent observables	5
3	ATLAS detector	6
4	Data and simulated event samples	8
5	Event reconstruction	10
6	Analysis strategy and event selection	11
7	Signal and background modelling	14
7.1	Signal modelling	14
7.2	Background modelling	15
8	Systematic uncertainties	16
8.1	Experimental systematic uncertainties	16
8.2	Theoretical systematic uncertainties	17
9	Results	18
9.1	Run-3 results	18
9.2	Combination of searches for CP violating effects using Run-2 and Run-3 results	23
10	Conclusion	25

1 Introduction

The observation of the Higgs boson at the Large Hadron Collider (LHC) by the ATLAS and CMS collaborations [1, 2] was a major success. Subsequent measurements have determined its spin, parity, mass, width, and couplings to gauge bosons and fermions with increasing precision [3–8]. These precise measurements make the Higgs boson an indispensable tool for testing the Standard Model (SM) and searching for physics beyond the Standard Model (BSM). In particular, the tensor structure of the Higgs boson’s couplings to vector bosons HVV (where $V = W, Z$) is a sensitive probe for BSM effects [9, 10], which motivates the search for anomalous contributions to the HVV vertex.

This article presents results from two studies of the HVV vertex in the vector-boson fusion (VBF) production of the Higgs boson, using $H(\rightarrow \gamma\gamma)jj$ events. Representative leading-order diagrams for the VBF production mode of the Higgs boson and its subsequent decay into two photons are depicted in Figure 1. The first study searches for the violation of combined charge conjugation and parity (CP) invariance in the Higgs-boson coupling to vector bosons. The second study probes the Higgs boson couplings to longitudinally and transversely polarised vector bosons. These studies are based on proton–proton (pp)

collision data corresponding to an integrated luminosity of 164 fb^{-1} collected with the ATLAS detector at $\sqrt{s} = 13.6 \text{ TeV}$ from 2022 to 2024.

Searches for CP-violating effects in Higgs-boson couplings are well motivated because the known sources of CP violation in nature are insufficient to explain the observed matter-antimatter asymmetry in our Universe through baryogenesis [11]. This strongly motivates further exploration, particularly as extended scalar sector models can naturally introduce new sources of CP violation [12]. At the same time, studies of Higgs-boson couplings to longitudinally polarised vector bosons are also of great importance. This is because the longitudinal polarisation states originate from the massless degrees of freedom arising from the Higgs field during electroweak symmetry breaking. Within the SM, the Higgs boson's coupling to these longitudinal states prevents the divergence of tree-level vector-boson scattering amplitudes at high energies [13]. However, if the Higgs boson were not a fundamental particle but a bound state, as predicted in models with a composite Higgs boson [14, 15], the Higgs-boson couplings to longitudinally and transversely polarised vector bosons may significantly deviate from their SM values.

Since the observation of the Higgs boson, the ATLAS and CMS collaborations have performed extensive searches for CP-violating effects in its couplings. During Run 1 of the LHC, these efforts primarily focused on Higgs boson decays into WW^* and ZZ^* [3]. Using 25 fb^{-1} of pp collision data collected at centre-of-mass energies of $\sqrt{s} = 7 \text{ TeV}$ and 8 TeV , both experiments provided the first limits on CP-odd contributions to the HVV vertex. With the same data sample, the first searches for CP-odd contributions in the Higgs boson production were performed, targeting the VBF process in the $H \rightarrow \tau\tau$ decay channel [16] and associated VH production in the $H \rightarrow b\bar{b}$ decay channel [17]. The LHC experiments later expanded these searches to various production processes, using the 140 fb^{-1} pp data sample of Run 2 at $\sqrt{s} = 13, \text{ TeV}$, including gluon–gluon fusion (ggF) in events with two associated jets [18, 19], as well as the VBF [19–24] and $t\bar{t}H$ [25–28] production modes. These studies used events with Higgs boson decays into WW^* , $\gamma\gamma$, ZZ^* , and $\tau\tau$. Building on the individual analyses, a combination of measurements of CP properties of Higgs boson interactions to vector bosons was also performed [29]. In addition, searches for CP violation in the interaction between the Higgs boson and τ -leptons were performed by probing the τ -lepton decay plane [30, 31]. To date, studies of Higgs-boson couplings to longitudinally and transversely polarised vector bosons have been performed only in $H(\rightarrow WW^* \rightarrow e\nu\mu\nu)jj$ events [18].

The two studies presented in this article probe CP- and polarisation-dependent observables constructed from the final-state particles in selected $\gamma\gamma jj$ events to test for deviations from the SM expectations. Analysis regions are defined based on requirements on the kinematic properties of the final-state particles and event-level quantities. To enhance the separation of the VBF signal from the background processes, a multi-class classifier based on a neural network is employed. The primary backgrounds to the VBF $H(\rightarrow \gamma\gamma)$ signal consist of final states with two photons and multiple jets and events where one or more jets are misidentified as photons. These backgrounds are determined using data-driven methods. Subleading backgrounds from other Higgs boson production modes are modelled via simulation, with their normalisations either constrained by a profile-likelihood fit to the data (in the case of the ggF production mode) or fixed to the Standard Model predictions. The results of the CP studies are interpreted within the Standard Model Effective Field Theory (SMEFT) framework [32] using the Warsaw basis [33, 34]. Complementing these CP studies, the results from the polarisation studies are interpreted as polarisation-dependent coupling scale factors between the Higgs boson and the vector bosons [35].

To maximise the sensitivity, the results of the CP study are combined with a previous analysis performed in $\gamma\gamma jj$ events in a data sample of proton–proton collisions at $\sqrt{s} = 13 \text{ TeV}$, corresponding to an integrated luminosity of 140 fb^{-1} [21]. Beyond the increased statistics provided by the larger data sample, the analysis presented in this article introduces several methodological improvements over the previous

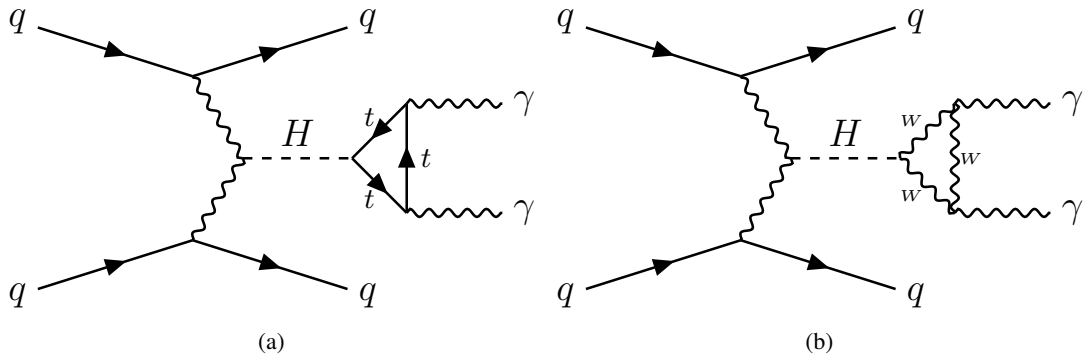


Figure 1: Representative lowest-order Feynman diagrams of vector-boson fusion production of a Higgs boson and subsequent decay into two photons $H \rightarrow \gamma\gamma$ via (a) a top-quark loop and (b) a W -boson loop.

Run-2 result, most notably the implementation of more sophisticated machine learning techniques for signal and background classification. Furthermore, the polarisation studies, performed here for the first time in the VBF $H(\rightarrow \gamma\gamma)$ channel, benefit significantly from the clean experimental signature and manageable background composition of the diphoton plus jets final state. In contrast, prior measurements in $H(\rightarrow WW^* \rightarrow e\nu\mu\nu)$ events were limited by the modelling of the complex background composition and the associated uncertainties, despite the larger Higgs boson branching fraction.

2 Theoretical framework and analysis methodology

2.1 CP Violation in the EFT Framework

For the studies testing the CP-invariance of the Higgs boson coupling to vector bosons, the SMEFT framework is used to parameterise possible deviations from the SM. The SMEFT framework supplements the SM Lagrangian with operators \mathcal{O}_i of mass-dimension $D > 4$ that are invariant under the SM gauge group $SU(3)_C \times SU(2)_L \times U(1)_Y$. The resulting effective Lagrangian is expressed as:

$$\mathcal{L}_{\text{SMEFT}} = \mathcal{L}_{\text{SM}} + \sum_i \frac{c_i^{(D)}}{\Lambda^{D-4}} \mathcal{O}_i^{(D)} \quad (1)$$

where Λ is the energy scale of new physics, and the dimensionless Wilson coefficients c_i govern the strength of the new interactions. Since the dimension-5 operator is typically ignored as it violates lepton number conservation [36], dimension-6 operators are expected to provide the leading contributions to physical observables.

Among the complete sets of dimension-6 operators, the Warsaw basis is the most widely adopted for LHC results [37]. In this basis, the three CP-odd operators $\mathcal{O}_{\Phi\widetilde{W}}$, $\mathcal{O}_{\Phi\widetilde{W}B}$, and $\mathcal{O}_{\Phi\widetilde{B}}$, along with their corresponding Wilson coefficients $c_{H\widetilde{W}}$, $c_{H\widetilde{W}B}$, and $c_{H\widetilde{B}}$, contribute to the HVV vertex. In the VBF $H \rightarrow \gamma\gamma$ process, these couplings affect both the production vertex and the loop-induced decay. While all three interactions modify the Higgs boson branching ratio, the $H \rightarrow \gamma\gamma$ decay itself remains insensitive to CP-violating effects. This is because in two-body decays of a spin-0 particle, all kinematic observables

are strictly determined by energy-momentum conservation. Consequently, the decay kinematics lack the degrees of freedom required to construct CP-sensitive observables. In contrast, the production vertex offers significant sensitivity. Given that VBF production is dominated by $W^+W^- \rightarrow H$ contributions, this analysis is primarily sensitive to $O_{\Phi\bar{W}}$ and focuses on constraining $c_{H\bar{W}}$, while all other Wilson coefficients affecting the HVV vertex are assumed to be zero.

2.2 Polarisation-dependent coupling-strength scale factors

To investigate the Higgs boson couplings to longitudinally and transversely polarised W and Z bosons, polarisation-dependent coupling-strength scale factors are introduced. Following the framework established in Ref. [35], these factors are defined as:

$$a_L = \frac{g_{HV_L V_L}}{g_{HVV}}, \quad a_T = \frac{g_{HV_T V_T}}{g_{HVV}} \quad (2)$$

where g_{HVV} denotes the SM HVV coupling strength, which is independent of the polarisation state, while $g_{HV_L V_L}$ and $g_{HV_T V_T}$ represent the measured polarisation-dependent couplings. In this study, the vector boson polarisations are defined in the Higgs boson rest frame such that the mixed-polarisation couplings $g_{HV_L V_T}$ vanish and do not contribute to the production process. This parameterisation of the coupling-strength focuses exclusively on these scale factors, and other BSM effects are not considered. The Standard Model is characterised by $a_L = a_T = 1$.

2.3 CP- and polarisation-dependent observables

Modifications to the HVV vertex from higher-dimensional operators impact the event kinematics and the total cross-section of Higgs boson production via VBF. The resulting squared matrix element, for a set of CP-odd couplings c_i , is then given by:

$$\begin{aligned} |\mathcal{M}|^2 &= \left| \mathcal{M}_{\text{SM}} + \sum_i \frac{c_i}{\Lambda^2} \mathcal{M}_{\text{BSM},i} \right|^2 \\ &= |\mathcal{M}_{\text{SM}}|^2 + 2 \sum_i \frac{c_i}{\Lambda^2} \text{Re}(\mathcal{M}_{\text{SM}}^* \mathcal{M}_{\text{BSM},i}) + \sum_i \sum_j \frac{c_i c_j}{\Lambda^4} \text{Re}(\mathcal{M}_{\text{BSM},i}^* \mathcal{M}_{\text{BSM},j}). \end{aligned} \quad (3)$$

The first term in the expansion corresponds to the squared SM matrix element. The second term (referred to in the following as ‘‘linear term’’) is composed of the cross terms between the SM and BSM couplings and represents the interference between the SM and BSM contributions. Finally, the third term accounts for the quadratic BSM contributions and the interference between different BSM terms (referred to in the following as ‘‘quadratic term’’). The SM and quadratic terms are CP-even. In contrast, the linear term is CP-odd and provides a potential source of CP-violating effects in the Higgs boson couplings. Because the linear term is CP-odd, its integral over a CP-symmetric phase space vanishes. Consequently, it does not contribute to the total cross-section. While the contributions from the quadratic term increases the total cross-section, its effect is not exploited in the current analysis because the observed event rate may be simultaneously influenced by contributions from BSM CP-even operators.

To maximise statistical sensitivity to CP-violating effects, an ‘‘Optimal Observable’’ (OO) is defined as the ratio of the interference term to the SM-only squared matrix element. For a specific CP-odd coupling c_i , this is given by:

$$OO_i = \frac{2\text{Re}(\mathcal{M}_{\text{SM}}^* \mathcal{M}_{\text{BSM},i})}{|\mathcal{M}_{\text{SM}}|^2}. \quad (4)$$

By construction, these observables are CP-odd. In the absence of CP violation and assuming negligible contributions from rescattering [38] (i.e. new particles being on the mass shell in loop corrections to the HVV vertex), their distributions are symmetric around a vanishing mean. Consequently, any observed asymmetry would provide direct evidence of CP violation in the HVV vertex, a feature not shared by CP-even observables derived from squared matrix elements. In this analysis, the OO observable is evaluated for the operator $\mathcal{O}_{\Phi\widetilde{W}}$ and the corresponding Wilson coefficient $c_{H\widetilde{W}}$. Figure 2 (a) illustrates the distribution of the OO for SM VBF Higgs boson production (where $c_{H\widetilde{W}} = 0$) and for two BSM scenarios where $c_{H\widetilde{W}} \neq 0$. These distributions, shown after the selection requirements described in Section 6, demonstrate how the mean of the distribution shifts toward positive or negative values depending on the sign of the $c_{H\widetilde{W}}$ parameter.

The matrix elements used in the construction of the OO are calculated at leading-order (LO) accuracy in QCD using MADGRAPH5_AMC@NLO [39], with the NNPDF3.0NLO [40] set of parton distribution functions (PDFs). These matrix elements are evaluated using the four-momenta of the Higgs boson, reconstructed from the two selected photons, and the two VBF-tagged jets. At the reconstruction level, the momentum fractions of the initial-state partons are derived in the reference frame of the ATLAS detector as:

$$x_{1,2}^{\text{reco}} = \frac{m_{Hjj} \cdot e^{\pm y_{Hjj}}}{\sqrt{s}} \quad (5)$$

by exploiting energy and momentum conservation, where m_{Hjj} and y_{Hjj} are the invariant mass and rapidity of the Higgs boson + dijet system, and \sqrt{s} is the centre-of-mass energy. A detailed description of this calculation can be found in Ref. [22].

A simple polarisation-dependent observable, suggested in Ref. [35] for constraining the coupling-strength scale factors a_L and a_T , is the absolute azimuthal angular difference between the two VBF-tagged jets ($\Delta\Phi_{jj}$). This variable is highly sensitive to the polarisation states of the vector bosons in the VBF production mode. Consequently, $\Delta\Phi_{jj}$ is employed in this analysis to provide sensitivity to these polarisation-dependent scale factors. Figure 2 (b) shows the distribution of the $\Delta\Phi_{jj}$ observable for SM VBF Higgs boson production (where $a_L = a_T = 1$) and for four BSM scenarios where either a_L or a_T are varied.

3 ATLAS detector

The ATLAS detector [42, 43] at the LHC covers nearly the entire solid angle around the collision point.¹ It consists of an inner tracking detector surrounded by a thin superconducting solenoid, electromagnetic (EM)

¹ ATLAS uses a right-handed coordinate system with its origin at the nominal interaction point (IP) in the centre of the detector and the z -axis along the beam pipe. The x -axis points from the IP to the centre of the LHC ring, and the y -axis points upwards. Polar coordinates (r, ϕ) are used in the transverse plane, ϕ being the azimuthal angle around the z -axis. The pseudorapidity is defined in terms of the polar angle θ as $\eta = -\ln \tan(\theta/2)$ and is equal to the rapidity $y = \frac{1}{2} \ln \left(\frac{E+p_z}{E-p_z} \right)$ in the relativistic limit. Angular distance is measured in units of $\Delta R \equiv \sqrt{(\Delta y)^2 + (\Delta\phi)^2}$. The transverse energy is defined as $E_T = E/\cosh(\eta)$.

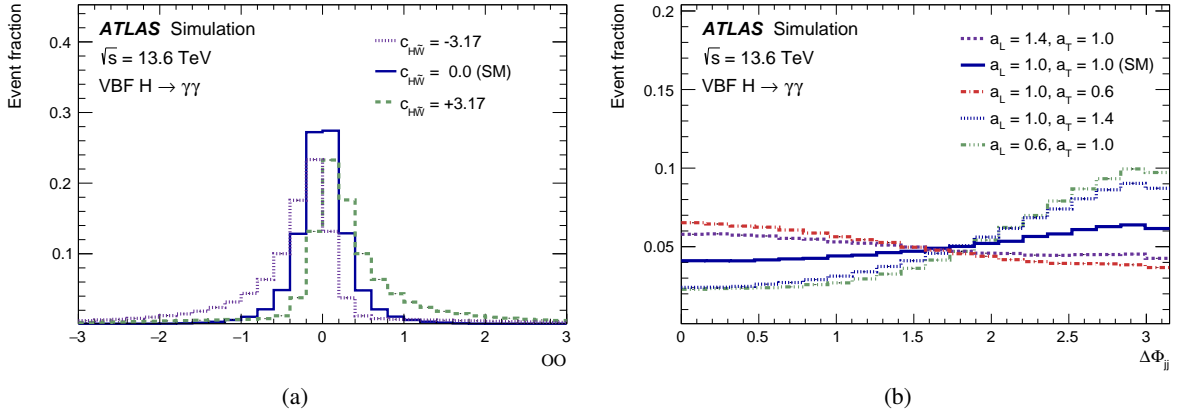


Figure 2: Distributions of (a) the OO observable shown for various configurations of the Wilson coefficient $c_{H\bar{W}}$, and (b) the $\Delta\Phi_{jj}$ observable for various configurations of the a_L and a_T parameters. These comparisons are performed in VBF events at the reconstruction level using the predictions of the MADGRAPH5_AMC@NLO + PYTHIA 8 [39, 41] generators.

and hadronic calorimeters, and a muon spectrometer incorporating three large superconducting air-core toroidal magnets.

The inner-detector system (ID) is immersed in a 2 T axial magnetic field and provides charged-particle tracking in the range of $|\eta| < 2.5$. The high-granularity silicon pixel detector covers the interaction region and typically provides four measurements per track, the first hit generally being in the insertable B-layer (IBL). It is followed by the SemiConductor Tracker (SCT), which usually provides eight measurements per track. These silicon detectors are complemented by the transition radiation tracker (TRT), which enables radially extended track reconstruction up to $|\eta| = 2.0$. The TRT also provides electron identification information based on the fraction of hits (typically 30 in total) above a higher energy-deposit threshold corresponding to transition radiation.

The calorimeter system covers the pseudorapidity range $|\eta| < 4.9$. Within the region $|\eta| < 3.2$, electromagnetic calorimetry is provided by barrel and endcap high-granularity lead/liquid-argon (LAr) calorimeters, with an additional thin LAr presampler covering $|\eta| < 1.8$ to correct for energy loss in material upstream of the calorimeters. Hadronic calorimetry is provided by the steel/scintillator-tile calorimeter, segmented into three barrel structures within $|\eta| < 1.7$, and two copper/LAr hadronic endcap calorimeters. The solid angle coverage is completed with forward copper/LAr and tungsten/LAr calorimeter modules optimised for electromagnetic and hadronic energy measurements, respectively.

The muon spectrometer (MS) comprises separate trigger and high-precision tracking chambers measuring the deflection of muons in a magnetic field generated by the superconducting air-core toroidal magnets. The field integral of the toroids ranges between 2.0 and 6.0 T m across most of the detector. Three layers of precision chambers, each consisting of layers of monitored drift tubes, cover the region $|\eta| < 2.7$, except in the innermost layer of the endcap region, where layers of small-strip thin-gap chambers and Micromegas chambers both provide precision tracking in the region $1.3 < |\eta| < 2.7$. The muon trigger system covers the range $|\eta| < 2.4$ with resistive-plate chambers in the barrel, thin-gap chambers in the endcap regions, and the small-strip thin-gap chambers and Micromegas chambers in the innermost layer of the endcap.

The luminosity is measured mainly by the LUCID–2 detector that records Cherenkov light produced in the quartz windows of photomultipliers located close to the beampipe.

Events were selected by the first-level trigger system implemented in custom hardware, followed by selections made by algorithms implemented in software in the high-level trigger [44]. The first-level trigger accepted events from the 40 MHz bunch crossings at a rate close to 100 kHz, which the high-level trigger further reduced to record complete events to disk at an average rate of about 3 kHz.

A software suite [45] is used in data simulation, in the reconstruction and analysis of real and simulated data, in detector operations, and in the trigger and data acquisition systems of the experiment.

4 Data and simulated event samples

The pp collision data at $\sqrt{s} = 13.6$ TeV used in these analyses were recorded with the ATLAS detector between 2022 and 2024, corresponding to a total integrated luminosity of $163.9 \pm 3.1 \text{ fb}^{-1}$ [46]. The data are required to satisfy criteria ensuring that the detector was in good operating condition [47]. Monte Carlo (MC) simulation samples were used to model the signal processes, assist in background estimates, and derive modelling uncertainties. All MC simulation samples were processed using a hybrid approach: the geometry and response of the ATLAS Inner Detector and muon spectrometer were simulated using GEANT4 [48] (G4), while the calorimeter response was modelled using AtlFast3 (AF3) [49]. AF3 combines parameterised approaches with machine-learning techniques to simulate particle showers with a level of precision comparable to GEANT4, while being significantly faster. For example, for single photons with an energy of 65 GeV and a pseudorapidity of $0.20 < |\eta| < 0.25$, AF3 is approximately 150 times faster than G4 when the calorimeter simulation alone is considered [49]. The studies presented in this article are the first by the ATLAS Collaboration to exclusively use MC samples produced with the AF3 detector simulation.

To study the CP properties of the Higgs boson couplings to vector bosons, the VBF production of the Higgs boson and the subsequent decay of the Higgs boson into photons were simulated at LO accuracy in QCD using the matrix element (ME) generator MADGRAPH5_AMC@NLO 3.3.1, the NNPDF3.0_{NLO} PDF set, and the FeynRules model [50] SMEFTsim_U35_MwScheme [51, 52]. PYTHIA 8.306 [41] with the A14 set of tuned parameters [53] was used to model the parton shower, hadronisation, and the underlying event. While signal samples were generated for a discrete set of $c_{H\bar{W}}$ values ($c_{H\bar{W}} \in \{-3.17, 0.0, 1.5, 3.17\}$ at $\Lambda = 1$ TeV), parameter morphing [54, 55] was used to model the signal across a continuous range of coupling scenarios by interpolating between the simulated basis points². These specific $c_{H\bar{W}}$ values were chosen to maximise the statistical stability of the morphing procedure throughout the target parameter space.

For the studies of the Higgs boson couplings to longitudinally and transversely polarised W and Z bosons, the VBF production of the Higgs boson and the subsequent decay into photons were simulated at LO in QCD using MADGRAPH5_AMC@NLO 2.8.3.2 and the NNPDF2.3_{NLO} [56] PDF set. The helicity amplitudes used in the ME generation of the Higgs boson production were modified to account for deviations in the Higgs boson coupling strengths to the polarised vector bosons within the Higgs boson rest frame, following the prescriptions in Ref. [35]. Signal samples were produced for the following benchmark scenarios: $(a_L, a_T) \in \{(1.0, 1.0), (1.4, 1.0), (1.2, 1.0), (1.0, 1.4), (1.0, 1.2), (1.0, 0.6), (0.6, 1.0)\}$. Parton shower,

² The signal samples corresponding to $c_{H\bar{W}} \in \{-3.17, 0.0, 3.17\}$ were used to build the morphing basis, while the signal sample corresponding to $c_{H\bar{W}} = 1.5$ was used to validate the morphing basis.

hadronisation, and the underlying event were simulated using the PYTHIA 8.308 generator with the A14 set of tuned parameters.

In both analyses, the diphoton background processes are categorised into two distinct components: resonant and non-resonant. The resonant background consists of $\gamma\gamma$ production from other Higgs boson modes, including gluon–gluon fusion (ggF), associated production with a vector boson (VH), and production in association with a pair of top- or bottom-quarks ($t\bar{t}H$ or $b\bar{b}H$) or a single top quark (tHq and tHW). Conversely, the non-resonant component includes continuum diphoton production in association with jets. Additional contributions from events where one or more jets are falsely reconstructed as photons (γj or jj), are estimated by using a data-driven approach, as described in Section 7.

The Higgs boson background processes (ggF, VH , $t\bar{t}H$ and $b\bar{b}H$) were simulated using the POWHEG Box v2 [57–60] generator with the PDF4LHC21 PDF set [61]. PYTHIA 8.310 was subsequently employed to model the parton showering, hadronisation, and the underlying event. Matrix elements for the ggF and VH processes were calculated at next-to-leading-order (NLO) accuracy in QCD for diagrams with up to one extra parton following the MiNLO [62–64] approach, though the $gg \rightarrow ZH$ process was computed only at LO accuracy. The $t\bar{t}H$ and $b\bar{b}H$ processes were also simulated at NLO accuracy in QCD. Finally, the production of a Higgs boson in association with a single top quark (tHq and tHW) was simulated using the MADGRAPH5_AMC@NLO generator and the NNPDF3.0_{NLO} PDF set to calculate the MEs at NLO accuracy, while PYTHIA with the A14 tune was used for the modelling of the parton shower, hadronisation, and underlying event.

The production of non-resonant diphoton + jets ($\gamma\gamma$ +jets) events was simulated using the SHERPA 2.2.14 [65] generator with the NNPDF3.0_{NNLO} [40] PDF set. The ME was calculated based on the COMIX [66] and OPENLOOPS [67–69] libraries at NLO accuracy in QCD for diagrams with up to one additional parton emissions, and LO accuracy in QCD for diagrams with two or three additional parton emissions. The MEPS@NLO prescription [70–73] was used to merge the ME and the SHERPA parton shower [74], which is based on a set of tuned parameters developed by the SHERPA authors. A dynamic merging cut [75] of 10 GeV was used and photons were required to be isolated according to a smooth-cone isolation criterion [76].

All simulated events were generated at a centre-of-mass energy \sqrt{s} of 13.6 TeV and were normalised to the state-of-the-art cross-section predictions³ [37]. Simulated events containing Higgs bosons were generated with a Higgs boson mass of 125.0 GeV, a Higgs boson’s width of 4.07 MeV, and a branching ratio of $(2.27 \pm 0.07) \times 10^{-3}$ for the $H \rightarrow \gamma\gamma$ decay [37]. Furthermore, EVTGEN 2.1.1 [77] is used for all event samples except for the ones produced with SHERPA to unify the properties of the bottom and charm hadron decays.

The effect of multiple interactions in the same and neighbouring bunch crossings (pile-up) was modelled by overlaying [78] the simulated hard-scattering event with inelastic pp events generated from a mix of EPOS 2.0.1.4 [79] and PYTHIA 8.308 [80]. The EPOS events were generated with the EPOS LHC tune [81] and the PYTHIA events with the A3 tune [82] and the NNPDF2.3_{LO} [56] set of PDFs. PYTHIA pileup events include either a high transverse momentum (p_T) jet, a prompt photon, or a lepton from a b -hadron decay, while EPOS was filtered to simulate all remaining pileup events in the overlay sample. The individual simulations were first reweighted to ensure a smooth connection across jet p_T then the combination reweighted to match the distribution of the actual number of interactions per bunch crossing (μ) measured

³ The VBF BSM signal hypotheses were normalised by applying a global correction factor, defined as the ratio of the higher-order cross-section to the leading-order cross section of the SM hypothesis to ensure a consistent treatment of higher-order effects across all coupling scenarios.

in data⁴ during the 2022, 2023, and 2024 runs of the LHC. A summary of all Monte Carlo samples used in the two analyses are presented in Table 1.

Table 1: Summary of the Monte Carlo generators employed to produce the various signal and background processes used for this analysis. The perturbative accuracy (in QCD and, if relevant, in EW corrections) of the total production cross section σ_{prod} is stated for each process [37]. The order at which the corresponding matrix elements are calculated in the Monte Carlo simulation is not necessarily the same as in the cross-section calculation.

Process	Generator	Perturbative accuracy of σ_{prod}
VBF $H \rightarrow \gamma\gamma$ ($c_{H\bar{W}}$ variations)	MADGRAPH5_AMC@NLO 3.3.1 + PYTHIA 8.306	NNLO (QCD) + NLO (EW)
VBF $H \rightarrow \gamma\gamma$ (a_L and a_T variations)	MADGRAPH5_AMC@NLO 2.8.3.2 + PYTHIA 8.308	NNLO (QCD) + NLO (EW)
$gg \rightarrow H \rightarrow \gamma\gamma$	POWHEG BOX v2 + PYTHIA 8.310	NNLO (QCD) + NLO (EW)
$VH(\rightarrow \gamma\gamma)$	POWHEG BOX v2 + PYTHIA 8.310	NNLO (QCD) + NLO (EW)
$b\bar{b}H(\rightarrow \gamma\gamma)$	POWHEG BOX v2 + PYTHIA 8.310	NLO
$t\bar{t}H(\rightarrow \gamma\gamma)$	POWHEG BOX v2 + PYTHIA 8.310	NLO (QCD) + NLO (EW)
tHq	MADGRAPH5_AMC@NLO 3.5.1 + PYTHIA 8.309	NLO
tHW	MADGRAPH5_AMC@NLO 3.5.3 + PYTHIA 8.310	NLO
$pp \rightarrow \gamma\gamma$	SHERPA 2.2.14	NLO

5 Event reconstruction

Charged-particle tracks are reconstructed in the ID using either the standard reconstruction algorithm [83] or an alternative procedure that accounts for bremsstrahlung energy losses during pattern recognition [84]. Tracks matched to EM calorimeter clusters [85] are refitted using a Gaussian Sum Filter (GSF) algorithm to improve the track parameter estimate. These GSF tracks are used for the reconstruction of converted photons, while standard tracks are used for the reconstruction of collision vertices [86].

Photons are reconstructed from variable-size topological clusters [87] built from electromagnetic calorimeter cells with energy deposits significantly above the noise threshold [84]. Photon candidates are classified as converted if matched to either two tracks forming a conversion vertex in the silicon detectors or a single track originating from the silicon detectors consistent with an electron but lacking hits in the innermost pixel layer. Otherwise, they are classified as unconverted. All photon candidates must have $E_T > 25$ GeV and fall within the acceptance region of the finely segmented first layer of the EM calorimeter ($|\eta| < 2.37$), excluding the transition region between the barrel and end cap calorimeters, $1.37 < |\eta| < 1.52$. Their energy measurement is calibrated using methods described in Ref. [88], including dedicated corrections for samples simulated with AF3.

Photon candidates must fulfil the identification criteria of the *Tight* operating point [89], which are based on the shape of the electromagnetic shower in the EM calorimeter and the leakage of energy into the hadronic calorimeter. To suppress non-prompt photons from hadron decays, candidates must satisfy both calorimeter- and track-based isolation requirements. The calorimeter-based isolation variable is defined as the sum of cluster transverse energies in a cone of $\Delta R = 0.2$ around the photon candidate, with corrections for energy leakage, pile-up, and the underlying event. This variable is required to be less than 5% of the photon's transverse energy. Similarly, the track-based isolation requires the scalar sum of p_T for all tracks

⁴ The average (most probable) number of interactions per bunch crossing were 42 (50) during the 2022 run, 51 (58) in the 2023 run, and 54 (63) in the 2024 run.

with $p_T > 1$ GeV, matched to the primary vertex and not associated with a conversion vertex, to be less than 5% of the photon’s transverse energy.

Jets are reconstructed using the anti- k_t algorithm [90] as implemented in the FASTJET package [91], with a radius parameter $R = 0.4$ and particle-flow objects as input [92]. Jets are required to have $p_T > 20$ GeV and $|\eta| < 4.4$. To mitigate pile-up contamination, two multivariate classifiers are applied: one based on calorimeter and tracking information for jets with $p_T < 60$ GeV and $|\eta| < 2.4$ [93], and another based on jet shapes and topological correlations for jets with $p_T < 120$ GeV and $|\eta| > 2.5$ [94]. Jet momenta are corrected for passive material losses, non-compensating calorimeter response, and average pile-up contributions [95, 96].

To resolve ambiguities when physics objects are reconstructed in close proximity, an overlap removal procedure is applied. The two leading photons are always retained, while jets within $\Delta R = 0.4$ of a photon are removed.

The primary vertex is selected using a neural-network algorithm [97] trained to distinguish the hard-scatter vertex of an $H \rightarrow \gamma\gamma$ event from pile-up vertices. The algorithm utilises information from all reconstructed vertices and the kinematic properties of the diphoton system. This provides a vertex selection efficiency of 92.1% (77.1%) for VBF Higgs boson events with (without) a converted photon. The algorithm’s performance was validated using $Z \rightarrow e^+e^-$ data from Run-3 pp collisions by treating electrons as unconverted photon candidates, showing good agreement between data and simulation. Following vertex selection, the four-momenta and properties of all selected photons and jets in the event are recomputed relative to this vertex.

6 Analysis strategy and event selection

Candidate events consistent with the $H(\rightarrow \gamma\gamma) + 2$ jets final state are selected using diphoton triggers [44, 98], which require the leading and subleading photons to have $E_T > 35$ GeV and $E_T > 25$ GeV, respectively. These triggers also apply online identification requirements based on calorimeter shower-shape variables, corresponding to the *Medium* operating point. Within the defined kinematic regions, the combined trigger efficiency for VBF Higgs boson production is around 99%.

To be considered for the final analysis, candidate events must contain at least two photons. The Higgs boson candidate is reconstructed from the two highest- E_T photons, requiring an invariant mass ($m_{\gamma\gamma}$) in the range of 105-160 GeV. To suppress contributions from non-resonant $\gamma\gamma +$ jets production, the leading and subleading photons must satisfy $E_T/m_{\gamma\gamma} > 0.35$ and 0.25 , respectively. Furthermore, at least two jets with $p_T > 30$ GeV are required. To enrich the sample with events having a VBF-like topology, the two leading jets must have a pseudorapidity gap $|\Delta\eta_{jj}| > 2.0$ and satisfy a Zeppenfeld variable [99] requirement of $\eta^{\text{Zepp}} = |\eta_{\gamma\gamma} - (\eta_{j_1} + \eta_{j_2})/2| < 5$, where $\eta_{\gamma\gamma}$ is the pseudorapidity of the diphoton system, and η_{j_1} and η_{j_2} are the pseudorapidities of the leading and subleading jets in the event. These requirements are applied identically to both the CP and polarisation studies.

To further separate the VBF signal from the dominant ggF Higgs boson and $\gamma\gamma +$ jets backgrounds, a multi-class neural network (NN) is employed. The network is trained using simulated MC samples for the VBF signal (assuming $c_{H\bar{W}} = 0.0$) and the ggF background, while a data-driven approach, as described below, is used to model the continuum background. The network processes 16 different input features describing the VBF topology, the Higgs boson kinematics, and the combined Higgs boson + jets system. The list of input features includes:

- **VBF topology** observables characterising the VBF tagged jets, including the transverse momentum and pseudorapidity of the two leading jets, the invariant dijet mass (m_{jj}), the pseudorapidity gap between the two jets ($\Delta\eta_{jj}$), the transverse momentum of the dijet system ($p_{T,jj}$), the multiplicity of jets with $|\eta| < 2.5$ ($N^{\text{central jets}}$), and the minimum angular separation between any pair of photons and jets ($\min \Delta R_{\gamma j}$).
- **Higgs boson kinematics** observables describing the diphoton system, including the angular separation between the two photons ($\Delta R_{\gamma\gamma}$), the diphoton transverse momentum normalised to the invariant mass ($p_{T,\gamma\gamma}/m_{\gamma\gamma}$), and the diphoton transverse momentum projected onto the diphoton thrust axis normalised to the invariant mass ($p_{T,\gamma\gamma}/m_{\gamma\gamma}$).
- **Higgs boson + jets system** observables correlating the Higgs boson and the dijet system, including the azimuthal angular difference between the two photons and the two jets ($\Delta\Phi_{\gamma\gamma,jj}$), the Zeppenfeld observable (η^{Zepp}), the Collins–Soper angle of the diphoton system in the $\gamma\gamma jj$ rest frame ($\cos \Theta^*(\gamma\gamma, jj)$), and the transverse momentum of the Higgs boson + dijets system ($p_{T,\gamma\gamma jj}$).

The most important input features in the training are the m_{jj} , $\Delta\eta_{jj}$, $\min \Delta R_{\gamma j}$, $\Delta R_{\gamma\gamma}$, and $p_{T,\gamma\gamma}/m_{\gamma\gamma}$ observables.

The classifier, implemented in PyTorch [100], follows a sequential architecture consisting of three hidden layers with 128, 64, and 32 nodes, respectively. Each hidden layer applies a linear transformation to the outputs of the preceding layer, followed by layer normalisation and a ReLU activation function. The architecture concludes with a final linear layer containing three output nodes (logits) corresponding to the VBF signal, the ggF Higgs boson background, and the non-resonant $\gamma\gamma$ + jets background. During training, the multi-class cross-entropy loss is applied directly to the logits, while for inference the logits are transformed using a softmax function to predict the probability of an event belonging to one of the three target processes. A dropout rate of 0.1 is applied after the second and third hidden layers to mitigate overtraining. To prevent the classifier from sculpting the $m_{\gamma\gamma}$ spectrum, the training minimises a combined loss function: a cross-entropy term for classification and an auxiliary distance correlation term to reduce the correlation of the network response from the $m_{\gamma\gamma}$ observable [101]. The model is optimised using the Adam algorithm [102] with a learning rate of 1×10^{-5} and an early stopping criterion that terminates training if the validation loss fails to improve by at least the required tolerance of 5×10^{-5} over five epochs.

A significant challenge in training the NN is the accurate representation of non-resonant $\gamma\gamma$ and γ + jets backgrounds, as standard Monte Carlo simulations often provide an insufficient description of these components in topologies typical of VBF production. To address this, a newly developed data-driven approach based on a flow-matching method [103, 104] is used to generate the training sample for these processes. This approach uses sideband data ($m_{\gamma\gamma} \leq 120$ GeV or $m_{\gamma\gamma} > 130$ GeV) as input to an algorithm that learns the probability density distributions and high-dimensional correlations of all input features to the NN training, allowing for the generation of a high-statistics, data-derived continuum background sample approximately 20 times larger than the data sideband sample. The flow-matching model is based on a Transformer encoder architecture with an embedded timestep, paired with a multi-layer perceptron (MLP) decoder that maps the encoded representations back to the feature space. Training is conducted over 300 steps using the AdamW optimiser [105] with a learning rate of 1×10^{-4} . To generate the final sample, the model is sampled in reverse steps using a Dormand–Prince solver [106] with an adaptive step size over 40 steps. This procedure results in a robust, high-statistics representation of the non-resonant background, which is essential for the subsequent NN training and optimisation. Although trained exclusively with sideband data, the generated sample is also found to be an accurate representation of

the non-resonant backgrounds in the signal peak region ($120 \text{ GeV} < m_{\gamma\gamma} \leq 130 \text{ GeV}$). Moreover, the underlying flow-matching model reproduces the correlation coefficients between all 16 input features to within 1% of those observed in data.

To protect against potential biases, a two-fold cross-validation scheme is employed when training the NN. Events are randomly divided into two equal-sized subsamples, A and B , with independent networks trained on each. The network trained on A is used to evaluate B , and vice-versa. Half of the data are analysed with the NNs trained on sample A , and the other half with the NNs trained on sample B . Finally, the output distributions from both NNs are merged for both simulated and collision data. To validate this procedure, the performance of the two independent NNs was compared on both simulation and data, and found to be consistent within statistical uncertainties.

The predictions of the three output nodes are combined into a single discriminant:

$$D_{NN} = \log \left(\frac{p_{\text{VBF}}}{(f_{\text{ggF}} \cdot p_{\text{ggF}} + (1 - f_{\text{ggF}}) \cdot p_{\text{Continuum}})} \right) \quad (6)$$

where f_{ggF} is the fraction of expected ggF Higgs boson events relative to the total background, which is determined to be $f_{\text{ggF}} = 0.022$. Furthermore, the p_i terms represent the probabilities for the various signal and background hypotheses as predicted by the NN.

The D_{NN} -score distribution is used to define analysis regions with varying signal purities. While the boundaries of these regions are chosen to maximise the overall sensitivity to the Wilson coefficient $c_{H\bar{W}}$, they are equally appropriate for the polarisation study. Following this optimisation procedure, events are placed into three categories labelled as “tight”, “medium”, and “loose” based on their D_{NN} -score values. The tight category, which targets the highest signal purity, is defined by $D_{NN} \geq 3.7$, while the medium and loose categories encompass the intervals $2.1 \leq D_{NN} < 3.7$ and $-0.5 \leq D_{NN} < 2.1$, respectively. Events with a D_{NN} score below -0.5 are discarded, as the addition of a further low-purity category was found to provide no significant improvement to the overall sensitivity of the two analyses.

Each of the three signal categories is further subdivided into eight sub-categories defined by disjoint intervals of either the OO or $\Delta\Phi_{jj}$ observable, resulting in a total of 24 non-overlapping regions used per analysis. The interval boundaries for the OO observable are defined as $[-\infty, -0.70, -0.34, -0.15, 0.00, 0.15, 0.34, 0.70, \infty]$, while the $\Delta\Phi_{jj}$ observable is divided into eight equidistant intervals in the range of $[0, \pi]$. Using the signal and background yields determined for each region (see Section 7), the OO and $\Delta\Phi_{jj}$ distributions are exploited to search for CP-violating effects and polarisation-dependent couplings, respectively.

The distribution of the D_{NN} -scores observed in the data from the $m_{\gamma\gamma}$ sidebands is presented in Figure 3. For comparison, the figure also includes the D_{NN} -score templates for the non-resonant background (comprising the $\gamma\gamma + \text{jets}$ and the $\gamma + \text{jets}$ processes obtained as detailed in Section 7.2), the resonant ggF Higgs boson background, and the VBF signal. The boundaries of the three signal regions are indicated by vertical dashed lines. As illustrated, the loose category is only moderately populated by the VBF signal. However, it contains a significant fraction of events from ggF Higgs boson production. This high concentration of resonant background in the lower-score region provides an important handle to constrain the normalisation of the ggF Higgs boson background directly from the data, thereby reducing the systematic uncertainties associated with its contribution in the more signal-pure categories.

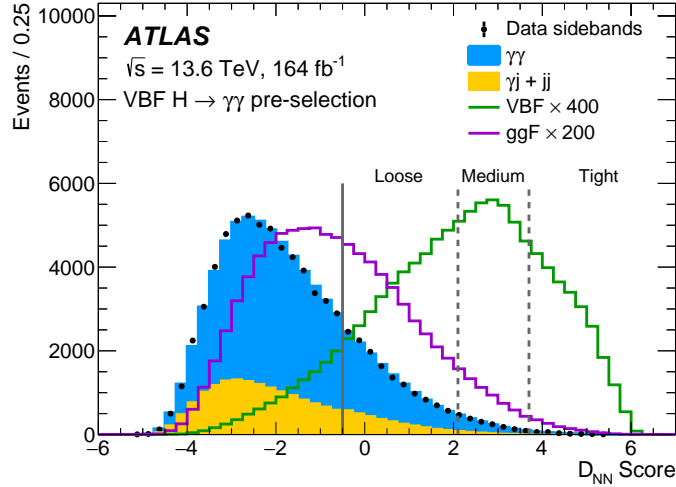


Figure 3: Comparison of the NN response score (D_{NN}) distributions for the VBF signal, the ggF background, and the non-resonant background, overlaid with sideband data. The non-resonant background includes simulated $\gamma\gamma$ continuum events as well as $\gamma + j$ and jj processes where one or more jets are misidentified as photons; the latter are estimated from control regions in data as detailed in Section 7. The VBF signal and ggF background are scaled by factors of 400 and 200 relative to their SM expectations, respectively. Vertical dashed lines indicate the thresholds used to define the signal categories, while events with a D_{NN} score below the lowest threshold (solid line) are excluded from the analysis.

7 Signal and background modelling

The yields for the signal, as well as the resonant and non-resonant backgrounds, are determined via a simultaneous unbinned maximum-likelihood fit to the individual diphoton invariant mass ($m_{\gamma\gamma}$) spectra of all analysis regions. These regions are defined by dividing the signal categories into discrete intervals of the OO or $\Delta\Phi_{jj}$ observables, as described in Section 6. Within each interval, the shape of the $m_{\gamma\gamma}$ distribution is modelled independently in the range of 105 to 160 GeV using analytic functional forms to describe the signal and background components.

7.1 Signal modelling

The $m_{\gamma\gamma}$ distributions of the VBF signal and the resonant backgrounds from other Higgs boson production modes are modelled in each category with a double-sided Crystal Ball (DSCB) function [107, 108], following the approach in Ref. [109]. The function consists of a Gaussian core describing the central peak, supplemented by two independent power-law tails at lower and higher $m_{\gamma\gamma}$ values. The total signal model includes six shape parameters and one overall normalisation factor. Among the shape parameters, the mean and width of the Gaussian core represent the signal peak position and the experimental resolution, respectively, while the remaining four parameters describe the tail behaviour. In each category, these six parameters are determined via fits to simulated signal samples, comprising the various Higgs boson production modes weighted by their SM cross-sections, and are later either fixed (for the tail parameters) or constrained within uncertainties originating from the photon energy calibration. Finally, the overall normalisation factor is determined from the fit to data. Systematic uncertainties associated with the signal modelling are detailed in Section 8.

7.2 Background modelling

The non-resonant background in the selected diphoton sample primarily consists of continuum $\gamma\gamma$ production, along with the γj and jj processes where one or more jets (j) are misidentified as photons. For each signal category, subdivided into intervals of OO or $\Delta\Phi_{jj}$, the relative contribution of each background component is measured in data using a double two-dimensional sideband method [110]. This technique uses 15 control regions in data in which either one photon (for the γj process) or both photons (for the jj process) fail to satisfy the identification or isolation criteria. The continuum background is on average found to be composed of approximately 79% $\gamma\gamma$ events, 19% γj , and 2% jj events. The $\gamma\gamma$ fraction changes smoothly across the analysis regions and ranges from 66% to 97%.

The $m_{\gamma\gamma}$ shape for the continuum $\gamma\gamma$ background is derived from simulated background samples after applying the full event selection described in Section 6. In contrast, the shapes for the γj and jj components are obtained from data control samples defined by inverting the identification requirements for one or both photons, while keeping all other selection criteria. The ratio of the $m_{\gamma\gamma}$ distributions of these data-driven components to those of the simulated $\gamma\gamma$ sample is well-described by a second-order polynomial. A fit to this ratio is used to derive a $m_{\gamma\gamma}$ -dependent weight, which is applied to the simulated $\gamma\gamma$ sample to produce a final set of background templates that incorporate the contributions and kinematics of the γj and jj processes. These templates, defined over the range $105 \leq m_{\gamma\gamma} < 160$ GeV in 55 uniform-width bins, are used solely to evaluate the spurious signal and select the background functional forms as described below. The final analysis results are then obtained by fitting the chosen analytic functions directly to the data.

Three classes of analytic functions are evaluated as candidates for modelling the non-resonant background in each category. They include exponential functions of first- to third-order polynomials, Bernstein polynomials of third to fifth order [111], and first-order power-law functions. The background function for each OO or $\Delta\Phi_{jj}$ region is selected independently based on the magnitude of the “spurious signal” [1] and the overall fit quality. The spurious signal, defined as the systematic bias in the fitted signal yield resulting from the functional form choice, is estimated by performing signal-plus-background fits to the background templates. This procedure is repeated by scanning the Higgs boson mass distribution in the range of 121 to 129 GeV in steps of 0.5 GeV, with the absolute maximum of the fitted signal yield across the scan taken as the spurious signal value.

To be considered, a function must satisfy two criteria: a χ^2 p-value greater than 0.1% and a spurious signal yield less than 20% of the statistical uncertainty of the fitted signal yield or 10% of the expected signal yield. If multiple functions meet these requirements, the one with the fewest degrees of freedom is chosen. In cases where no function initially satisfies the spurious signal criteria, the χ^2 requirement is removed. For both the CP and polarisation studies, these criteria were not met in two out of the 24 analysis regions due to large statistical fluctuations in the background templates. In these instances, the candidate functions were instead fitted directly to the sideband data to confirm they provided a sufficiently accurate description of the $m_{\gamma\gamma}$ shape. The final spurious signal value is incorporated as a systematic uncertainty in the signal yield to account for potential biases in the background modelling. Furthermore, uncertainties in the γj and jj fractions are found to have a negligible impact on the outcome of the spurious-signal test and are therefore neglected in the final fit.

8 Systematic uncertainties

Systematic uncertainties considered in the two analyses can be grouped into two main areas: uncertainties in the modelling of the $m_{\gamma\gamma}$ distribution for the signal and background processes, and uncertainties in the predicted VBF signal and ggF background yields in each category arising from experimental or theory sources. These systematic uncertainties are incorporated into the likelihood model as nuisance parameters (NPs) [112], as detailed in Section 9. Further information about the relevant uncertainties is provided below.

8.1 Experimental systematic uncertainties

Most experimental uncertainties primarily affect the expected yields of the VBF signal and the ggF background. The photon identification and isolation efficiencies are corrected to match those observed in data using dedicated measurements [89]. These correction factors, along with their corresponding uncertainties, are determined as a function of the photon E_T and $|\eta|$ using control samples of prompt photons from $\gamma + \text{jets}$ events, radiative $Z \rightarrow \ell^+ \ell^- \gamma$ decays, and electrons from $Z \rightarrow e^+ e^-$ decays. In the latter case, electrons are used as a proxy for photons due to their similar electromagnetic shower signatures, with Smirnov transformations applied to account for residual differences between their respective shower-shape distributions. The impact on the event yields from uncertainties in the photon identification and isolation efficiencies range from 3.6% to 5.7% and from 1.6% to 2.0%, respectively, for both the VBF signal and the ggF background. The uncertainty in the efficiency of the diphoton trigger is estimated by using radiative Z boson decays and events from pre-scaled lower-threshold triggers [98]. The resulting uncertainties are typically around 0.2%.

The photon energy scale and resolution are corrected to account for energy loss in upstream and inactive material, leakage effects, and imperfect modelling of electromagnetic showers and electronics response. These corrections, and the relevant uncertainties, are derived from control samples of electrons from Z boson decays and of photons from radiative $Z \rightarrow \ell^+ \ell^- \gamma$ decays [88]. The resulting uncertainties in the predicted yields of the VBF signal and the ggF background range from 0.2% to 0.5%.

Uncertainties in the jet energy scale (JES) and resolution (JER) are estimated by using control samples where jets recoil against well-calibrated reference objects, such as a photon or a Z boson. These uncertainties incorporate contributions from *in situ* calibration measurements, the dependence on pile-up activity, and the jet flavour composition [95]. To account for an observed mismodelling of jets at large pseudorapidity ($|\eta| > 3.2$) resulting from an energy shift measured in the forward calorimeters, an additional systematic uncertainty is introduced. Furthermore, JES and JER uncertainty terms are included to account for the non-closure between the G4 and AF3 simulations. The performance of the jet vertex tagging algorithm, employed to suppress contributions from pile-up jets, is corrected to match the efficiencies observed in data [93]. The associated correction factors and their systematic uncertainties are fully propagated through both studies. Summing these individual contributions, the total uncertainty in the VBF signal yields ranges from 4% to 11%, while the ggF background uncertainty ranges from 7% to 25% across all analysis regions.

Uncertainties in the modelling of pile-up activity in the simulation are accounted for by varying the value of the visible inelastic cross-section used for reweighting the simulation to match the data [113]. The resulting uncertainties in the VBF signal and the ggF background yields range from 0.1% to 1.4%.

Dedicated uncertainties are evaluated to account for residual discrepancies between the G4 and AF3 simulations. These uncertainties are determined by comparing the predicted event yields of the VBF signal and the ggF background using samples where the calorimeter responses are simulated with either AF3 or G4. The comparisons are performed independently for each signal category and within each OO and $\Delta\Phi_{jj}$ interval. The resulting yield differences are assigned as additional systematic uncertainties, which are typically on the order of 5% for both processes.

Finally, a global luminosity uncertainty of 1.9% is applied to the normalisation of the simulated signal and background samples. This uncertainty is determined following the methodology discussed in Ref. [46], using the LUCID-2 detector [114] for the primary luminosity measurements.

Beyond their impact on the expected event yields, the uncertainties in the energy scale and energy resolution of the photon candidates also affect the shape of the $m_{\gamma\gamma}$ distribution for both the VBF signal and the Higgs boson background processes. Most notably, these include uncertainties in the energy scale and energy resolution of the photon candidates. The photon energy scale uncertainties are propagated as shifts to the peak position of the DSCB function. The resulting impact is typically less than 0.3% relative to the nominal peak position, depending on the specific signal category and the OO or $\Delta\Phi_{jj}$ interval. Similarly, the photon energy resolution uncertainties are propagated to the Gaussian width of the DSCB shape. This variation has a relative impact ranging from 6% to 14%, depending on the event category and the corresponding OO or $\Delta\Phi_{jj}$ interval.

The modelling of the non-resonant $\gamma\gamma + \text{jets}$ background is subject to the choice of the analytic functional form. The resulting uncertainties in the background estimate for each interval of the OO and $\Delta\Phi_{jj}$ distributions are quantified via the spurious signal yield, as detailed in Section 7. For each of the tested background functions, the spurious signal is smaller than 30% of the statistical uncertainty of the expected signal yield.

8.2 Theoretical systematic uncertainties

Uncertainties in the theoretical modelling of the simulated VBF signal and the ggF background processes are taken into account. These modelling uncertainties arise from missing higher-order terms in the perturbative QCD calculations, the modelling of parton showers and the PDF set, and uncertainties in the value of the strong coupling constant α_S .

Uncertainties in the modelling of the PDF sets are evaluated following the PDF4LHC recommendations [115], while the impact of the α_S uncertainty is assessed by varying the nominal value ($\alpha_S = 0.118$) by ± 0.001 . These effects result in yield variations of approximately 2% and 0.5%, respectively.

Furthermore, uncertainties due to missing higher-order terms in the perturbative expansion are evaluated by varying the renormalisation and factorisation scales, μ_R and μ_F . For the VBF signal process, these uncertainties are estimated by individually varying μ_R and μ_F by a factor of 2 or 0.5 relative to their nominal value. Six combinations are considered: $(\mu_R, \mu_F) = (0.5, 0.5), (0.5, 1.0), (1.0, 0.5), (1.0, 2.0), (2.0, 1.0),$ and $(2.0, 2.0)$ times their nominal value. The final uncertainty is defined as the envelope of these variations, taking the maximal upward and downward deviations from the nominal predictions. These variations result in an uncertainty of up to 10% on the expected signal yields. For the ggF background process, a simple variation of the renormalisation and factorisation scales is insufficient, as it tends to underestimate the actual uncertainties. Instead, the procedure detailed in Ref. [116] is followed. This approach provides 18 individual nuisance parameters covering effects from jet migration, the Higgs boson

p_T shape, VBF topology selection, and top-quark-mass dependence. These uncertainties are typically less than 15% of the expected ggF background yields.

The modelling of the parton shower, underlying event, and hadronisation is assessed separately for the VBF signal and ggF background processes. This is achieved by replacing PYTHIA8.310 with HERWIG7.2.3 with the H7UE set of tuned parameters [117] for the event simulation. The uncertainties estimated from the differences between the resulting yield predictions typically do not exceed 10% for the VBF signal and 15% for the ggF background process.

Since the other Higgs boson production modes (ZH , WH , $b\bar{b}H$, $t\bar{t}H$, tWH , and $tHjb$) contribute only minimally to the signal regions probed in the two analyses, only uncertainties in their cross sections are taken into account. These uncertainties include effects from varying the renormalisation and factorisation scales, the PDF set, and α_s . The exact values are taken from Ref. [37].

9 Results

An unbinned maximum-likelihood fit is used for the statistical interpretation of the results from both the CP- and polarisation studies. Fits are performed independently for each parameter of interest (POI): $c_{H\widetilde{W}}$, a_L , and a_T . In each case, a simultaneous fit is conducted on the $m_{\gamma\gamma}$ distributions across the 24 analysis regions. Systematic uncertainties are implemented as nuisance parameters (NPs) with their correlations maintained across regions. The normalisations of the VBF signal and ggF background processes are parameterised via the normalisation scale factors, μ_{VBF} and μ_{ggF} , which are treated in most fit configurations as free parameters common to all regions. The normalisations of the other Higgs boson production processes are constrained to the SM predictions within their respective theoretical uncertainties.

The expected performance is evaluated using Asimov data samples [118] generated under the SM hypothesis. For fits to the Asimov data sample, the background shape and yield are fixed based on a fit to the data sidebands, excluding the signal peak region (120 to 130 GeV). As described in Section 4, parameter morphing is used to interpolate between a discrete set of simulated coupling values for $c_{H\widetilde{W}}$, a_L , and a_T to model the signal across a continuous range of coupling scenarios.

To obtain the final results, the fitting procedure is applied individually to each coupling parameter hypothesis, where the background prediction is only affected through variations of the normalisation factors and the NPs. A negative log-likelihood (NLL) curve is constructed as a function of the relevant coupling parameters. The value at the NLL minimum is taken as the best-fit estimate of the corresponding POI, while the associated confidence level (CL) intervals are determined from the appropriate deviation of the NLL from its minimum.

9.1 Run-3 results

In the fit configurations for the CP studies, the normalisation scale factors μ_{VBF} and μ_{ggF} are treated as free-floating parameters. By allowing these parameters to float, the analysis relies solely on the shape of the OO distribution, thereby reducing sensitivity to BSM CP-even contributions that could modify the total cross-section. However, as the quadratic BSM terms can modulate the OO distribution in a symmetric manner, they may still influence the measured shape. Consequently, the constraints on $c_{H\widetilde{W}}$ are derived

using two distinct parameterisations: one including only the linear terms in the morphing procedure, and another accounting for both the linear and quadratic terms.

For the polarisation studies, the parameters a_L and a_T are determined in two separate fit configurations. When one parameter is treated as the POI, the other is fixed to its SM value. Two distinct types of fits are considered: a shape-only fit, where both μ_{VBF} and μ_{ggF} are treated as free parameters, and a shape+rate fit, where μ_{ggF} is floated while μ_{VBF} is fixed to unity. The shape-only fit relies exclusively on the shape information of the $\Delta\Phi_{jj}$ distribution to distinguish between different signal hypotheses, whereas the shape+rate fit incorporates both the distribution shape and the total event yield. In the shape+rate fit, the signal normalisation is not free to adjust to the data but instead follows the cross section predicted for each (a_L, a_T) hypothesis, allowing rate information to contribute to the constraints of the POI. The two parameters show distinct sensitivities: a_L significantly modifies the total yield because the longitudinal polarisation vectors of the massive gauge bosons are proportional to the energy and can lead to large enhancements in the total cross section, whereas a_T has a comparatively weaker impact on the normalisation. Consequently, a_L is more strongly constrained by rate information, while the sensitivity to a_T is primarily driven by the shape of the $\Delta\Phi_{jj}$ distribution.

Figure 4 depicts the weighted OO and $\Delta\Phi_{jj}$ distributions summed across all three signal categories. Events are weighted by $\ln(1 + S/B)$, where S and B are the post-fit yields of signal and background events, respectively. The post-fit distribution of the diphoton invariant mass summed over all analysis categories and the intervals of the optimal observable is shown in Figure 5, where the events in each category are weighted by $\ln(1 + S/B)$. The signal and background contributions are fixed to the best-fit values from the $c_{H\widetilde{W}}$ interpretations.

The results of the likelihood scans for the CP studies are presented in Figure 6. The resulting best-fit value, as well as the expected and observed 95% CL intervals, are detailed in Figure 7 for the fit using the linear+quadratic parameterisation. The corresponding normalisation scale factors for the VBF signal and ggF background, at the best-fit estimate of $c_{H\widetilde{W}}$, are found to be $\mu_{\text{VBF}} = 1.01^{+0.24}_{-0.20}$ and $\mu_{\text{ggF}} = 1.27^{+0.56}_{-0.45}$, respectively. The 68% (95%) CL limits with linear-only terms shift by approximately 3.0% (8.6%), indicating a negligible impact of the quadratic terms on the exclusion limits. Figure 7 also shows a comparison of the expected and observed best-fit values and 95% CL intervals of the Run-2 VBF $H \rightarrow \gamma\gamma$ analysis and the statistical combination of the Run-2 and Run-3 results.

The results of the likelihood scans for the polarisation studies are presented in Figure 8. The scans over a_L (a_T) are shown in the upper (lower) panel, and the resulting best-fit values and the 95% CL intervals are detailed in Figure 9. The corresponding normalisation factors μ_{VBF} and μ_{ggF} are consistent within one standard deviation with those obtained from the CP studies. The asymmetry of the likelihood curves from the shape+rate fits stems from the non-linear dependence of the cross-section on the coupling parameters (see Ref. [35]). Conversely, the asymmetry in the shape-only fits is primarily driven by the background distribution, as the concentration of background at low $\Delta\Phi_{jj}$ values in the most sensitive signal category creates a lopsided sensitivity. For $a_L < a_T$, the VBF signal shifts toward larger $\Delta\Phi_{jj}$ values where the background is low, whereas for $a_L > a_T$, the signal overlaps more significantly with the background at low $\Delta\Phi_{jj}$ values.

The results from both the CP and polarisation studies are consistent with the SM expectations.

A breakdown of the impacts of various uncertainty sources on each POI, evaluated at the 68% CL, is summarised in Table 2. For all fits, the statistical uncertainty is the dominant component. Among the leading systematic uncertainties are those related to the modelling of the VBF signal process, the spurious signal, the energy scale and resolution of jets, and the energy resolution of photons. Generally, fits

exploiting both shape and rate information show increased sensitivity to experimental and modelling uncertainties compared with fits using only shape information.

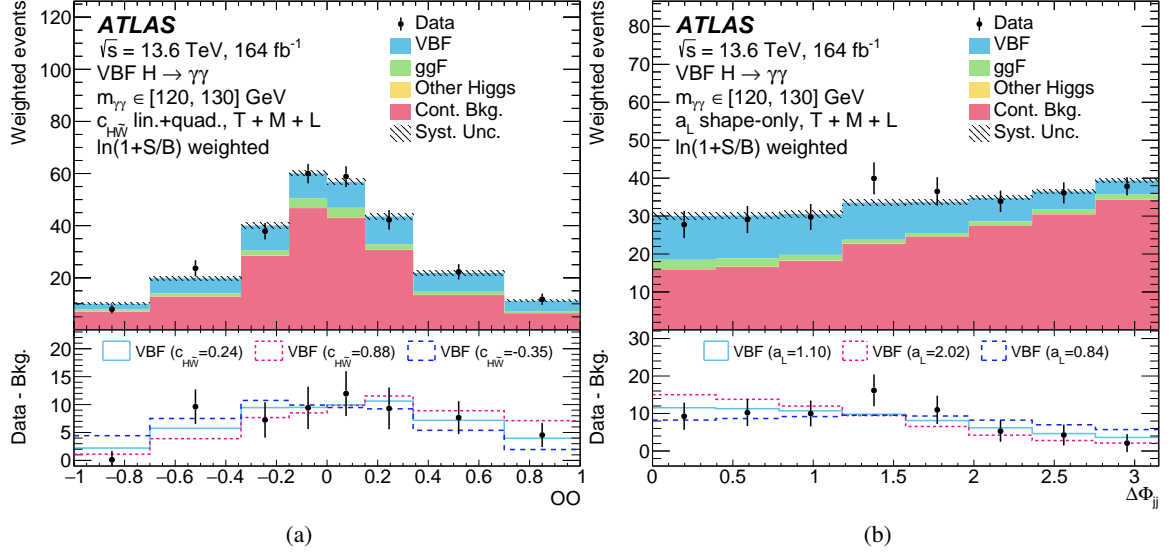


Figure 4: Post-fit distributions of (a) the optimal observable and (b) $\Delta\Phi_{jj}$ for events in the combined tight (T), medium (M), and loose (L) analysis regions within the invariant diphoton mass window $m_{\gamma\gamma} \in [120, 130]$ GeV. The signal and background yields are fixed to the best-fit values from the $c_{H\bar{W}}$ and a_L interpretations. Contributions from the three regions are summed, weighted by $\ln(1 + S/B)$, where S and B are the best-fit signal and background yields, respectively. The overflow and underflow are included in the outermost bins. The uncertainty band includes all systematic uncertainties. The lower panels show the background-subtracted data compared with the best-fit VBF prediction and two BSM scenarios corresponding to the two POI values excluded at exactly 95% CL by fits using only shape information.

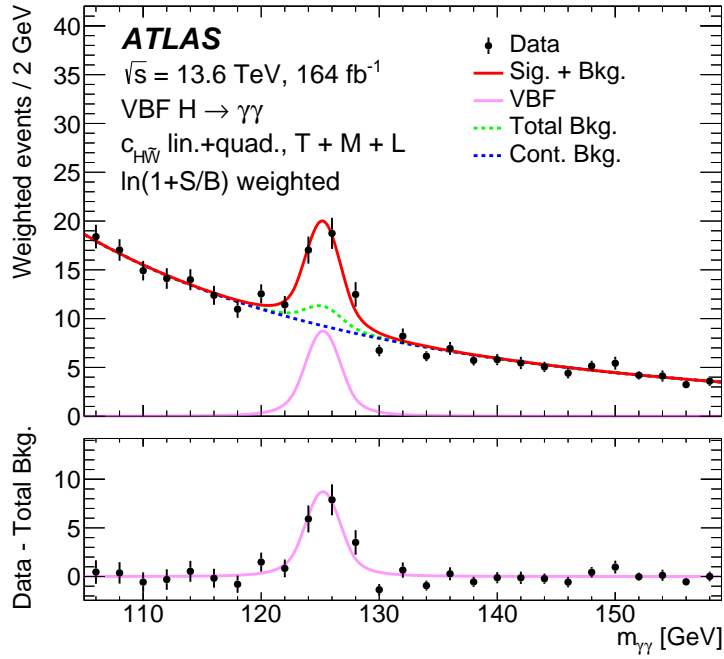


Figure 5: Weighted post-fit distribution of the data events compared with the signal and background contributions for the $m_{\gamma\gamma}$ spectrum, summed over the tight (T), medium (M), and loose (L) analysis regions and optimal observable intervals. Events are weighted by $\ln(1 + S/B)$, where S and B are the best-fit signal and background yields in each analysis region and optimal observable interval. The signal and background contributions are fixed to the values obtained from the best fit at $c_{H\tilde{W}} = 0.24$.

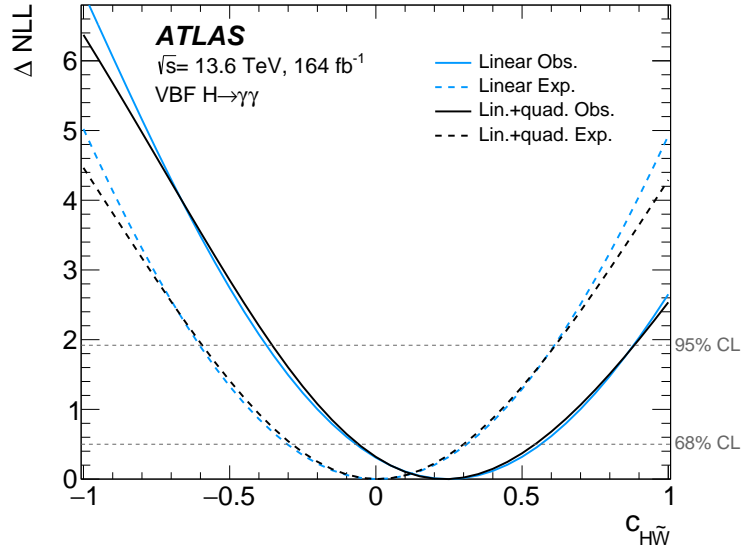


Figure 6: Expected and observed likelihood curves as a function of the Wilson coefficient $c_{H\tilde{W}}$. Fits using parameterisations with linear-only terms and linear+quadratic terms are shown. The dashed horizontal lines indicate the ΔNLL values corresponding to the 68% and 95% CL intervals. Results are obtained assuming a new physics scale of $\Lambda = 1$ TeV.

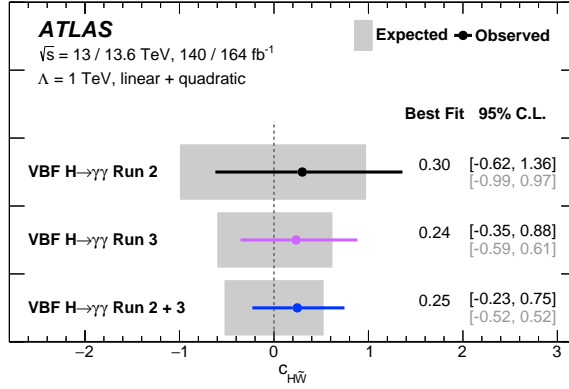


Figure 7: The expected and observed measurements of the Wilson coefficient $c_{H\bar{W}}$ in the VBF $H \rightarrow \gamma\gamma$ channel. Results are shown for integrated luminosities of 140 fb^{-1} at $\sqrt{s} = 13 \text{ TeV}$ [21] and 164 fb^{-1} at $\sqrt{s} = 13.6 \text{ TeV}$, and for the statistical combination of both data samples (as presented in Sec. 9.2). The dots and 95% CL bars show the best-fit values with statistical and systematic uncertainties, and the grey bands centred at zero show the expected 95% CL intervals. The best fit values and 95% CL observed (expected) limits are also explicitly stated on the right-hand side of the plot in black (grey). Results are obtained assuming a new physics scale of $\Lambda = 1 \text{ TeV}$.

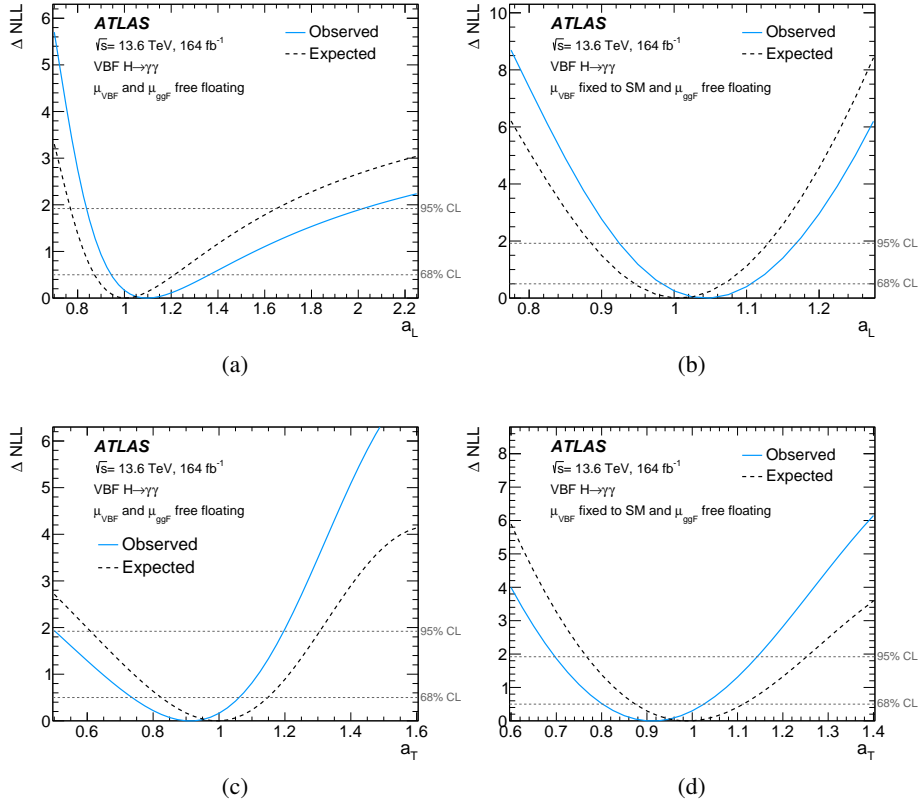


Figure 8: Expected and observed likelihood curves as a function of the longitudinally (a, b) and transversely (c, d) polarised couplings. Fits using shape-only (a, c) and shape+rate (b, d) information are shown. For all figures, the dashed horizontal lines indicate the ΔNLL values corresponding to the 68% and 95% CL intervals.

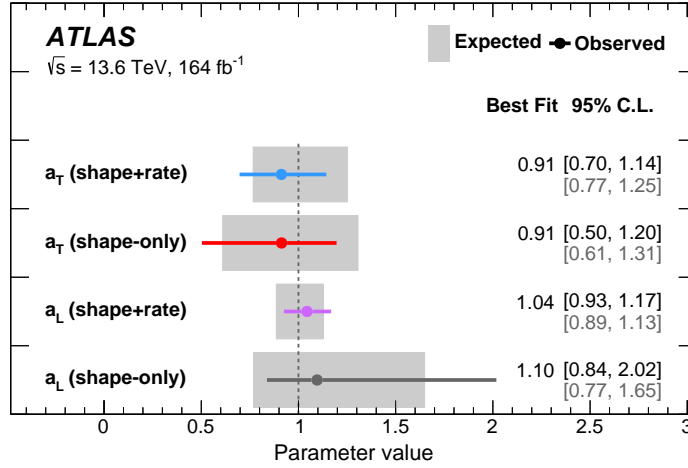


Figure 9: The expected and observed measurements of the polarisation-dependent coupling-strength scale factors for an integrated luminosity of 164 fb^{-1} at $\sqrt{s} = 13.6 \text{ TeV}$. The dots and 95% CL bars show the best-fit values with statistical and systematic uncertainties, and the grey bands centred at one show the expected 95% CL intervals. The best fit values and 95% CL observed (expected) limits are also explicitly stated on the right-hand side of the plot in black (grey).

Table 2: Breakdown of the relative contributions to the uncertainty in the best-fit parameters of interest (i.e. either $c_{H\bar{W}}$, a_L , or a_T) for the CP and polarisation studies. The relative impact of each group of nuisance parameters is defined as the square root of the difference between the squares of the total uncertainty obtained when treating all nuisance parameters as free and the uncertainty obtained when that group of nuisance parameters is fixed to their best-fit values, normalised to the total uncertainty. The statistical uncertainty component is determined by fixing all nuisance parameters to their best-fit values. The sum in quadrature of the individual components may differ from the total uncertainty due to correlations between the different groups of nuisance parameters.

Source	$c_{H\bar{W}}$ (Linear-only)	$c_{H\bar{W}}$ (Linear+quad.)	a_L (shape-only)	a_L (shape+rate)	a_T (shape-only)	a_T (shape+rate)
Total statistical	99%	99%	98%	79%	98%	89%
Total systematic	10%	7.4%	20%	61%	20%	45%
Spurious Signal	12%	11%	9.1%	7.4%	9.3%	7.4%
G4-AF3 discrepancies	3.3%	4.8%	2.1%	18%	3.3%	12%
Photons	< 1%	< 1%	2.9%	22%	3.9%	16%
Jets	7.0%	9.3%	10%	38%	12%	24%
Luminosity + Pile-up	1.6%	1.9%	< 1%	9.4%	< 1%	7.0%
VBF theory	5.8%	5.4%	8.8%	31%	9.5%	23%
ggF theory	2.9%	4.0%	5.0%	5.1%	6.1%	5.9%
Other Higgs boson theory	< 1%	< 1%	< 1%	< 1%	< 1%	< 1%

9.2 Combination of searches for CP violating effects using Run-2 and Run-3 results

The results obtained from the Run-3 dataset are combined with the previous ATLAS search for CP-violating effects in VBF $H \rightarrow \gamma\gamma$ events using Run-2 data [21]. To maximise the sensitivity to $c_{H\bar{W}}$, a simultaneous fit to the Run-2 and Run-3 datasets is performed. Theoretical uncertainties in the parton shower model, are treated as fully correlated across both datasets. The QCD scale uncertainty is correlated for the ggF process but uncorrelated for the VBF signal. This accounts for the different uncertainty calculation procedures

employed in the Run-2 and Run-3 analyses. Most experimental uncertainties are treated as fully correlated, with exceptions for photon and jet energy scale uncertainties related to specific corrections for the AF3 simulation, photon leakage effects, and the extrapolation between Run-2 and Run-3 conditions. All other systematic uncertainties are treated as uncorrelated. The spurious signal and parton shower uncertainties represent the dominant systematic components in the combination. The impact of the specific correlation scheme was evaluated and found to be negligible, as the total uncertainty is dominated by the statistical component.

The joint likelihood is constructed as the product of the individual likelihood functions from the Run-2 and Run-3 analyses. Correlated systematic sources share a common NP. In this combination, the normalisation scale factor μ_{ggF} is treated as a free-floating parameter in the Run-2 component of the fit to ensure a consistent treatment across both datasets. This approach results in a $\sim 5\%$ broadening of the $c_{H\bar{W}}$ constraint relative to the original Run-2 publication, where μ_{ggF} was constrained to its SM prediction within theoretical uncertainties.

Confidence level intervals are determined for the parameterisations with linear-only and linear+quadratic terms. The expected and observed profile likelihood scans for the Run-2, Run-3, and combined datasets are shown in Figure 10. For the fit with the linear+quadratic parameterisation, the best-fit value is found to be $c_{H\bar{W}} = 0.25$. The observed 68% (95%) CL intervals for $c_{H\bar{W}}$ are determined to be $[0.01, 0.49]$ ($[-0.23, 0.75]$) compared to the expected intervals of $[-0.26, 0.26]$ ($[-0.52, 0.52]$). The corresponding normalisation scale factors at the best-fit point are $\mu_{VBF} = 1.14 \pm 0.12$ and $\mu_{ggF} = 1.43^{+0.59}_{-0.47}$. For the combined fit, the impact of the quadratic terms on the CL intervals is negligible. The best-fit value, and the expected and observed 95% CL intervals for the combined fit are also presented alongside the individual Run-2 and Run-3 results in Figure 7.

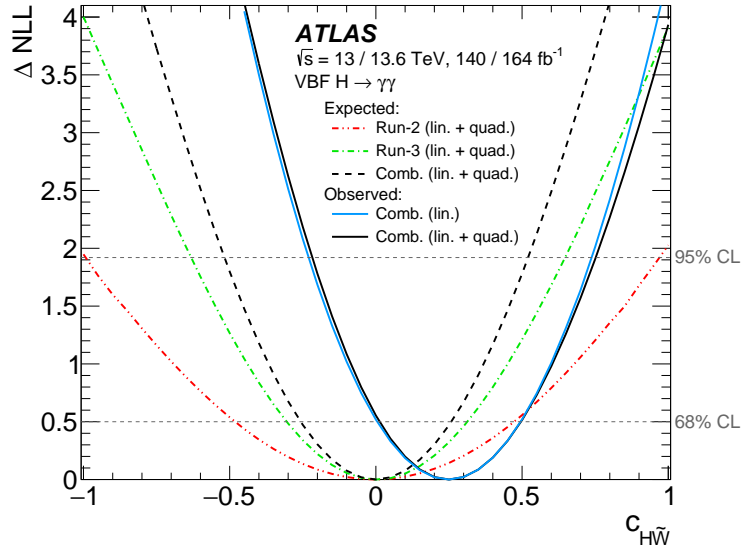


Figure 10: Expected and observed likelihood curve as a function of the Wilson coefficient $c_{H\bar{W}}$. The results are shown for the individual Run-2 and Run-3 datasets, as well as for the combined fit of both datasets. Scans are performed using both the full linear+quadratic and linear-only parameterisations. The dashed horizontal lines indicate the ΔNLL values corresponding to the 68% and 95% CL intervals. Results are obtained assuming a new physics scale of $\Lambda = 1 \text{ TeV}$.

10 Conclusion

This article presents constraints on the CP structure and the polarisation-dependent coupling strengths of the HVV coupling, probed via the vector-boson fusion production mode. The results are obtained using the $H(\rightarrow \gamma\gamma)jj$ final state in data corresponding to an integrated luminosity of 164 fb^{-1} of proton–proton collision data at $\sqrt{s} = 13.6 \text{ TeV}$, recorded with the ATLAS detector during 2022–2024. Significant improvements with respect to previous results are achieved through the implementation of a new neural network-based classification algorithm and the larger analysed data sample.

The CP-odd Wilson coefficient $c_{H\overline{W}}$, parameterising CP-violating effects in the HVV coupling, and the coupling-strength scale factors for longitudinally and transversely polarised vector bosons, are constrained using kinematic observables. Based on the shape of an Optimal Observable, the 68% (95%) CL intervals for $c_{H\overline{W}}$ are determined to be $[-0.06, 0.54]$ ($[-0.35, 0.88]$). Compared with a similar analysis of $H(\rightarrow \gamma\gamma)jj$ events using 140 fb^{-1} of $\sqrt{s} = 13 \text{ TeV}$ data, these Run-3 constraints show a 38% improvement, with 29% arising from refined analysis techniques, most notably the implementation of a new NN-based classification algorithm. To maximise sensitivity, the Run-2 and Run-3 results are combined, narrowing the 68% (95%) CL intervals for $c_{H\overline{W}}$ to $[0.01, 0.49]$ ($[-0.23, 0.75]$), which represents a total improvement of 50% over the Run-2 results.

Two fit configurations are used to determine the polarisation-dependent scale factors. Using shape information from the $\Delta\Phi_{jj}$ distribution alone, the 68% (95%) CL intervals are $a_L \in [0.94, 1.36]$ ($[0.84, 2.02]$) and $a_T \in [0.74, 1.06]$ ($[0.50, 1.20]$). When both shape and rate information are used, the constraints are significantly strengthened to $a_L \in [0.98, 1.11]$ ($[0.93, 1.17]$) and $a_T \in [0.80, 1.03]$ ($[0.70, 1.14]$). These measurements represent the first determination of polarisation-dependent coupling strength scale factors in $H(\rightarrow \gamma\gamma)jj$ events. Compared with previous results in $H(\rightarrow WW^* \rightarrow e\nu\mu\nu)jj$ events using 36.1 fb^{-1} of $\sqrt{s} = 13 \text{ TeV}$ data, the current analysis provides a major improvement in sensitivity. Using shape information alone, this analysis provides 95% CL intervals for a_L and a_T , whereas the sensitivity of the previous analysis was insufficient to reach those confidence levels. Furthermore, when comparing the results from fits that use both shape and rate information, the widths of the 95% CL intervals for a_L and a_T are reduced by more than a factor of three relative to the results obtained in $H(\rightarrow WW^* \rightarrow e\nu\mu\nu)jj$ events.

All results are consistent with the SM expectations, as no significant CP-odd contributions or deviations in polarisation-dependent couplings are observed. Notably, these studies represent a significant advancement as the first ATLAS results to rely exclusively on the AF3 detector simulation of the ATLAS calorimeter system for all Monte Carlo samples, demonstrating the viability of this fast simulation tool.

Acknowledgements

We thank CERN for the very successful operation of the LHC and its injectors, as well as the support staff at CERN and at our institutions worldwide without whom ATLAS could not be operated efficiently.

The crucial computing support from all WLCG partners is acknowledged gratefully, in particular from CERN, the ATLAS Tier-1 facilities at TRIUMF/SFU (Canada), NDGF (Denmark, Norway, Sweden), CC-IN2P3 (France), KIT/GridKA (Germany), INFN-CNAF (Italy), NL-T1 (Netherlands), PIC (Spain), RAL (UK) and BNL (USA), the Tier-2 facilities worldwide and large non-WLCG resource providers. Major contributors of computing resources are listed in Ref. [119].

We gratefully acknowledge the support of ANPCyT, Argentina; YerPhI, Armenia; ARC, Australia; BMWFW and FWF, Austria; ANAS, Azerbaijan; CNPq and FAPESP, Brazil; NSERC, NRC and CFI, Canada; CERN; ANID, Chile; CAS, MOST and NSFC, China; Minciencias, Colombia; MEYS CR, Czech Republic; DNRf and DNSRC, Denmark; IN2P3-CNRS and CEA-DRF/IRFU, France; SRNSFG, Georgia; BMFT, HGF and MPG, Germany; GSRI, Greece; RGC and Hong Kong SAR, China; ICHEP and Academy of Sciences and Humanities, Israel; INFN, Italy; MEXT and JSPS, Japan; CNRST, Morocco; NWO, Netherlands; RCN, Norway; MNiSW, Poland; FCT, Portugal; MNE/IFA, Romania; MSTDI, Serbia; MSSR, Slovakia; ARIS and MVZI, Slovenia; DSI/NRF, South Africa; MICIU/AEI, Spain; SRC and Wallenberg Foundation, Sweden; SERI, SNSF and Cantons of Bern and Geneva, Switzerland; NSTC, Taipei; TENMAK, Türkiye; STFC/UKRI, United Kingdom; DOE and NSF, United States of America.

Individual groups and members have received support from BCKDF, CANARIE, CRC and DRAC, Canada; CERN-CZ, FORTE and PRIMUS, Czech Republic; COST, ERC, ERDF, Horizon 2020 and Marie Skłodowska-Curie Actions, European Union; Investissements d'Avenir Labex, Investissements d'Avenir Idex and ANR, France; DFG and AvH Foundation, Germany; Herakleitos, Thales and Aristeia programmes co-financed by EU-ESF and the Greek NSRF, Greece; BSF-NSF and MINERVA, Israel; NCN and NAWA, Poland; La Caixa Banking Foundation, CERCA and AGAUR programs from Generalitat de Catalunya and PROMETEO and GenT Programmes Generalitat Valenciana, Spain; Göran Gustafssons Stiftelse, Sweden; The Royal Society and Leverhulme Trust, United Kingdom; Eric and Wendy Schmidt Fund for Strategic Innovation, United States of America.

In addition, individual members wish to acknowledge support from Chile: Agencia Nacional de Investigación y Desarrollo (ANID FONDECYT reg. 1230987, FONDECYT 1230812, FONDECYT 1240864, Fondecyt 3240661, Fondecyt Regular 1240721); China: Chinese Ministry of Science and Technology (MOST-2023YFA1605700, MOST-2023YFA1609300), National Natural Science Foundation of China (NSFC 12275265, NSFC-W2543005); Czech Republic: Czech Science Foundation (GACR - 24-11373S), Ministry of Education Youth and Sports (ERC-CZ-LL2327, FORTE CZ.02.01.01/00/22_008/0004632), PRIMUS Research Programme (PRIMUS/21/SCI/017); EU: H2020 European Research Council (ERC - 101002463); European Union: European Research Council (BARD No. 101116429, ERC - 948254, ERC 101089007), European Regional Development Fund (HE COFUND GA No.101081355, ERDF), Marie Skłodowska-Curie Actions (GAP-101168829); France: Agence Nationale de la Recherche (ANR-21-CE31-0013, ANR-22-EDIR-0002, ANR-24-CE31-0504-01); Germany: Deutsche Forschungsgemeinschaft (DFG - 469666862); China: Research Grants Council (GRF); Italy: Ministero dell'Università e della Ricerca (NextGenEU 153D23001490006 M4C2.1.1, NextGenEU I53D23000820006 M4C2.1.1, NextGenEU I53D23001490006 M4C2.1.1, SOE2024_0000023); Japan: Japan Society for the Promotion of Science (JSPS KAKENHI JP25H0063, JSPS KAKENHI JP22H01227, JSPS KAKENHI JP22H04944, JSPS KAKENHI JP22KK0227, JSPS KAKENHI JP24K23939, JSPS KAKENHI JP24KK0251, JSPS KAKENHI JP25H00650, JSPS KAKENHI JP25H01291, JSPS KAKENHI JP25K01023); Poland: Polish National Science Centre (NCN 2021/42/E/ST2/00350, NCN OPUS 2023/51/B/ST2/02507, NCN OPUS nr 2022/47/B/ST2/03059, NCN UMO-2019/34/E/ST2/00393, UMO-2022/47/O/ST2/00148, UMO-2023/49/B/ST2/04085, UMO-2023/51/B/ST2/00920, UMO-2024/53/N/ST2/00869); Spain: Agència de Gestió d'Ajuts Universitaris i de Recerca. (AGAUR - 2023 BP 00141), Ministry of Science and Innovation (RYC2019-028510-I, RYC2020-030254-I, RYC2021-031273-I, RYC2022-038164-I), Ministerio de Ciencia, Innovación y Universidades/Agencia Estatal de Investigación (PID2022-142604OB-C22); Sweden: Carl Trygger Foundation (Carl Trygger Foundation CTS 22:2312), Swedish Research Council (Swedish Research Council 2023-04654, VR 2021-03651, VR 2022-03845, VR 2022-04683, VR 2023-03403, VR 2024-05451, VR 2025-05940), Knut and Alice Wallenberg Foundation (KAW 2023.0366); Switzerland: Swiss National Science Foundation (SNSF - PCEFP2_194658); United Kingdom: The Binks Trust, Royal Society

(NIF-R1-231091); United States of America: U.S. Department of Energy (ECA DE-AC02-76SF00515), John Templeton Foundation (John Templeton Foundation 63206), Neubauer Family Foundation.

References

- [1] ATLAS Collaboration, *Observation of a new particle in the search for the Standard Model Higgs boson with the ATLAS detector at the LHC*, *Phys. Lett. B* **716** (2012) 1, arXiv: [1207.7214 \[hep-ex\]](#).
- [2] CMS Collaboration, *Observation of a new boson at a mass of 125 GeV with the CMS experiment at the LHC*, *Phys. Lett. B* **716** (2012) 30, arXiv: [1207.7235 \[hep-ex\]](#).
- [3] ATLAS Collaboration, *Study of the spin and parity of the Higgs boson in diboson decays with the ATLAS detector*, *Eur. Phys. J. C* **75** (2015) 476, arXiv: [1506.05669 \[hep-ex\]](#), Erratum: *Eur. Phys. J. C* **76** (2016) 152.
- [4] ATLAS Collaboration, *Combined Measurement of the Higgs Boson Mass from the $H \rightarrow \gamma\gamma$ and $H \rightarrow ZZ^* \rightarrow 4\ell$ Decay Channels with the ATLAS Detector Using $\sqrt{s} = 7, 8,$ and 13 TeV pp Collision Data*, *Phys. Rev. Lett.* **131** (2023) 251802, arXiv: [2308.04775 \[hep-ex\]](#).
- [5] ATLAS Collaboration, *Measurement of off-shell Higgs boson production in the $H^* \rightarrow ZZ \rightarrow 4\ell$ decay channel using a neural simulation-based inference technique in 13 TeV pp collisions with the ATLAS detector*, *Rept. Prog. Phys.* **88** (2025) 057803, arXiv: [2412.01548 \[hep-ex\]](#).
- [6] CMS Collaboration, *Measurement of the Higgs boson width and evidence of its off-shell contributions to ZZ production*, *Nature Physics* **18** (2022) 1329, arXiv: [2202.06923 \[hep-ex\]](#).
- [7] ATLAS Collaboration, *A detailed map of Higgs boson interactions by the ATLAS experiment ten years after the discovery*, *Nature* **607** (2022) 52, arXiv: [2207.00092 \[hep-ex\]](#), Erratum: *Nature* **612** (2022) E24.
- [8] CMS Collaboration, *A portrait of the Higgs boson by the CMS experiment ten years after the discovery*, *Nature* **607** (2022) 60, arXiv: [2207.00043 \[hep-ex\]](#), Erratum: *Nature* **623** (2023) E4.
- [9] I. Anderson et al., *Constraining Anomalous HVV Interactions at Proton and Lepton Colliders*, *Phys. Rev. D* **89** (2014) 035007, arXiv: [1309.4819 \[hep-ph\]](#).
- [10] G. F. Giudice, C. Grojean, A. Pomarol, and R. Rattazzi, *The Strongly-Interacting Light Higgs*, *JHEP* **06** (2007) 045, arXiv: [hep-ph/0703164](#).
- [11] A. D. Sakharov, *Violation of CP invariance, C asymmetry, and baryon asymmetry of the universe*, *Sov. Phys. Usp.* **34** (1991) 392.
- [12] G. C. Branco et al., *Theory and phenomenology of two-Higgs-doublet models*, *Phys. Rept.* **516** (2012) 1, arXiv: [1106.0034 \[hep-ph\]](#).
- [13] B. W. Lee, C. Quigg, and H. B. Thacker, *Strength of Weak Interactions at Very High Energies and the Higgs Boson Mass*, *Phys. Rev. Lett.* **38** (1977) 883.
- [14] D. B. Kaplan and H. Georgi, *$SU(2) \times U(1)$ Breaking by Vacuum Misalignment*, *Phys. Lett. B* **136** (1984) 183.

- [15] D. B. Kaplan, H. Georgi, and S. Dimopoulos, *Composite Higgs Scalars*, *Phys. Lett. B* **136** (1984) 187.
- [16] ATLAS Collaboration, *Test of CP invariance in vector-boson fusion production of the Higgs boson using the Optimal Observable method in the ditau decay channel with the ATLAS detector*, *Eur. Phys. J. C* **76** (2016) 658, arXiv: [1602.04516 \[hep-ex\]](#).
- [17] CMS Collaboration, *Combined search for anomalous pseudoscalar HVV couplings in $VH(H \rightarrow b\bar{b})$ production and $H \rightarrow VV$ decay*, *Phys. Lett. B* **759** (2016) 672, arXiv: [1602.04305 \[hep-ex\]](#).
- [18] ATLAS Collaboration, *Constraints on Higgs boson properties using $WW^*(\rightarrow e\nu\mu\nu)jj$ production in 36.1 fb^{-1} of $\sqrt{s} = 13\text{ TeV}$ pp collisions with the ATLAS detector*, *Eur. Phys. J. C* **82** (2022) 622, arXiv: [2109.13808 \[hep-ex\]](#).
- [19] CMS Collaboration, *Constraints on anomalous Higgs boson couplings to vector bosons and fermions from the production of Higgs bosons using the $\tau\tau$ final state*, *Phys. Rev. D* **108** (2023) 032013, arXiv: [2205.05120 \[hep-ex\]](#).
- [20] ATLAS Collaboration, *Test of CP-invariance of the Higgs boson in vector-boson fusion production and its decay into four leptons*, *JHEP* **05** (2024) 105, arXiv: [2304.09612 \[hep-ex\]](#).
- [21] ATLAS Collaboration, *Test of CP Invariance in Higgs Boson Vector-Boson-Fusion Production Using the $H \rightarrow \gamma\gamma$ Channel with the ATLAS Detector*, *Phys. Rev. Lett.* **131** (2023) 061802, arXiv: [2208.02338 \[hep-ex\]](#).
- [22] ATLAS Collaboration, *Test of CP invariance in vector-boson fusion production of the Higgs boson in the $H \rightarrow \tau\tau$ channel in proton–proton collisions at $\sqrt{s} = 13\text{ TeV}$ with the ATLAS detector*, *Phys. Lett. B* **805** (2020) 135426, arXiv: [2002.05315 \[hep-ex\]](#).
- [23] ATLAS Collaboration, *Probing the Higgs boson CP properties in vector-boson fusion production in the $H \rightarrow \tau^+\tau^-$ channel with the ATLAS detector*, *JHEP* **10** (2025) 092, arXiv: [2506.19395 \[hep-ex\]](#).
- [24] ATLAS Collaboration, *Measurements of Higgs boson production via gluon–gluon fusion and vector-boson fusion using $H \rightarrow WW^* \rightarrow \ell\nu\ell\nu$ decays in pp collisions with the ATLAS detector and their effective field theory interpretations*, *Eur. Phys. J. C* **85** (2025) 1403, arXiv: [2504.07686 \[hep-ex\]](#).
- [25] ATLAS Collaboration, *CP Properties of Higgs Boson Interactions with Top Quarks in the $t\bar{t}H$ and tH Processes Using $H \rightarrow \gamma\gamma$ with the ATLAS Detector*, *Phys. Rev. Lett.* **125** (2020) 061802, arXiv: [2004.04545 \[hep-ex\]](#).
- [26] ATLAS Collaboration, *Probing the CP nature of the top-Higgs Yukawa coupling in $t\bar{t}H$ and tH events with $H \rightarrow b\bar{b}$ decays using the ATLAS detector at the LHC*, *Phys. Lett. B* **849** (2024) 138469, arXiv: [2303.05974 \[hep-ex\]](#).
- [27] CMS Collaboration, *Search for CP violation in $t\bar{t}H$ and tH production in multilepton channels in proton–proton collisions at $\sqrt{s} = 13\text{ TeV}$* , *JHEP* **07** (2023) 092, arXiv: [2208.02686 \[hep-ex\]](#).
- [28] CMS Collaboration, *Measurements of $t\bar{t}H$ Production and the CP Structure of the Yukawa Interaction between the Higgs Boson and Top Quark in the Diphoton Decay Channel*, *Phys. Rev. Lett.* **125** (2020) 061801, arXiv: [2003.10866 \[hep-ex\]](#).

- [29] ATLAS Collaboration, *Combination of measurements of CP properties of Higgs boson interactions to vector bosons using Run 2 proton–proton collisions at $\sqrt{s} = 13$ TeV with the ATLAS detector*, (2026), CERN-EP-2026-071.
- [30] ATLAS Collaboration, *Measurement of the CP properties of Higgs boson interactions with τ -leptons with the ATLAS detector*, *Eur. Phys. J. C* **83** (2023) 563, arXiv: 2212.05833 [hep-ex].
- [31] CMS Collaboration, *Analysis of the CP structure of the Yukawa coupling between the Higgs boson and τ leptons in proton–proton collisions at $\sqrt{s} = 13$ TeV*, *JHEP* **06** (2022) 012, arXiv: 2110.04836 [hep-ex].
- [32] I. Brivio, and M. Trott, *The Standard Model as an Effective Field Theory*, *Phys. Rept.* **793** (2019) 1, arXiv: 1706.08945 [hep-ph].
- [33] W. Buchmüller, and D. Wyler, *Effective lagrangian analysis of new interactions and flavour conservation*, *Nucl. Phys. B* **268** (1986) 621.
- [34] B. Grzadkowski, M. Iskrzyński, M. Misiak, and J. Rosiek, *Dimension-Six Terms in the Standard Model Lagrangian*, *JHEP* **10** (2010) 085, arXiv: 1008.4884 [hep-ph].
- [35] J. Brehmer, J. Jaeckel, and T. Plehn, *Polarized WW Scattering on the Higgs Pole*, *Phys. Rev. D* **90** (2014) 054023, arXiv: 1404.5951 [hep-ph].
- [36] S. Weinberg, *Baryon- and Lepton-Nonconserving Processes*, *Phys. Rev. Lett.* **43** (1979) 1566.
- [37] D. de Florian et al., *Handbook of LHC Higgs Cross Sections: 4. Deciphering the Nature of the Higgs Sector*, (2017), arXiv: 1610.07922 [hep-ph].
- [38] J. Brehmer, F. Kling, T. Plehn, and T. M. P. Tait, *Better Higgs-CP Tests Through Information Geometry*, *Phys. Rev. D* **97** (2018) 095017, arXiv: 1712.02350 [hep-ph].
- [39] J. Alwall et al., *The automated computation of tree-level and next-to-leading order differential cross sections, and their matching to parton shower simulations*, *JHEP* **07** (2014) 079, arXiv: 1405.0301 [hep-ph].
- [40] NNPDF Collaboration, R. D. Ball et al., *Parton distributions for the LHC run II*, *JHEP* **04** (2015) 040, arXiv: 1410.8849 [hep-ph].
- [41] T. Sjöstrand et al., *An introduction to PYTHIA 8.2*, *Comput. Phys. Commun.* **191** (2015) 159, arXiv: 1410.3012 [hep-ph].
- [42] ATLAS Collaboration, *The ATLAS Experiment at the CERN Large Hadron Collider*, *JINST* **3** (2008) S08003.
- [43] ATLAS Collaboration, *The ATLAS experiment at the CERN Large Hadron Collider: a description of the detector configuration for Run 3*, *JINST* **19** (2024) P05063, arXiv: 2305.16623 [physics.ins-det].
- [44] ATLAS Collaboration, *The ATLAS trigger system for LHC Run 3 and trigger performance in 2022*, *JINST* **19** (2024) P06029, arXiv: 2401.06630 [hep-ex].

- [45] ATLAS Collaboration, *Software and computing for Run 3 of the ATLAS experiment at the LHC*, *Eur. Phys. J. C* **85** (2025) 234, arXiv: 2404.06335 [hep-ex],
Erratum: *Eur. Phys. J. C* **85** (2025) 907.
- [46] ATLAS Collaboration, *Preliminary luminosity calibration of the ATLAS 13.6 TeV data recorded in 2024 and combination with the 2022 and 2023 measurements*, ATL-DAPR-PUB-2025-001, 2025,
URL: <https://cds.cern.ch/record/2948582>.
- [47] ATLAS Collaboration,
ATLAS data quality operations and performance for 2015–2018 data-taking,
JINST **15** (2020) P04003, arXiv: 1911.04632 [physics.ins-det].
- [48] S. Agostinelli et al., *GEANT4 – a simulation toolkit*, *Nucl. Instrum. Meth. A* **506** (2003) 250.
- [49] ATLAS Collaboration, *AtlFast3: The Next Generation of Fast Simulation in ATLAS*,
Comput. Softw. Big Sci. **6** (2022) 7, arXiv: 2109.02551 [hep-ex].
- [50] A. Alloul, N. D. Christensen, C. Degrande, C. Duhr and B. Fuks,
FeynRules 2.0 - A complete toolbox for tree-level phenomenology,
Comput. Phys. Commun. **185** (2014) 2250, arXiv: 1310.1921 [hep-ph].
- [51] I. Brivio, Y. Jiang and M. Trott, *The SMEFTsim package, theory and tools*, *JHEP* **12** (2017) 070,
arXiv: 1709.06492 [hep-ph].
- [52] I. Brivio, *SMEFTsim 3.0 — a practical guide*, *JHEP* **04** (2021) 073,
arXiv: 2012.11343 [hep-ph].
- [53] ATLAS Collaboration, *ATLAS Pythia 8 tunes to 7 TeV data*, ATL-PHYS-PUB-2014-021, 2014,
URL: <https://cds.cern.ch/record/1966419>.
- [54] ATLAS Collaboration, *Search for the Standard Model Higgs boson produced in association with top quarks and decaying into $b\bar{b}$ in pp collisions at $\sqrt{s} = 8$ TeV with the ATLAS detector*,
Eur. Phys. J. C **75** (2015) 349, arXiv: 1503.05066 [hep-ex].
- [55] M. Baak, S. Gadatsch, R. Harrington and W. Verkerke, *Interpolation between multi-dimensional histograms using a new non-linear moment morphing method*,
Nucl. Instrum. Meth. A **771** (2015) 39, arXiv: 1410.7388 [physics.data-an].
- [56] NNPDF Collaboration, R. D. Ball et al., *Parton distributions with LHC data*,
Nucl. Phys. B **867** (2013) 244, arXiv: 1207.1303 [hep-ph].
- [57] S. Frixione, G. Ridolfi and P. Nason,
A positive-weight next-to-leading-order Monte Carlo for heavy flavour hadroproduction,
JHEP **09** (2007) 126, arXiv: 0707.3088 [hep-ph].
- [58] P. Nason, *A new method for combining NLO QCD with shower Monte Carlo algorithms*,
JHEP **11** (2004) 040, arXiv: hep-ph/0409146.
- [59] S. Frixione, P. Nason and C. Oleari,
Matching NLO QCD computations with parton shower simulations: the POWHEG method,
JHEP **11** (2007) 070, arXiv: 0709.2092 [hep-ph].
- [60] S. Alioli, P. Nason, C. Oleari and E. Re, *A general framework for implementing NLO calculations in shower Monte Carlo programs: the POWHEG BOX*, *JHEP* **06** (2010) 043,
arXiv: 1002.2581 [hep-ph].
- [61] R. D. Ball et al., *The PDF4LHC21 combination of global PDF fits for the LHC Run III*,
J. Phys. G **49** (2022) 080501, arXiv: 2203.05506 [hep-ph].

- [62] K. Hamilton, P. Nason and G. Zanderighi, *MINLO: multi-scale improved NLO*, [JHEP **10** \(2012\) 155](#), arXiv: [1206.3572 \[hep-ph\]](#).
- [63] J. M. Campbell et al., *NLO Higgs boson production plus one and two jets using the POWHEG BOX, MadGraph4 and MCFM*, [JHEP **07** \(2012\) 092](#), arXiv: [1202.5475 \[hep-ph\]](#).
- [64] K. Hamilton, P. Nason, C. Oleari and G. Zanderighi, *Merging H/W/Z + 0 and 1 jet at NLO with no merging scale: a path to parton shower + NNLO matching*, [JHEP **05** \(2013\) 082](#), arXiv: [1212.4504 \[hep-ph\]](#).
- [65] E. Bothmann et al., *Event generation with Sherpa 2.2*, [SciPost Phys. **7** \(2019\) 034](#), arXiv: [1905.09127 \[hep-ph\]](#).
- [66] T. Gleisberg and S. Höche, *Comix, a new matrix element generator*, [JHEP **12** \(2008\) 039](#), arXiv: [0808.3674 \[hep-ph\]](#).
- [67] F. Buccioni et al., *OpenLoops 2*, [Eur. Phys. J. C **79** \(2019\) 866](#), arXiv: [1907.13071 \[hep-ph\]](#).
- [68] F. Cascioli, P. Maierhöfer and S. Pozzorini, *Scattering Amplitudes with Open Loops*, [Phys. Rev. Lett. **108** \(2012\) 111601](#), arXiv: [1111.5206 \[hep-ph\]](#).
- [69] A. Denner, S. Dittmaier and L. Hofer, *COLLIER: A fortran-based complex one-loop library in extended regularizations*, [Comput. Phys. Commun. **212** \(2017\) 220](#), arXiv: [1604.06792 \[hep-ph\]](#).
- [70] S. Höche, F. Krauss, M. Schönherr and F. Siegert, *A critical appraisal of NLO+PS matching methods*, [JHEP **09** \(2012\) 049](#), arXiv: [1111.1220 \[hep-ph\]](#).
- [71] S. Höche, F. Krauss, M. Schönherr and F. Siegert, *QCD matrix elements + parton showers. The NLO case*, [JHEP **04** \(2013\) 027](#), arXiv: [1207.5030 \[hep-ph\]](#).
- [72] S. Catani, F. Krauss, B. R. Webber and R. Kuhn, *QCD Matrix Elements + Parton Showers*, [JHEP **11** \(2001\) 063](#), arXiv: [hep-ph/0109231](#).
- [73] S. Höche, F. Krauss, S. Schumann and F. Siegert, *QCD matrix elements and truncated showers*, [JHEP **05** \(2009\) 053](#), arXiv: [0903.1219 \[hep-ph\]](#).
- [74] S. Schumann and F. Krauss, *A parton shower algorithm based on Catani–Seymour dipole factorisation*, [JHEP **03** \(2008\) 038](#), arXiv: [0709.1027 \[hep-ph\]](#).
- [75] F. Siegert, *A practical guide to event generation for prompt photon production with Sherpa*, [J. Phys. G **44** \(2017\) 044007](#), arXiv: [1611.07226 \[hep-ph\]](#).
- [76] S. Frixione, *Isolated photons in perturbative QCD*, [Phys. Lett. B **429** \(1998\) 369](#), arXiv: [hep-ph/9801442](#).
- [77] D. J. Lange, *The EvtGen particle decay simulation package*, [Nucl. Instrum. Meth. A **462** \(2001\) 152](#).
- [78] ATLAS Collaboration, *Emulating the impact of additional proton–proton interactions in the ATLAS simulation by presampling sets of inelastic Monte Carlo events*, [Comput. Softw. Big Sci. **6** \(2022\) 3](#), arXiv: [2102.09495 \[hep-ex\]](#).

- [79] K. Werner, F.-M. Liu and T. Pierog, *Parton ladder splitting and the rapidity dependence of transverse momentum spectra in deuteron–gold collisions at the BNL Relativistic Heavy Ion Collider*, *Phys. Rev. C* **74** (2006) 044902, arXiv: [hep-ph/0506232](https://arxiv.org/abs/hep-ph/0506232).
- [80] C. Bierlich et al., *A comprehensive guide to the physics and usage of PYTHIA 8.3*, *SciPost Phys. Codebases* (2022) 8, arXiv: [2203.11601](https://arxiv.org/abs/2203.11601) [[hep-ph](#)].
- [81] T. Pierog, I. Karpenko, J. M. Katzy, E. Yatsenko and K. Werner, *EPOS LHC: Test of collective hadronization with data measured at the CERN Large Hadron Collider*, *Phys. Rev. C* **92** (2015) 034906, arXiv: [1306.0121](https://arxiv.org/abs/1306.0121) [[hep-ph](#)].
- [82] ATLAS Collaboration, *The Pythia 8 A3 tune description of ATLAS minimum bias and inelastic measurements incorporating the Donnachie–Landshoff diffractive model*, ATL-PHYS-PUB-2016-017, 2016, URL: <https://cds.cern.ch/record/2206965>.
- [83] ATLAS Collaboration, *Performance of the ATLAS track reconstruction algorithms in dense environments in LHC Run 2*, *Eur. Phys. J. C* **77** (2017) 673, arXiv: [1704.07983](https://arxiv.org/abs/1704.07983) [[hep-ex](#)].
- [84] ATLAS Collaboration, *Electron reconstruction and identification in the ATLAS experiment using the 2015 and 2016 LHC proton–proton collision data at $\sqrt{s} = 13$ TeV*, *Eur. Phys. J. C* **79** (2019) 639, arXiv: [1902.04655](https://arxiv.org/abs/1902.04655) [[physics.ins-det](#)].
- [85] W. Lampl et al., *Calorimeter Clustering Algorithms: Description and Performance*, ATL-LARG-PUB-2008-002, 2008, URL: <https://cds.cern.ch/record/1099735>.
- [86] ATLAS Collaboration, *Vertex Reconstruction Performance of the ATLAS Detector at $\sqrt{s} = 13$ TeV*, ATL-PHYS-PUB-2015-026, 2015, URL: <https://cds.cern.ch/record/2037717>.
- [87] ATLAS Collaboration, *Topological cell clustering in the ATLAS calorimeters and its performance in LHC Run 1*, *Eur. Phys. J. C* **77** (2017) 490, arXiv: [1603.02934](https://arxiv.org/abs/1603.02934) [[hep-ex](#)].
- [88] ATLAS Collaboration, *Electron and photon energy calibration with the ATLAS detector using LHC Run 2 data*, *JINST* **19** (2024) P02009, arXiv: [2309.05471](https://arxiv.org/abs/2309.05471) [[hep-ex](#)].
- [89] ATLAS Collaboration, *Electron and photon efficiencies in LHC Run 2 with the ATLAS experiment*, *JHEP* **05** (2024) 162, arXiv: [2308.13362](https://arxiv.org/abs/2308.13362) [[hep-ex](#)].
- [90] M. Cacciari, G. P. Salam and G. Soyez, *The anti- k_t jet clustering algorithm*, *JHEP* **04** (2008) 063, arXiv: [0802.1189](https://arxiv.org/abs/0802.1189) [[hep-ph](#)].
- [91] M. Cacciari, G. P. Salam and G. Soyez, *FastJet user manual*, *Eur. Phys. J. C* **72** (2012) 1896, arXiv: [1111.6097](https://arxiv.org/abs/1111.6097) [[hep-ph](#)].
- [92] ATLAS Collaboration, *Jet reconstruction and performance using particle flow with the ATLAS Detector*, *Eur. Phys. J. C* **77** (2017) 466, arXiv: [1703.10485](https://arxiv.org/abs/1703.10485) [[hep-ex](#)].
- [93] ATLAS Collaboration, *Performance of pile-up mitigation techniques for jets in pp collisions at $\sqrt{s} = 8$ TeV using the ATLAS detector*, *Eur. Phys. J. C* **76** (2016) 581, arXiv: [1510.03823](https://arxiv.org/abs/1510.03823) [[hep-ex](#)].
- [94] ATLAS Collaboration, *Forward jet vertex tagging using the particle flow algorithm*, ATL-PHYS-PUB-2019-026, 2019, URL: <https://cds.cern.ch/record/2683100>.

- [95] ATLAS Collaboration, *Jet energy scale and resolution measured in proton–proton collisions at $\sqrt{s} = 13$ TeV with the ATLAS detector*, *Eur. Phys. J. C* **81** (2021) 689, arXiv: [2007.02645 \[hep-ex\]](#).
- [96] ATLAS Collaboration, *In situ calibration of large-radius jet energy and mass in 13 TeV proton–proton collisions with the ATLAS detector*, *Eur. Phys. J. C* **79** (2019) 135, arXiv: [1807.09477 \[hep-ex\]](#).
- [97] ATLAS Collaboration, *Measurement of Higgs boson production in the diphoton decay channel in pp collisions at center-of-mass energies of 7 and 8 TeV with the ATLAS detector*, *Phys. Rev. D* **90** (2014) 112015, arXiv: [1408.7084 \[hep-ex\]](#).
- [98] ATLAS Collaboration, *Performance of electron and photon triggers in ATLAS during LHC Run 2*, *Eur. Phys. J. C* **80** (2020) 47, arXiv: [1909.00761 \[hep-ex\]](#).
- [99] J. R. Andersen, K. Arnold, and D. Zeppenfeld, *Azimuthal Angle Correlations for Higgs Boson plus Multi-Jet Events*, *JHEP* **06** (2010) 091, arXiv: [1001.3822 \[hep-ph\]](#).
- [100] A. Paszke et al., *PyTorch: An Imperative Style, High-Performance Deep Learning Library*, 2019, arXiv: [1912.01703 \[cs.LG\]](#).
- [101] G. Kasieczka, and D. Shih, *Robust Jet Classifiers through Distance Correlation*, *Phys. Rev. Lett.* **125** (2020) 122001, arXiv: [2001.05310 \[hep-ph\]](#).
- [102] D. P. Kingma and J. Ba, *Adam: A method for stochastic optimization*, (2017), arXiv: [1412.6980 \[cs.LG\]](#), URL: <https://arxiv.org/abs/1412.6980>.
- [103] R. T. Q. Chen, Y. Rubanova, J. Bettencourt, and D. Duvenaud, *Neural Ordinary Differential Equations*, (2019), arXiv: [1806.07366 \[cs.LG\]](#).
- [104] C. Daumann, M. Donega, J. Erdmann, M. Galli, J. L. Späh, and D. Valsecchi, *One Flow to Correct Them all: Improving Simulations in High-Energy Physics with a Single Normalising Flow and a Switch*, *Computing and Software for Big Science* **8** (2024) 15, arXiv: [2403.18582 \[hep-ph\]](#).
- [105] I. Loshchilov and F. Hutter, *Decoupled Weight Decay Regularization*, 2019, arXiv: [1711.05101 \[cs.LG\]](#), URL: <https://arxiv.org/abs/1711.05101>.
- [106] J. R. Dormand and P. J. Prince, *A family of embedded Runge-Kutta formulae*, *Journal of Computational and Applied Mathematics* **6** (1980) 19.
- [107] M. Oreglia, *A Study of the Reactions $\psi' \rightarrow \gamma\gamma\psi$* , Appendix D, PhD thesis: Stanford University, 1980, URL: <https://www-public.slac.stanford.edu/sciDoc/docMeta.aspx?slacPubNumber=slac-r-236>.
- [108] ATLAS Collaboration, *Search for Scalar Diphoton Resonances in the Mass Range 65–600 GeV with the ATLAS Detector in pp Collision Data at $\sqrt{s} = 8$ TeV*, *Phys. Rev. Lett.* **113** (2014) 171801, arXiv: [1407.6583 \[hep-ex\]](#).
- [109] ATLAS Collaboration, *Measurements of Higgs boson properties in the diphoton decay channel with 36 fb^{-1} of pp collision data at $\sqrt{s} = 13$ TeV with the ATLAS detector*, *Phys. Rev. D* **98** (2018) 052005, arXiv: [1802.04146 \[hep-ex\]](#).
- [110] ATLAS Collaboration, *Measurement of the isolated diphoton cross section in pp collisions at $\sqrt{s} = 7$ TeV with the ATLAS detector*, *Phys. Rev. D* **85** (2012) 012003, arXiv: [1107.0581 \[hep-ex\]](#).

- [111] S. N. Bernstein, *Démonstration du Théorème de Weierstrass fondée sur le calcul des Probabilités*, Comm. Soc. Math. Kharkov **13** (1912) 1.
- [112] J. S. Conway, ‘Incorporating Nuisance Parameters in Likelihoods for Multisource Spectra’, *PHYSTAT 2011*, 2011 115, arXiv: [1103.0354 \[physics.data-an\]](#).
- [113] ATLAS Collaboration, *Measurement of the Inelastic Proton–Proton Cross Section at $\sqrt{s} = 13$ TeV with the ATLAS Detector at the LHC*, *Phys. Rev. Lett.* **117** (2016) 182002, arXiv: [1606.02625 \[hep-ex\]](#).
- [114] G. Avoni et al., *The new LUCID-2 detector for luminosity measurement and monitoring in ATLAS*, *JINST* **13** (2018) P07017.
- [115] J. Butterworth et al., *PDF4LHC recommendations for LHC Run II*, *J. Phys. G* **43** (2016) 023001, arXiv: [1510.03865 \[hep-ph\]](#).
- [116] ATLAS Collaboration, *Evaluation of QCD uncertainties for Higgs boson production through gluon fusion and in association with two top quarks for simplified template cross-section measurements*, ATL-PHYS-PUB-2023-031, 2023, URL: <https://cds.cern.ch/record/2878797>.
- [117] J. Bellm et al., *Herwig 7.2 release note*, *Eur. Phys. J. C* **80** (2020) 452, arXiv: [1912.06509 \[hep-ph\]](#).
- [118] G. Cowan, K. Cranmer, E. Gross and O. Vitells, *Asymptotic formulae for likelihood-based tests of new physics*, *Eur. Phys. J. C* **71** (2011) 1554, arXiv: [1007.1727 \[physics.data-an\]](#), Erratum: *Eur. Phys. J. C* **73** (2013) 2501.
- [119] ATLAS Collaboration, *ATLAS Computing Acknowledgements*, ATL-SOFT-PUB-2026-001, 2026, URL: <https://cds.cern.ch/record/2952666>.

The ATLAS Collaboration

G. Aad ¹⁰², E. Aakvaag ¹⁷, B. Abbott ¹²¹, S. Abdelhameed ^{83b}, K. Abeling ⁵⁴, N.J. Abicht ⁴⁸, S.H. Abidi ³⁰, M. Aboeela ⁴⁴, A. Abouhorma ^{36e}, H. Abramowicz ¹⁵⁴, B.S. Acharya ^{68a,68b,m}, A. Ackermann ^{62a}, C. Adam Bourdarios ⁴, L. Adamczyk ^{85a}, S.V. Addepalli ¹⁴⁶, M.J. Addison ¹⁰¹, J. Adelman ¹¹⁷, A. Adiguzel ^{22c}, T. Adye ¹³⁵, A.A. Affolder ¹³⁷, Y. Afik ³⁹, M.N. Agaras ¹³, A. Aggarwal ¹⁰⁰, C. Agheorghiesei ^{28c}, A. Ahmad ^{83a}, F. Ahmadov ^{38,ad}, S. Ahuja ⁹⁵, S. Ahuja ¹⁶⁵, X. Ai ^{113c}, G. Aielli ^{75a,75b}, A. Aikot ¹⁶⁵, M. Ait Tamlihat ^{36e}, T.P.A. Åkesson ⁹⁸, D. Akiyama ¹⁷⁰, N.N. Akolkar ²⁵, S. Aktas ¹⁶⁸, G.L. Alberghi ^{24b}, J. Albert ¹⁶⁷, U. Alberti ²⁰, P. Albicocco ⁵², S. Alderweireldt ⁵¹, Z.L. Alegria ¹²², M. Aleksa ³⁷, I.N. Aleksandrov ³⁸, C. Alexa ^{28b}, T. Alexopoulos ¹⁰, F. Alfonsi ^{24b}, M. Algren ⁵⁵, M. Alhroob ¹⁶⁹, B. Ali ¹³³, H.M.J. Ali ^{91,v}, S. Ali ³², S.W. Alibocus ⁹², M. Aliev ^{34c}, G. Alimonti ^{70a}, C. Allaire ⁶⁵, B.M.M. Allbrooke ¹⁴⁹, D.R. Allen ¹²², J.S. Allen ¹⁰¹, J.F. Allen ⁵¹, C.S. Alley ¹, E.R. Almazan ¹³⁷, A. Aloisio ^{71a,71b}, F. Alonso ⁹⁰, C. Alpigiani ¹⁴⁰, A. Alvarez Fernandez ¹⁰⁰, M. Alves Cardoso ⁵⁵, M.G. Alviggi ^{71a,71b}, M. Aly ¹⁰¹, Y. Amaral Coutinho ^{81b}, C. Amelung ³⁷, M. Amerl ¹⁰¹, T. Amezza ¹²⁸, B. Amini ⁵³, K. Amirie ¹⁵⁸, A. Amirkhanov ³⁸, D. Amperiadou ¹⁵⁵, S. An ⁸², C. Anastopoulos ¹⁴², T. Andeen ¹¹, J.K. Anders ⁹², A.C. Anderson ⁵⁸, A. Andreazza ^{70a,70b}, S. Angelidakis ⁹, A. Angerami ⁴¹, A.V. Anisenkov ³⁸, A. Annovi ^{73a}, C. Antel ³⁷, E. Antipov ¹⁴⁸, M. Antonelli ⁵², F. Anulli ^{74a}, M. Aoki ⁸², T. Aoki ¹⁵⁶, M.A. Aparo ¹³, L. Aperio Bella ⁴⁷, M. Apicella ³¹, C. Appelt ¹⁵⁴, A. Apyan ²⁷, M. Arampatzi ¹⁰, S.J. Arbiol Val ⁸⁶, C. Arcangeletti ⁵², A.T.H. Arce ⁵⁰, M. Arcuri ^{43b,43a}, J-F. Arguin ¹⁰⁸, S. Argyropoulos ¹⁵⁵, J.-H. Arling ⁴⁷, O. Arnaez ⁴, H. Arnold ¹⁴⁸, G. Artoni ^{74a,74b}, H. Asada ¹¹¹, S. Asatryan ¹⁷⁵, N.A. Asbah ³⁷, R.A. Ashby Pickering ¹⁶⁹, A.M. Aslam ⁹⁵, J. Assahsah ^{36d}, K. Assamagan ³⁰, R. Astalos ^{29a}, K.S.V. Astrand ⁹⁸, S. Atashi ¹⁶², R.J. Atkin ^{34a}, H. Atmani ^{36f}, P.A. Atmasiddha ¹²⁹, K. Augsten ¹³³, A.D. Auriol ⁴⁰, V.A. Austrup ¹⁰¹, A.S. Avad ⁹⁴, G. Avolio ³⁷, A. Azzam ¹³, D. Babal ^{29b}, H. Bachacou ¹³⁶, K. Bachas ^{155,p}, A. Bachiu ³⁵, E. Bachmann ⁴⁹, M.J. Backes ^{62a}, A. Badea ³⁹, T.M. Baer ¹⁰⁶, M. Bahmani ¹⁹, D. Bahner ⁵³, K. Bai ¹²⁴, L. Baines ⁹⁴, O.K. Baker ¹⁷⁴, D. Bakshi Gupta ⁸, L.E. Balabram Filho ^{81b}, V. Balakrishnan ¹²¹, R. Balasubramanian ⁴, P. Balek ^{85a}, E. Ballabene ^{24b,24a}, F. Balli ¹³⁶, L.M. Baltes ^{62a}, W.K. Balunas ¹²⁷, I. Bamwidhi ^{83c}, E. Banas ⁸⁶, M. Bandieramonte ¹³⁰, A. Bandyopadhyay ²⁵, S. Bansal ²⁵, L. Barak ¹⁵⁴, M. Barakat ⁴⁷, E.L. Barberio ¹⁰⁵, D. Barberis ^{18b}, M. Barbero ¹⁰², M.Z. Barel ¹¹⁶, T. Barillari ¹¹⁰, M-S. Barisits ³⁷, T. Barklow ¹⁴⁶, P. Baron ¹³⁴, D.A. Baron Moreno ¹⁰¹, A. Baroncelli ⁶¹, A.J. Barr ¹²⁷, J.D. Barr ⁹⁶, F. Barreiro ⁹⁹, J. Barreiro Guimarães da Costa ¹⁴, M.G. Barros Teixeira ^{131a}, F. Bartels ^{62a}, R. Bartoldus ¹⁴⁶, A.E. Barton ⁹¹, P. Bartos ^{29a}, M. Baselga ⁴⁸, S. Bashiri ⁸⁶, A. Bassalat ^{65,b}, M.J. Basso ^{159a}, S. Bataju ⁴⁴, R. Bate ¹⁶⁶, R.L. Bates ⁵⁸, S. Batlamous ⁹⁹, M. Battaglia ¹³⁷, D. Battulga ¹⁹, M. Bauce ^{74a,74b}, L. Bauckhage ⁴⁷, P. Bauer ²⁵, L.T. Bayer ⁴⁷, L.T. Bazzano Hurrell ³¹, T. Beau ¹²⁸, J.Y. Beaucamp ⁹⁰, S. Beauceron ¹²⁸, P.H. Beauchemin ¹⁶¹, P. Bechtle ²⁵, H.P. Beck ^{20,o}, K. Becker ¹⁶⁹, A.J. Beddall ⁸⁰, V.A. Bednyakov ³⁸, C.P. Bee ¹⁴⁸, L.J. Beemster ¹⁶, M. Begalli ^{81d}, M. Begel ³⁰, J.K. Behr ⁴⁷, J.F. Beirer ³⁷, F. Beisiegel ²⁵, M. Belfkir ^{83c}, G. Bella ¹⁵⁴, L. Bellagamba ^{24b}, A. Bellerive ³⁵, C.D. Bellgraph ⁶⁷, P. Bellos ²¹, I. Benaoumeur ²¹, D. Bencheikroun ^{36a}, F. Bendebba ^{36a}, Y. Benhammou ¹⁵⁴, K.C. Benkendorfer ¹⁶⁷, L. Beresford ⁴⁷, M. Beretta ⁵², E. Bergeas Kuutmann ¹⁶³, N. Berger ⁴, B. Bergmann ¹³³, J. Beringer ^{18a}, M. Berkat ¹³⁶, G. Bernardi ⁵, C. Bernius ¹⁴⁶, F.U. Bernlochner ²⁵, A. Berrocal Guardia ¹³, T. Berry ⁹⁵, P. Berta ¹³⁴, A. Berti ^{131a},

R. Bertrand [id](#)¹⁰², S. Bethke [id](#)¹¹⁰, A. Betti [id](#)^{74a,74b}, T.F. Beumker [id](#)¹⁷³, A.J. Bevan [id](#)⁹⁴, L. Bezio [id](#)⁵⁵, N.K. Bhalla [id](#)⁵³, S. Bharthuar [id](#)¹¹⁰, S. Bhatta [id](#)¹⁴⁸, P. Bhattacharai [id](#)¹⁴⁶, Z.M. Bhatti [id](#)¹¹⁸, K.D. Bhide [id](#)⁵³, V.S. Bhopatkar [id](#)¹²², R.M. Bianchi [id](#)¹³⁰, G. Bianco [id](#)^{24b,24a}, O. Biebel [id](#)¹⁰⁹, M. Biglietti [id](#)^{76a}, P. Bijl [id](#)⁵³, C.S. Billingsley [id](#)⁴⁴, Y. Bimondi [id](#)^{36f}, M. Bindi [id](#)⁵⁴, A. Bingham [id](#)¹⁷³, A. Bingul [id](#)^{22b}, C. Bini [id](#)^{74a,74b}, G.A. Bird [id](#)³³, M. Biroš [id](#)¹³⁴, S. Biryukov [id](#)¹⁴⁹, T. Bisanz [id](#)⁴⁸, E. Bisceglie [id](#)^{24b,24a}, J.P. Biswal [id](#)¹³⁵, D. Biswas [id](#)¹⁴⁴, M. Biyabi [id](#)¹⁴, I. Bloch [id](#)⁴⁷, A. Blue [id](#)⁵⁸, U. Blumenschein [id](#)⁹⁴, V.S. Bobrovnikov [id](#)³⁸, L. Boccardo [id](#)^{56b,56a}, M. Boehler [id](#)⁵³, B. Boehm [id](#)¹⁶⁸, D. Bogavac [id](#)¹³, L.S. Boggia [id](#)¹²⁸, V. Boisvert [id](#)⁹⁵, P. Bokan [id](#)¹⁶³, T. Bold [id](#)^{85a}, M. Bomben [id](#)⁵, M. Bona [id](#)⁹⁴, M. Boonekamp [id](#)¹³⁶, A.G. Borbély [id](#)⁵⁸, G. Borissov [id](#)⁹¹, A. Borkar [id](#)¹⁶⁸, D. Bortoletto [id](#)¹²⁷, M. Borysova [id](#)¹⁷¹, D. Boscherini [id](#)^{24b}, M. Bosman [id](#)¹³, K. Bouaouda [id](#)^{36a}, L. Boudet [id](#)¹³⁶, J. Boudreau [id](#)¹³⁰, E.V. Bouhova-Thacker [id](#)⁹¹, D. Boumediene [id](#)⁴⁰, R. Bouquet [id](#)^{56b,56a}, A. Boveia [id](#)¹²⁰, D. Boye [id](#)³⁰, I.R. Boyko [id](#)³⁸, L. Bozianu [id](#)⁵⁵, J. Bracink [id](#)²¹, N. Brahimi [id](#)⁴, G. Brandt [id](#)¹⁷³, O. Brandt [id](#)³³, B. Brau [id](#)¹⁰³, R. Brenner [id](#)¹⁷¹, L. Brenner [id](#)¹¹⁶, R. Brenner [id](#)¹⁶³, S. Bressler [id](#)¹⁷¹, M. Brettell [id](#)⁹⁶, G. Brianti [id](#)¹¹⁶, D. Britton [id](#)⁵⁸, D. Britzger [id](#)¹¹⁰, I. Brock [id](#)²⁵, R. Brock [id](#)¹⁰⁷, H. Bronson [id](#)¹²⁹, G. Brooijmans [id](#)⁴¹, A.J. Brooks [id](#)⁶⁷, E.M. Brooks [id](#)^{159b}, E. Brost [id](#)³⁰, L.M. Brown [id](#)^{167,159a}, L.E. Bruce [id](#)⁶⁰, T.L. Bruckler [id](#)¹²⁷, P.A. Bruckman de Renstrom [id](#)⁸⁶, B. Brüers [id](#)⁴⁷, A. Bruni [id](#)^{24b}, G. Bruni [id](#)^{24b}, D. Brunner [id](#)^{46a,46b}, M. Bruschi [id](#)^{24b}, N. Bruscinò [id](#)^{74a,74b}, T. Buanes [id](#)¹⁷, Q. Buat [id](#)¹⁴⁰, D. Buchin [id](#)¹¹⁰, A.G. Buckley [id](#)⁵⁸, J. Bucko [id](#)¹³⁴, M. Bühring [id](#)⁴⁹, O. Bulekov [id](#)⁸⁰, B.A. Bullard [id](#)¹⁴⁶, T.O. Buratovich [id](#)⁹⁰, S. Burdin [id](#)⁹², C.D. Burgard [id](#)⁴⁸, A.M. Burger [id](#)⁸⁹, B. Burghgrave [id](#)⁸, O. Burlayenko [id](#)⁵³, J. Burleson [id](#)¹⁶⁴, J.C. Burzynski [id](#)¹²¹, V. Büscher [id](#)¹⁰⁰, P.J. Bussey [id](#)⁵⁸, O. But [id](#)²⁵, J.M. Butler [id](#)²⁶, C.M. Buttar [id](#)⁵⁸, J.M. Butterworth [id](#)⁹⁶, P. Butti [id](#)³⁷, W. Buttinger [id](#)¹³⁵, C.J. Buxo Vazquez [id](#)¹⁰⁷, A.R. Buzykaev [id](#)³⁸, S. Cabrera Urbán [id](#)¹⁶⁵, L. Cadamuro [id](#)⁶⁵, H. Cai [id](#)³⁷, Y. Cai [id](#)^{24b,112c,24a}, Y. Cai [id](#)^{112a}, M.A. Cairo [id](#)¹²⁹, V.M.M. Cairo [id](#)³⁷, O. Cakir [id](#)^{3a}, N. Calace [id](#)³⁷, P. Calafiura [id](#)^{18a}, G. Calderini [id](#)¹²⁸, P. Calfayan [id](#)³⁵, L. Calic [id](#)⁹⁸, G. Callea [id](#)⁵⁸, L.P. Caloba [id](#)^{81b}, D. Calvet [id](#)⁴⁰, S. Calvet [id](#)⁴⁰, R. Camacho Toro [id](#)¹²⁸, S. Camarda [id](#)³⁷, D. Camarero Munoz [id](#)²⁷, P. Camarri [id](#)^{75a,75b}, C. Camincher [id](#)³⁷, M. Campanelli [id](#)⁹⁶, A. Camplani [id](#)⁴², V. Canale [id](#)^{71a,71b}, A.C. Canbay [id](#)^{3a}, E. Canonero [id](#)⁹⁵, J. Cantero [id](#)¹⁶⁵, F. Capocasa [id](#)²⁷, P. Cappelli [id](#)²⁷, M. Capua [id](#)^{43b,43a}, A. Carbone [id](#)^{70a,70b}, R. Cardarelli [id](#)^{75a}, J.C.J. Cardenas [id](#)⁸, M.P. Cardiff [id](#)²⁷, G. Carducci [id](#)^{43b,43a}, T. Carli [id](#)³⁷, G. Carlino [id](#)^{71a}, J.I. Carlotto [id](#)¹³, B.T. Carlson [id](#)^{130,q}, E.M. Carlson [id](#)¹⁶⁷, L. Carminati [id](#)^{70a,70b}, A. Carnelli [id](#)⁴, M. Carnesale [id](#)³⁷, S. Caron [id](#)¹¹⁵, E. Carquin [id](#)^{138g}, I.B. Carr [id](#)¹⁰⁵, S. Carrá [id](#)^{72a,72b}, G. Carratta [id](#)^{24b,24a}, C. Carrion Martinez [id](#)¹⁶⁵, A.M. Carroll [id](#)¹²⁴, N. Cartalade [id](#)⁴⁰, M.P. Casado [id](#)^{13,h}, P. Casolaro [id](#)^{71a,71b}, M. Caspar [id](#)⁴⁷, F. Cassinese [id](#)⁹⁰, W.R. Castiglioni [id](#)³⁹, F.L. Castillo [id](#)⁴, V. Castillo Gimenez [id](#)¹⁶⁵, N.F. Castro [id](#)^{131a,131e}, A. Catinaccio [id](#)³⁷, J.R. Catmore [id](#)¹²⁶, T. Cavaliere [id](#)⁴, V. Cavaliere [id](#)³⁰, E. Celebi [id](#)⁸⁰, S. Cella [id](#)³⁰, V. Cepaitis [id](#)⁵⁵, K. Cerny [id](#)¹²³, A.S. Cerqueira [id](#)^{81a}, A. Cerri [id](#)^{73a,ap}, L. Cerrito [id](#)^{75a,75b}, F. Cerutti [id](#)^{18a}, B. Cervato [id](#)^{70a,70b}, A. Cervelli [id](#)^{24b}, G. Cesarini [id](#)⁵², S.A. Cetin [id](#)⁸⁰, V.C. Chabalala [id](#)^{34j}, P.M. Chabrilat [id](#)¹²⁸, R. Chakkappai [id](#)⁶⁵, S. Chakraborty [id](#)¹⁶⁹, A. Chambers [id](#)⁶⁰, J. Chan [id](#)^{18a}, J.D. Chapman [id](#)³³, E. Chapon [id](#)¹³⁶, D.G. Charlton [id](#)²¹, C. Chauhan [id](#)¹³², Y. Che [id](#)^{112a}, S. Chekanov [id](#)⁶, G.A. Chelkov [id](#)^{38,a}, H. Chen [id](#)³⁰, J. Chen [id](#)^{141a}, J. Chen [id](#)¹⁴⁵, M. Chen [id](#)⁵⁹, S. Chen [id](#)⁸⁷, S.J. Chen [id](#)^{112a}, X. Chen [id](#)^{141a}, X. Chen [id](#)^{15,ai}, Z. Chen [id](#)⁶¹, C.L. Cheng [id](#)¹⁷², H.C. Cheng [id](#)^{63a}, S. Cheong [id](#)¹⁴⁶, A. Cheplakov [id](#)³⁸, E. Cherepanova [id](#)¹¹⁶, E. Cheu [id](#)⁷, K. Cheung [id](#)⁶⁴, L. Chevalier [id](#)¹³⁶, G. Chiarelli [id](#)^{73a}, G. Chiodini [id](#)^{69a}, A.S. Chisholm [id](#)²¹, J.L. Chisholm [id](#)¹⁶⁶, A. Chitan [id](#)^{28b}, M. Chitishvili [id](#)¹⁶⁵, M.V. Chizhov [id](#)^{38,r}, K. Choi [id](#)¹¹, Y. Chou [id](#)¹⁴⁰, E.Y.S. Chow [id](#)¹¹⁵, G. Christou [id](#)⁵¹, K.L. Chu [id](#)¹⁷¹, M.C. Chu [id](#)^{63a}, Z. Chubinidze [id](#)⁵², J. Chudoba [id](#)¹³², J.J. Chwastowski [id](#)⁸⁶, D. Cieri [id](#)¹¹⁰, K.M. Ciesla [id](#)^{85a}, V. Cindro [id](#)⁹³, A. Ciocio [id](#)^{18a}, F. Ciotto [id](#)^{71a,71b}, Z.H. Citron [id](#)¹⁷¹, M. Citterio [id](#)^{70a}, D.A. Ciubotaru [id](#)^{28b}, A. Clark [id](#)⁵⁵, P.J. Clark [id](#)⁵¹, N. Clarke Hall [id](#)⁹⁶, C. Clarry [id](#)¹⁵⁸, S.E. Clawson [id](#)⁴⁷, C. Clement [id](#)^{46a,46b}, L. Clissa [id](#)^{24b,24a}, Y. Coadou [id](#)¹⁰², M. Cobal [id](#)^{68a,68c},

A. Coccaro ^{56b}, M.G. Cochran Branson ¹⁴⁰, R.F. Coelho Barrue ^{131a}, R. Coelho Lopes De Sa ¹⁰³,
 S. Coelli ^{70a}, M.M. Cohen ¹²⁹, L.S. Colangeli ¹⁵⁸, B. Cole ⁴¹, P. Collado Soto ⁹⁹, J. Collot ⁵⁹,
 M.R. Coluccia ^{69a}, I. Combes ⁶⁵, P. Conde Muiño ^{131a,131g}, L.H.J. Condren ¹⁶², M.P. Connell ^{34c},
 S.H. Connell ^{34c}, E.I. Conroy ¹²⁷, M. Contreras Cossio ¹¹, F. Conventi ^{71a,ak},
 A.M. Cooper-Sarkar ¹²⁷, L. Corazzina ^{74a,74b}, F.A. Corchia ^{24b,24a}, A. Cordeiro Oudot Choi ¹⁴⁰,
 L.D. Corpe ⁴⁰, M. Corradi ^{74a,74b}, F. Corriveau ^{104,ab}, A. Cortes-Gonzalez ¹⁵⁶, M.J. Costa ¹⁶⁵,
 F. Costanza ⁴, D. Costanzo ¹⁴², J. Couthures ⁴, G. Cowan ⁹⁵, K. Cranmer ¹⁷², L. Cremer ⁴⁸,
 D. Cremonini ^{24b,24a}, S. Crépe-Renaudin ⁵⁹, F. Crescioli ¹²⁸, T. Cresta ^{72a,72b}, M. Cristinziani ¹⁴⁴,
 M. Cristoforetti ^{77a,77b}, T.M. Critchley ⁵⁵, E. Critelli ⁹⁶, A. Cueto ⁹⁹, H. Cui ⁹⁶, Z. Cui ⁷,
 B.M. Cunnett ¹⁴⁹, W.R. Cunningham ⁵⁸, E. Cuppini ¹¹⁰, F. Curcio ¹⁶⁵, J.R. Curran ⁵¹,
 M.J. Da Cunha Sargedas De Sousa ^{56b,56a}, J.V. Da Fonseca Pinto ^{81b}, C. Da Via ¹⁰¹,
 W. Dabrowski ^{85a}, T. Dado ³⁷, S. Dahbi ¹⁵¹, T. Dai ¹⁰⁶, D. Dal Santo ²⁰, C. Dallapiccola ¹⁰³,
 M. Dam ⁴², G. D'amen ³⁰, V. D'Amico ¹⁰⁹, J.R. Dandoy ³⁵, M. D'Andrea ^{56b,56a},
 D. Dannheim ³⁷, G. D'anniballe ^{73a,73b}, M. Danninger ¹⁴⁵, V. Dao ¹⁴⁸, G. Darbo ^{56b},
 F. Dattola ⁴⁷, S. D'Auria ^{70a,70b}, A. D'Avanzo ^{71a,71b}, T. Davidek ¹³⁴, J. Davidson ¹⁶⁹,
 I. Dawson ⁹⁴, K. De ⁸, C. De Almeida Rossi ¹⁵⁸, N. De Biase ⁴⁷, S. De Castro ^{24b,24a},
 N. De Groot ¹¹⁵, P. de Jong ¹¹⁶, H. De la Torre ¹¹⁷, A. De Maria ^{112a}, S. De Miranda Rimes ^{81d},
 A. De Salvo ^{74a}, U. De Sanctis ^{75a,75b}, F. De Santis ^{69a,69b}, A. De Santo ¹⁴⁹,
 J.B. De Vivie De Regie ⁵⁹, K.G. De Vries ¹¹⁶, J. Debevc ⁹³, D.V. Dedovich ³⁸, J. Degens ⁹²,
 A.M. Deiana ⁴⁴, J. Del Peso ⁹⁹, L. Delagrangé ²⁷, F. Deliot ¹³⁶, C.M. Delitzsch ⁴⁸,
 M. Della Pietra ^{71a,71b}, D. Della Volpe ⁵⁵, A. Dell'Acqua ³⁷, L. Dell'Asta ^{70a,70b}, M. Delmastro ⁴,
 C.C. Delogu ^{56b,56a}, P.A. Delsart ⁵⁹, S. Demers ¹⁷⁴, M. Demichev ³⁸, H. Denizli ^{22a,1},
 M.G. Depala ⁹², L. D'Eramo ⁴⁰, D. Derendarz ⁸⁶, L. Derin ^{56b,56a}, F. Derue ¹²⁸, P. Dervan ^{92,*},
 A.M. Desai ¹, K. Desch ²⁵, F.A. Di Bello ^{73a,73b}, A. Di Ciaccio ^{75a,75b}, L. Di Ciaccio ⁴,
 D. Di Croce ³⁷, C. Di Donato ^{71a,71b}, A. Di Girolamo ³⁷, G. Di Gregorio ⁶⁵, A. Di Luca ^{77a,77b},
 B. Di Micco ^{76a,76b}, R. Di Nardo ^{76a,76b}, K.F. Di Petrillo ³⁹, M. Diamantopoulou ³⁵, F.A. Dias ¹¹⁶,
 M.A. Diaz ^{138a,138b}, A.R. Didenko ³⁸, M. Didenko ¹⁶⁵, S.D. Diefenbacher ^{18a}, E.B. Diehl ¹⁰⁶,
 S. Díez Cornell ⁴⁷, C. Diez Pardos ¹⁴⁴, C. Dimitriadi ¹⁴⁷, A. Dimitrievska ²¹, A. Dimri ¹⁴⁸,
 Y. Ding ⁶¹, J. Dingfelder ²⁵, T. Dingley ¹²⁷, I-M. Dinu ^{28b}, S.J. Dittmeier ^{62b}, F. Dittus ³⁷,
 M. Divisek ¹³⁴, B. Dixit ⁹², F. Djama ¹⁰², T. Djobava ^{152b}, C. Doglioni ^{101,98}, A. Dohnalova ^{29a},
 Z. Dolezal ¹³⁴, K. Domijan ^{85a}, K.M. Dona ³⁹, M. Donadelli ^{81d}, B. Dong ¹⁰⁷, J. Donini ⁴⁰,
 A. D'Onofrio ^{71a,71b}, M. D'Onofrio ⁹², J. Dopke ¹³⁵, A. Doria ^{71a}, N. Dos Santos Fernandes ^{131a},
 I.A. Dos Santos Luz ^{81e}, P. Dougan ⁴⁴, M.T. Dova ⁹⁰, A.T. Doyle ⁵⁸, M.P. Drescher ⁵⁴,
 E. Dreyer ¹⁷¹, I. Drivas-koulouris ¹⁰, M. Drnevich ¹¹⁸, D. Du ⁶¹, T. Du ³⁹, T.A. du Pree ¹¹⁶,
 Z. Duan ^{112a}, M. Dubau ⁴, F. Dubinin ³⁸, M. Dubovsky ^{29a}, E. Duchovni ¹⁷¹, G. Duckeck ¹⁰⁹,
 P.K. Duckett ⁹⁶, O.A. Ducu ^{28b}, D. Duda ⁵¹, A. Dudarev ³⁷, M.M. Dudek ⁸⁶, E.R. Duden ²⁷,
 M. D'uffizi ¹⁰¹, L. Duflost ⁶⁵, M. Dührssen ³⁷, I. Duminica ^{28g}, A.E. Dumitriu ^{28b},
 M. Dunford ^{62a}, T. Duong ⁴, A. Duperrin ¹⁰², A.F. Duque Bran ⁴⁰, H. Duran Yildiz ^{3a},
 A. Durglishvili ^{152b}, G.I. Dyckes ^{18a}, M. Dyndal ^{85a}, B.S. Dziedzic ³⁷, G.H. Eberwein ¹²⁷,
 B. Eckerova ^{29a}, J.C. Egan ⁹⁶, S. Eggebrecht ⁵⁴, E. Egidio Purcino De Souza ^{81e}, G. Eigen ¹⁷,
 K. Einsweiler ^{18a}, T. Ekelof ¹⁶³, P.A. Ekman ⁹⁸, S. El Farkh ^{36b}, Y. El Ghazali ⁶¹,
 H. El Jarrari ¹⁰⁴, A. El Moussaouy ^{36a}, I. Elbaz ¹⁵⁴, D. Elitez ³⁷, M. Ellert ¹⁶³,
 F. Ellinghaus ¹⁷³, T.A. Elliot ⁹⁵, J. Elmsheuser ³⁰, M. Elsayy ^{83b}, M. Elsing ³⁷,
 D. Emelianov ¹³⁵, Y. Enari ⁸², S. Epari ¹⁰⁸, D. Ernani Martins Neto ⁸⁶, F. Ernst ³⁷,
 M. Escalier ⁶⁵, C. Escobar ¹⁶⁵, R. Estevam De Paula ^{81c}, E. Etzion ¹⁵⁴, G. Evans ^{131a,131b},
 H. Evans ⁶⁷, L.S. Evans ⁴⁷, S. Ezzarqtouni ^{36a}, F. Fabbri ^{24b,24a}, L. Fabbri ^{24b,24a}, G. Facini ⁹⁶,
 V. Fadeyev ¹³⁷, D. Fakoudis ¹⁰⁰, S. Falciano ^{74a}, L.F. Falda Ulhoa Coelho ²⁷, F. Fallavollita ¹¹⁰,

G. Falsetti ^{43b,43a}, J. Faltova ¹³⁴, C. Fan ¹⁶⁴, K.Y. Fan ^{63b}, Y. Fan ¹⁴, Y. Fang ^{14,112c}, M. Fanti ^{70a,70b}, M. Faraj ^{68a,68c}, Z. Farazpay ⁹⁷, A. Farbin ⁸, A. Farilla ^{76a}, K. Farman ¹⁵¹, J.N. Farr ¹⁷⁴, M.S. Farrington ⁶⁰, S.M. Farrington ^{135,51}, F. Fassi ^{36e}, D. Fassouliotis ⁹, L. Fayard ⁶⁵, G. Fazzino ^{62b}, P. Federic ¹³⁴, P. Federicova ¹³², M. Feickert ¹⁷², L. Feligioni ¹⁰², D.E. Fellers ^{18a}, C. Feng ^{113b}, Y. Feng ¹⁴, Z. Feng ⁶⁵, B. Fernandez Barbadillo ⁹¹, P. Fernandez Martinez ⁶⁶, C. Fernandez Ruiz ³³, J. Ferrando ⁹¹, A. Ferrari ¹⁶³, P. Ferrari ^{116,115}, R. Ferrari ^{72a}, D. Ferrere ⁵⁵, C. Ferretti ¹⁰⁶, M.P. Fewell ¹, D. Fiacco ^{74a,74b}, F. Fiedler ¹⁰⁰, P. Fiedler ¹³³, S. Filimonov ³⁸, M.S. Filip ^{28b,s}, A. Filipčič ⁹³, E.K. Filmer ^{159a}, F. Filthaut ¹¹⁵, M.C.N. Fiolhais ^{131a,131c,c}, L. Fiorini ¹⁶⁵, W.C. Fisher ¹⁰⁷, T. Fitschen ¹⁰¹, I. Fleck ¹⁴⁴, P. Fleischmann ¹⁰⁶, T. Flick ¹⁷³, M. Flores ^{34d,ag}, L.R. Flores Castillo ^{63a}, M. Foll ¹²⁶, F.M. Follega ^{77a,77b}, N. Fomin ³³, J.H. Foo ¹⁵⁸, A. Formica ¹³⁶, M. Fornasiero ¹⁴⁹, A.C. Forti ¹⁰¹, N. Forti ^{24b,24a}, E. Fortin ¹⁰², A.W. Fortman ^{18a}, L. Foster ^{18a}, L. Fountas ⁹, H. Fox ⁹¹, P. Francavilla ^{73a,73b}, S. Francescato ⁶⁰, S. Franchellucci ²⁰, M. Franchini ^{24b,24a}, S. Franchino ^{62a}, D. Francis ³⁷, L. Franco ⁴⁷, L. Franconi ⁴⁷, M. Franklin ⁶⁰, G. Frattari ³⁷, Y.Y. Frid ¹⁵⁴, N. Fritzsche ³⁷, A. Froch ⁵⁵, D. Froidevaux ³⁷, J.A. Frost ¹³⁵, Y. Fu ¹⁰⁷, S. Fuenzalida Garrido ^{138g}, Y.C. Fujikake ¹³⁷, M. Fujimoto ¹⁴⁸, K.Y. Fung ^{63a}, E. Furtado De Simas Filho ^{81e}, M. Furukawa ¹⁵⁶, M. Fuste Costa ⁴⁷, P. Fuste Martin ¹³, J. Fuster ¹⁶⁵, A. Gaa ⁵⁴, A. Gabrielli ^{24b,24a}, A. Gabrielli ¹⁵⁸, G. Gagliardi ^{56b,56a}, L.G. Gagnon ^{18a}, S. Galantzan ¹⁵⁴, J. Gallagher ¹, E.J. Gallas ¹²⁷, A.L. Gallen ¹⁶³, B.J. Gallop ¹³⁵, K.K. Gan ¹²⁰, Y. Gao ⁵¹, Z. Gao ^{112a}, A. Garabaglu ¹⁴⁰, F.M. Garay Walls ^{138a,138b}, C. García ¹⁶⁵, A. Garcia Alonso ¹¹⁶, A.G. Garcia Caffaro ¹⁷⁴, J.E. García Navarro ¹⁶⁵, M.A. Garcia Ruiz ^{23b}, M. Garcia-Sciveres ^{18a}, G.L. Gardner ¹²⁹, R.W. Gardner ³⁹, N. Garelli ¹⁶¹, R.B. Garg ¹⁴⁶, J.M. Gargan ³³, C.A. Garner ¹⁵⁸, C.M. Garvey ^{34a}, V.K. Gassmann ¹⁶¹, G. Gaudio ^{72a}, A.J. Gavin ⁹⁴, J. Gavranovic ⁹³, I.L. Gavrilenko ^{131a}, C. Gay ¹⁶⁶, G. Gaycken ¹²⁴, A. Gekow ¹²⁰, C. Gemme ^{56b}, M.H. Genest ⁵⁹, A.D. Gentry ¹¹⁴, S. George ⁹⁵, T. Geralis ⁴⁵, A.A. Gerwin ¹²¹, P. Gessinger-Befurt ³⁷, M. Ghani ¹⁶⁹, K. Ghorbanian ⁹⁴, A. Ghosal ¹⁴⁴, A. Ghosh ¹⁶², A. Ghosh ⁷, B. Giacobbe ^{24b}, S. Giagu ^{74a,74b}, A. Giannini ⁶¹, S.M. Gibson ⁹⁵, D.T. Gil ^{85b}, B.J. Gilbert ⁴¹, D. Gillberg ³⁵, G. Gilles ¹¹⁶, D.M. Gingrich ^{2,aj}, M.P. Giordani ^{68a,68c}, P.F. Giraud ¹³⁶, G. Giugliarelli ^{68a,68c}, D. Giugni ^{70a}, F. Giuli ^{75a,75b,al}, I. Gkialas ^{9,i}, B.C. Gladwyn ¹²⁷, C. Glasman ⁹⁹, M. Glazewska ²⁰, R.M. Gleason ¹⁶², G. Glemža ⁴⁷, I. Gnesi ^{24b,24a,am}, Y. Go ³⁰, M. Goblirsch-Kolb ³⁷, B. Gocke ⁴⁸, D. Godin ¹⁰⁸, B. Gokturk ^{22a}, S. Goldfarb ¹⁰⁵, T. Golling ⁵⁵, M.G.D. Gololo ^{34c}, A. Golub ¹⁴⁰, J.P. Gombas ¹⁰⁷, A. Gomes ^{131a,131b}, G. Gomes Da Silva ¹⁴⁴, A.J. Gomez Delegido ³⁷, R. Gonçalo ^{131a}, A. Gongadze ^{152c}, F. Gonnella ²¹, J.L. Gonski ¹⁴⁶, R.Y. González Andana ⁵¹, S. González de la Hoz ¹⁶⁵, M.V. Gonzalez Rodrigues ⁴⁷, R. Gonzalez Suarez ¹⁶³, S. Gonzalez-Sevilla ⁵⁵, L. Goossens ³⁷, B. Gorini ³⁷, E. Gorini ^{69a,69b}, A. Gorišek ⁹³, T.C. Gosart ¹²⁹, A.T. Goshaw ⁵⁰, M.I. Gostkin ³⁸, S. Goswami ¹²², C.A. Gottardo ³⁷, S.A. Gotz ¹⁰⁹, M. Goughri ^{36b}, A.G. Goussiou ¹⁴⁰, N. Govender ^{34c}, R.P. Grabarczyk ¹²⁷, I. Grabowska-Bold ^{85a}, K. Graham ³⁵, E. Gramstad ¹²⁶, S. Grancagnolo ^{69a,69b}, C.M. Grant ¹, P.M. Gravila ^{28f}, F.G. Gravili ^{69a,69b}, H.M. Gray ^{18a}, M. Greco ¹¹⁰, M.J. Green ¹, C. Grefe ²⁵, A.S. Grefsrud ¹⁷, I.M. Gregor ⁴⁷, K.T. Greif ¹⁶², P. Grenier ¹⁴⁶, S.G. Grewe ¹¹⁰, K. Grimm ³², S. Grinstein ^{13,x}, E. Gross ¹⁷¹, J. Grosse-Knetter ⁵⁴, L.H. Grossman ^{18b}, L. Guan ¹⁰⁶, G. Guerrieri ³⁷, R. Guevara ¹²⁶, R. Gugel ¹⁰⁰, J.A.M. Guhit ¹⁰⁶, A. Guida ¹⁹, E. Guilloton ¹⁶⁹, S. Guindon ³⁷, F. Guo ^{14,112c}, J. Guo ^{141a}, L. Guo ⁴⁷, L. Guo ^{112b,u}, Y. Guo ¹⁰⁶, Y. Guo ⁴¹, A. Gupta ⁴⁸, R. Gupta ¹³⁰, S. Gupta ²⁷, S. Gurbuz ²⁵, S.S. Gurdasani ⁴⁷, G. Gustavino ^{74a,74b}, P. Gutierrez ¹²¹, L.F. Gutierrez Zagazeta ¹²⁹, M. Gutsche ⁴⁹, C. Gutschow ⁹⁶, W. Guérin ⁸⁹, C. Gwenlan ¹²⁷,

C.B. Gwilliam [id⁹²](#), E.S. Haaland [id¹²⁶](#), A. Haas [id¹¹⁸](#), M. Habedank [id⁵⁸](#), C. Haber [id^{18a}](#),
 R.J. Haberle [id¹⁷¹](#), H.K. Hadavand [id⁸](#), A. Haddad [id⁴⁰](#), A. Hadeef [id⁴⁹](#), A.I. Hagan [id⁹¹](#), J.J. Hahn [id¹⁴⁴](#),
 M. Haleem [id¹⁶⁸](#), J. Haley [id¹²²](#), G.D. Hallewell [id¹⁰²](#), J.A. Hallford [id⁴⁷](#), K. Hamano [id¹⁶⁷](#),
 H. Hamdaoui [id¹⁶³](#), M. Hamer [id²⁵](#), S.E.D. Hammoud [id⁶⁵](#), E.J. Hampshire [id⁹⁵](#), L. Han [id^{112a}](#),
 L. Han [id⁶¹](#), S. Han [id¹⁴](#), K. Hanagaki [id⁸²](#), M. Hance [id¹³⁷](#), D.A. Hangal [id⁴¹](#), H. Hanif [id¹⁴⁵](#),
 M.D. Hank [id¹²⁹](#), J.B. Hansen [id⁴²](#), P.H. Hansen [id⁴²](#), T. Harenberg [id¹⁷³](#), S. Harkusha [id¹⁷⁵](#),
 M.L. Harris [id¹⁰³](#), Y.T. Harris [id²⁵](#), J. Harrison [id¹³](#), P.F. Harrison [id¹⁶⁹](#), M.L.E. Hart [id⁹⁶](#),
 N.M. Hartman [id¹¹⁰](#), N.M. Hartmann [id¹⁰⁹](#), R.Z. Hasan [id^{95,135}](#), Y. Hasegawa [id¹⁴³](#), D. Hashimoto [id¹¹¹](#),
 F. Haslbeck [id³⁷](#), S. Hassan [id¹²⁶](#), R. Hauser [id¹⁰⁷](#), M. Haviernik [id¹³⁴](#), C.M. Hawkes [id²¹](#),
 R.J. Hawkins [id³⁷](#), Y. Hayashi [id¹⁵⁶](#), D. Hayden [id¹⁰⁷](#), R.L. Hayes [id¹¹⁶](#), C.P. Hays [id¹²⁷](#), J.M. Hays [id⁹⁴](#),
 H.S. Hayward [id⁹²](#), M. He [id^{14,112c}](#), Y. He [id⁴⁷](#), Y. He [id⁹⁶](#), N.B. Heatley [id⁹⁴](#), V. Hedberg [id⁹⁸](#),
 J. Heilmann [id³⁵](#), S. Heim [id⁴⁷](#), T. Heim [id^{18a}](#), J.J. Heinrich [id¹²⁴](#), L. Heinrich [id¹¹⁰](#), J. Hejbal [id¹³²](#),
 M. Helbig [id⁴⁹](#), A. Held [id¹⁷²](#), S. Hellesund [id¹⁷](#), C.M. Helling [id¹⁶⁶](#), F.N.E. Henry [id⁵⁸](#), H. Herde [id⁹⁸](#),
 Y. Hernández Jiménez [id¹⁴⁸](#), G. Herten [id⁵³](#), R. Hertenberger [id¹⁰⁹](#), L. Hervas [id³⁷](#), M.E. Hespings [id¹⁰⁰](#),
 N.P. Hesse [id^{159a}](#), J. Hessler [id¹¹⁰](#), R. Hicks [id¹²⁹](#), M. Hidaoui [id^{36b}](#), N. Hidic [id¹³⁴](#), E. Hill [id¹⁵⁸](#),
 T.S. Hillersoy [id¹⁷](#), S.J. Hillier [id²¹](#), J.R. Hinds [id¹⁰⁷](#), F. Hinterkeuser [id²⁵](#), M. Hirose [id¹²⁵](#), S. Hirose [id¹⁶⁰](#),
 D. Hirschbuehl [id¹⁷³](#), B. Hiti [id⁹³](#), J. Hobbs [id¹⁴⁸](#), R. Hobincu [id^{28e}](#), N. Hod [id¹⁷¹](#), A.M. Hodges [id¹⁶⁴](#),
 M.C. Hodgkinson [id¹⁴²](#), B.H. Hodgkinson [id¹²⁷](#), A. Hoecker [id³⁷](#), D.D. Hofer [id¹⁰⁶](#), J. Hofer [id¹⁶⁵](#),
 J. Hofner [id¹⁰⁰](#), M. Holzbock [id³⁷](#), L.B.A.H. Hommels [id³³](#), V. Homsak [id¹²⁷](#), J.J. Hong [id⁶⁷](#),
 T.M. Hong [id¹³⁰](#), B.H. Hooberman [id¹⁶⁴](#), W.H. Hopkins [id⁶](#), M.C. Hoppesch [id¹⁶⁴](#), Y. Horii [id¹¹¹](#),
 M.E. Horstmann [id¹¹⁰](#), M.M. Horzela [id⁵⁴](#), S. Hou [id¹⁵¹](#), M.R. Housenga [id¹⁶⁴](#), J. Howarth [id⁵⁸](#),
 J. Hoya [id⁶](#), M. Hrabovsky [id¹²³](#), T. Hryn'ova [id⁴](#), P.J. Hsu [id⁶⁴](#), S.-C. Hsu [id¹⁴⁰](#), T. Hsu [id⁶⁵](#), M. Hu [id^{18a}](#),
 P. Hu [id^{63b}](#), Q. Hu [id⁶¹](#), S. Huang [id³³](#), X. Huang [id^{14,112c}](#), Y. Huang [id¹³⁴](#), Y. Huang [id^{112b}](#), Y. Huang [id¹⁴](#),
 Z. Huang [id⁶⁵](#), Z. Hubacek [id¹³³](#), F. Huegging [id²⁵](#), T.B. Huffman [id¹²⁷](#),
 M. Hufnagel Maranha De Faria [id^{81a}](#), C.A. Hugli [id⁴⁷](#), M. Huhtinen [id³⁷](#), S.K. Huiberts [id¹⁷](#),
 R. Hulsken [id¹⁰⁴](#), C.E. Hultquist [id^{18a}](#), D.L. Humphreys [id¹⁰³](#), N. Huseynov [id¹²](#), J. Huston [id¹⁰⁷](#),
 B. Huth [id³⁷](#), J. Huth [id⁶⁰](#), L. Huth [id⁴⁷](#), R. Hyneman [id⁷](#), G. Iacobucci [id⁵⁵](#), G. Iakovidis [id³⁰](#),
 L. Iconomidou-Fayard [id⁶⁵](#), J.P. Iddon [id³⁷](#), P. Iengo [id^{71a,71b}](#), Y. Iiyama [id¹⁵⁶](#), T. Iizawa [id¹⁵⁶](#),
 Y. Ikegami [id⁸²](#), D. Iliadis [id¹⁵⁵](#), N. Ilic [id¹⁵⁸](#), H. Imam [id^{36a}](#), G. Inacio Goncalves [id^{81d}](#),
 S.A. Infante Cabanas [id^{138c}](#), T. Ingebretsen Carlson [id^{46a,46b}](#), J.M. Inglis [id⁹⁴](#), G. Introzzi [id^{72a,72b}](#),
 M. Iodice [id^{76a}](#), V. Ippolito [id^{74a,74b}](#), R.K. Irwin [id⁹²](#), M. Ishino [id¹⁵⁶](#), W. Islam [id¹⁷²](#), C. Issever [id¹⁹](#),
 S. Istin [id^{22a,ar}](#), K. Itabashi [id¹²⁵](#), H. Ito [id¹⁷⁰](#), R. Iuppa [id^{77a,77b}](#), A. Ivina [id¹⁷¹](#), F. Ivone [id³⁷](#),
 S. Izumiyama [id¹¹¹](#), V. Izzo [id^{71a}](#), P. Jacka [id¹³³](#), P. Jackson [id¹](#), P.R. Jacobson [id⁵⁰](#), P. Jain [id⁴⁷](#),
 K. Jakobs [id⁵³](#), J. Jamieson [id⁵⁸](#), W. Jang [id¹⁵⁶](#), S. Jankovych [id¹¹⁶](#), B.K. Jashal [id¹³⁵](#), M. Javurkova [id¹⁰³](#),
 P. Jawahar [id¹⁰¹](#), L. Jeanty [id¹²⁴](#), J. Jejelava [id^{152a,ae}](#), P. Jenni [id^{53,f}](#), L. Jerala [id⁹³](#), C.E. Jessiman [id³⁵](#),
 H. Jia [id¹⁶⁶](#), J. Jia [id¹⁴⁸](#), X. Jia [id^{110,112c}](#), C. Jiang [id⁵¹](#), Q. Jiang [id^{63b}](#), S. Jiggins [id⁴⁷](#),
 M. Jimenez Ortega [id¹⁶⁵](#), J. Jimenez Pena [id¹³](#), S. Jin [id^{112a}](#), A. Jinaru [id^{28b}](#), O. Jinnouchi [id¹³⁹](#),
 P. Johansson [id¹⁴²](#), K.A. Johns [id⁷](#), J.W. Johnson [id¹³⁷](#), F.A. Jolly [id⁴⁷](#), D.M. Jones [id¹⁴⁹](#), E. Jones [id⁴⁷](#),
 K.S. Jones [id⁸](#), P. Jones [id³³](#), R.W.L. Jones [id⁹¹](#), T.J. Jones [id⁹²](#), H.L. Joos [id³⁷](#), R. Joshi [id¹²⁰](#),
 J. Jovicevic [id¹⁶](#), X. Ju [id^{18a}](#), J.J. Junggeburth [id³⁷](#), T. Junkermann [id^{62a}](#), A. Juste Rozas [id^{13,x}](#),
 M.K. Juzek [id⁸⁶](#), S. Kabana [id^{138f}](#), A. Kaczmarek [id⁸⁶](#), S.A. Kadir [id¹⁴⁶](#), M. Kado [id¹¹⁰](#), H. Kagan [id¹²⁰](#),
 M. Kagan [id¹⁴⁶](#), A. Kahn [id¹²⁹](#), C. Kahra [id¹⁰⁰](#), T. Kaji [id¹⁵⁶](#), E. Kajomovitz [id¹⁵³](#), N. Kakati [id¹⁷¹](#),
 N. Kakoty [id¹³](#), S. Kandel [id⁸](#), E. Kanellaki [id⁴⁵](#), N. Kanellos [id¹⁰](#), D. Kar [id^{34j,*}](#), E. Karentzos [id²⁵](#),
 K. Karki [id⁸](#), O. Karkout [id¹¹⁶](#), S.N. Karpov [id³⁸](#), Z.M. Karpova [id³⁸](#), V. Kartvelishvili [id^{91,152b}](#),
 E. Kasimi [id¹⁵⁵](#), J. Katzy [id⁴⁷](#), S. Kaur [id³⁵](#), R. Kavak [id¹⁶⁴](#), K. Kawade [id¹⁴³](#), M.P. Kawale [id¹²¹](#),
 C. Kawamoto [id⁸⁷](#), E.F. Kay [id³⁷](#), S. Kazakos [id¹⁰⁷](#), K. Kazakova [id¹⁰²](#), J.M. Keaveney [id^{34a}](#),
 R. Keeler [id¹⁶⁷](#), G.V. Kehris [id⁶⁰](#), J.S. Keller [id³⁵](#), J.M. Kelly [id¹⁶⁷](#), J.J. Kempster [id¹⁴⁹](#), O. Kepka [id¹³²](#),

J. Kerr [id^{159b}](#), B.P. Kerridge [id¹³⁵](#), B.P. Kerševan [id⁹³](#), L. Keszeghova [id^{29a}](#), R.A. Khan [id¹³⁰](#),
 A. Khanov [id¹²²](#), M. Kholodenko [id^{131a}](#), T.J. Khoo [id¹⁹](#), G. Khorialuli [id¹⁶⁸](#), Y. Khoulaki [id^{36a}](#),
 Y.A.R. Khwaira [id¹²⁸](#), D. Kim [id⁶](#), D.W. Kim [id^{18b}](#), Y.K. Kim [id³⁹](#), N. Kimura [id⁹⁶](#), M.K. Kingston [id⁵⁴](#),
 F. Kirfel [id²⁵](#), J. Kirk [id¹³⁵](#), A.E. Kiryunin [id¹¹⁰](#), S. Kita [id¹⁶⁰](#), O. Kivernyk [id²⁵](#), M. Klassen [id¹⁶¹](#),
 C. Klein [id³⁵](#), L. Klein [id¹⁶⁸](#), M.H. Klein [id⁴⁴](#), S.B. Klein [id⁵⁵](#), U. Klein [id⁹²](#), A. Klimentov [id³⁰](#),
 P. Kluit [id¹¹⁶](#), S. Kluth [id¹¹⁰](#), E. Kneringer [id⁷⁸](#), T.M. Knight [id¹⁵⁸](#), A. Knue [id⁴⁸](#), M. Kobel [id⁴⁹](#),
 D. Kobylanskii [id¹⁷¹](#), S.F. Koch [id³⁷](#), M. Kocian [id¹⁴⁶](#), P. Kodyš [id¹³⁴](#), D.M. Koeck [id¹²⁴](#), T. Koffas [id³⁵](#),
 K. Kojima [id⁸²](#), O. Kolay [id⁴⁹](#), I. Koletsou [id⁴](#), T. Komarek [id⁸⁶](#), S. Kondo [id¹⁵⁶](#), K. Köneke [id⁵⁴](#),
 A.X.Y. Kong [id¹](#), T. Kono [id¹¹⁹](#), N. Konstantinidis [id⁹⁶](#), P. Kontaxakis [id⁵⁵](#), B. Konya [id⁹⁸](#),
 R. Kopeliangsky [id⁴¹](#), S. Koperny [id^{85a}](#), R. Koppenhofer [id⁵³](#), K. Korcyl [id⁸⁶](#), K. Kordas [id^{155,d}](#),
 A. Korn [id⁹⁶](#), S. Korn [id⁵⁴](#), I. Korolkov [id¹³](#), B. Kortman [id¹¹⁶](#), O. Kortner [id¹¹⁰](#), S. Kortner [id¹¹⁰](#),
 W.H. Kostecka [id¹¹⁷](#), M. Kostov [id^{29a}](#), V.V. Kostyukhin [id¹⁴⁴](#), A. Kotskechagia [id³⁷](#), A. Kotwal [id⁵⁰](#),
 A. Koulouris [id³⁷](#), A. Kourkoumeli-Charalampidi [id^{72a,72b}](#), O. Kovanda [id¹²⁴](#), R. Kowalewski [id¹⁶⁷](#),
 W. Kozanecki [id¹²⁴](#), G. Kramberger [id⁹³](#), P. Kramer [id²⁵](#), A. Krasznahorkay [id¹⁰³](#), A.C. Kraus [id¹¹⁷](#),
 J.W. Kraus [id¹⁷³](#), J.A. Kremer [id⁴⁷](#), N.B. Krengel [id¹⁴⁴](#), T. Kresse [id¹⁵⁸](#), L. Kretschmann [id¹⁷³](#),
 J. Kretschmar [id⁹²](#), P. Krieger [id¹⁵⁸](#), K. Krizka [id²¹](#), K. Kroeninger [id⁴⁸](#), H. Kroha [id¹¹⁰](#), J. Kroll [id¹³²](#),
 J. Kroll [id¹²⁹](#), K.S. Krowpman [id¹⁰⁷](#), U. Kruchonak [id³⁸](#), H. Krüger [id²⁵](#), N. Krumnack [id⁷⁹](#), J. Krupa [id¹⁴⁶](#),
 M.C. Kruse [id⁵⁰](#), O. Kuchinskaia [id³⁸](#), S. Kuday [id^{3a}](#), S. Kuehn [id³⁷](#), R. Kuesters [id⁵³](#), T. Kuhl [id⁴⁷](#),
 V. Kukhtin [id³⁸](#), Y. Kulchitsky [id³⁸](#), S. Kuleshov [id^{138d,138b}](#), J. Kull [id¹](#), E.V. Kumar [id¹⁰⁹](#), M. Kumar [id^{34j}](#),
 N. Kumari [id⁴⁷](#), P. Kumari [id^{159b}](#), A. Kupco [id¹³²](#), O. Kuprash [id⁵³](#), H. Kurashige [id⁸⁴](#),
 L.L. Kurchaninov [id^{159a}](#), O. Kurdysh [id⁴](#), M. Kuze [id¹³⁹](#), A.K. Kvam [id¹⁰³](#), J. Kvita [id¹²³](#),
 N.G. Kyriacou [id¹⁴⁰](#), M. Laassiri [id³⁰](#), C. Lacasta [id¹⁶⁵](#), H. Lacker [id¹⁹](#), D. Lacour [id¹²⁸](#), E. Ladygin [id³⁸](#),
 A. Lafarge [id⁴⁰](#), B. Laforge [id¹²⁸](#), T. Lagouri [id¹⁷⁴](#), F.Z. Lahbabi [id^{36a}](#), S. Lai [id⁵⁴](#), W.S. Lai [id⁹⁶](#),
 I.K. Lakomic [id⁵⁴](#), J.E. Lambert [id¹⁶⁷](#), S. Lammers [id⁶⁷](#), W. Lampl [id⁷](#), C. Lampoudis [id¹⁵⁵](#),
 G. Lamprinoudis [id¹⁶⁸](#), A.N. Lancaster [id¹¹⁷](#), U. Landgraf [id⁵³](#), M.P.J. Landon [id⁹⁴](#), V.S. Lang [id⁵³](#),
 A.J. Lankford [id¹⁶²](#), F. Lanni [id³⁷](#), C.S. Lantz [id¹⁶⁴](#), K. Lantzsch [id²⁵](#), A. Lanza [id^{72a}](#),
 M. Lanzac Berrocal [id¹⁶⁵](#), T. Lari [id^{70a}](#), D. Larsen [id¹⁷](#), L. Larson [id¹¹](#), F. Lasagni Manghi [id^{24b}](#),
 M. Lassnig [id³⁷](#), H.C. Lau [id¹⁶⁷](#), S.D. Lawlor [id¹⁴²](#), R. Lazaridou [id¹⁶²](#), M. Lazzaroni [id^{70a,70b}](#), E.T.T. Le [id¹⁶²](#),
 H.D.M. Le [id¹⁰⁷](#), E.M. Le Boulicaut [id¹⁷⁴](#), D.O. Le Guennec [id¹³⁶](#), L.T. Le Pottier [id^{18a}](#), B. Leban [id^{24b,24a}](#),
 F. Ledroit-Guillon [id⁵⁹](#), T.F. Lee [id^{159b}](#), L.L. Leeuw [id^{34h}](#), M. Lefebvre [id¹⁶⁷](#), C. Leggett [id^{18a}](#),
 L.M. Lehmann [id¹¹⁶](#), G. Lehmann Miotto [id³⁷](#), M. Leigh [id⁵⁵](#), W.A. Leight [id¹⁰³](#), W. Leinonen [id¹¹⁵](#),
 A. Leisos [id^{155,t}](#), M.A.L. Leite [id^{81c}](#), C.E. Leitgeb [id¹⁹](#), R. Leitner [id¹³⁴](#), K.J.C. Leney [id⁴⁴](#), T. Lenz [id²⁵](#),
 S. Leone [id^{73a}](#), C. Leonidopoulos [id⁵¹](#), A. Leopold [id¹⁴⁷](#), J. LePage-Bourbonnais [id³⁵](#), R. Les [id¹⁰⁷](#),
 C.G. Lester [id³³](#), J. Levêque [id⁴](#), L.J. Levinson [id¹⁷¹](#), G. Levrini [id^{24b,24a}](#), M.P. Lewicki [id⁸⁶](#),
 C. Lewis [id¹⁴⁰](#), D.J. Lewis [id⁴](#), L. Lewitt [id¹⁴²](#), A. Li [id³⁰](#), B. Li [id^{113b}](#), C. Li [id¹⁰⁶](#), C-Q. Li [id¹¹⁰](#), H. Li [id^{113b}](#),
 H. Li [id¹⁰¹](#), H. Li [id¹⁵](#), H. Li [id⁶¹](#), H. Li [id^{113b}](#), J. Li [id^{141a}](#), L. Li [id^{141a}](#), R. Li [id¹⁷⁴](#), S. Li [id^{141b,141a}](#), T. Li [id⁵](#),
 Y. Li [id¹⁴](#), Z. Li [id^{14,112c}](#), Z. Li [id⁶¹](#), S. Liang [id^{14,112c}](#), Z. Liang [id¹⁴](#), M. Liberatore [id¹³⁶](#), B. Liberti [id^{75a}](#),
 G.B. Libotte [id^{81d}](#), K. Lie [id^{63c}](#), J. Lieber Marin [id^{81e}](#), H. Lien [id⁶⁷](#), H. Lin [id¹⁰⁶](#), S.F. Lin [id¹⁴⁸](#),
 L. Linden [id¹⁰⁹](#), R.E. Lindley [id⁷](#), J.H. Lindon [id³⁷](#), J. Ling [id⁶⁰](#), E. Lipeles [id¹²⁹](#), A. Lipniacka [id¹⁷](#),
 A. Lister [id¹⁶⁶](#), J.D. Little [id⁶⁷](#), B. Liu [id^{113a}](#), B.X. Liu [id^{112b}](#), D. Liu [id¹⁵³](#), D. Liu [id¹³⁷](#), E.H.L. Liu [id²¹](#),
 H. Liu [id^{112b}](#), J.K.K. Liu [id¹¹⁸](#), K. Liu [id^{141b}](#), K. Liu [id^{141b}](#), M. Liu [id⁶¹](#), M.Y. Liu [id⁶¹](#), P. Liu [id^{113b}](#),
 Q. Liu [id¹⁴⁶](#), S. Liu [id¹⁴⁸](#), X. Liu [id^{113b}](#), Y. Liu [id^{112b,112c}](#), Y. Liu [id¹⁶⁴](#), Y.L. Liu [id^{113b}](#), Y.W. Liu [id⁶¹](#),
 Z. Liu [id^{65,j}](#), S.L. Lloyd [id⁹⁴](#), E.M. Lobodzinska [id⁴⁷](#), P. Loch [id⁷](#), E. Lodhi [id¹⁵⁸](#), K. Lohwasser [id¹⁴²](#),
 E. Loiacono [id¹²²](#), J.D. Lomas [id²¹](#), I. Longarini [id¹⁶²](#), R. Longo [id^{24b,24a,am}](#), A. Lopez Solis [id¹³](#),
 N.A. Lopez-canelas [id⁷](#), N. Lorenzo Martinez [id⁴](#), A.M. Lory [id¹⁰⁹](#), M. Losada [id^{83b}](#),
 G. Löschke Centeno [id⁴](#), X. Lou [id^{14,112c}](#), P.A. Love [id⁹¹](#), M. Lu [id⁶⁵](#), S. Lu [id¹²⁹](#), Y.J. Lu [id¹⁵¹](#),
 H.J. Lubatti [id¹⁴⁰](#), C. Luci [id^{74a,74b}](#), F.L. Lucio Alves [id^{112a}](#), F. Luehring [id⁶⁷](#), B.S. Lunday [id¹²⁹](#),

O. Lundberg ¹⁴⁷, J. Lunde ³⁷, N.A. Luongo ⁶, M.S. Lutz ¹⁵⁸, A.B. Lux ²⁶, D. Lynn ³⁰, R. Lysak ¹³², V. Lysenko ¹³³, E. Lytken ⁹⁸, V. Lyubushkin ³⁸, T. Lyubushkina ³⁸, M.M. Lyukova ¹⁴⁸, H. Ma ³⁰, K. Ma ⁶¹, L.L. Ma ^{113b}, W. Ma ⁶¹, Y. Ma ^{113b}, J.C. MacDonald ¹⁰⁰, P.C. Machado De Abreu Farias ^{81e}, D. Macina ³⁷, R. Madar ⁴⁰, T. Madula ⁹⁶, J. Maeda ⁸⁴, T. Maeno ³⁰, P.T. Mafa ^{34f}, H. Maguire ¹⁴², M. Maheshwari ³³, V. Maiboroda ⁶⁵, G. Maineri ^{70a,70b}, A. Maio ^{131a,131b,131d}, K. Maj ^{85a}, O. Majersky ⁴⁷, S. Majewski ¹²⁴, A. Makita ¹⁵⁶, N. Makovec ⁶⁵, V. Maksimovic ¹⁶, B. Malaescu ¹²⁸, J. Malamant ¹²⁶, Pa. Malecki ⁸⁶, F. Malek ^{59,n}, M. Mali ⁹³, D. Malito ⁹⁵, A. Maloizel ⁵, A. Malvezzi Lopes ^{81d}, S. Malyukov ³⁸, J. Mamuzic ⁹³, G. Mancini ⁵², M.N. Mancini ²⁷, G. Manco ^{72a,72b}, S.S. Mandarray ¹⁴⁹, I. Mandić ⁹³, L. Manhaes de Andrade Filho ^{81a}, I.M. Maniatis ¹⁷¹, J. Manjarres Ramos ⁸⁹, D.C. Mankad ¹⁷¹, A. Mann ¹⁰⁹, T. Manoussos ³⁷, M.N. Mantinan ³⁹, S. Manzoni ³⁷, L. Mao ^{141a}, X. Mapekula ^{34c}, A. Marantis ¹⁵⁵, R.R. Marcelo Gregorio ¹, G. Marchiori ⁵, C. Marcon ^{70a}, E. Maricic ¹⁶, M. Marinescu ⁴⁷, S. Marium ⁴⁷, M. Marjanovic ¹²¹, A. Markhoos ⁵³, M. Markovitch ⁶⁵, M.K. Maroun ¹⁰³, M.C. Marr ¹⁴⁵, T.L. Marsault ¹³⁶, G.T. Marsden ¹⁰¹, Z. Marshall ^{18a}, S. Marti-Garcia ¹⁶⁵, J. Martin ⁹⁶, T.A. Martin ¹³⁵, V.J. Martin ⁵¹, B. Martin dit Latour ¹⁷, L. Martinelli ^{74a,74b}, V.I. Martinez Outschoorn ¹⁰³, P. Martinez Suarez ³⁷, S. Martin-Haugh ¹³⁵, G. Martinovicova ¹³⁴, V.S. Martoiu ^{28b}, A. Martone ⁸⁹, A.C. Martyniuk ⁹⁶, A. Marzin ³⁷, D. Mascione ^{77a,77b}, L. Masetti ¹⁰⁰, J. Masik ¹⁰¹, A.L. Maslennikov ³⁸, S.L. Mason ⁴¹, P. Massarotti ^{71a,71b}, P. Mastrandrea ^{73a,73b}, A. Mastroberardino ^{43b,43a}, R. Mastrofrancesco ^{72a,72b}, T. Masubuchi ¹²⁵, T.T. Mathew ¹²⁴, J. Matousek ¹³⁴, D.M. Mattern ⁴⁸, K. Mauer ⁴⁷, J. Maurer ^{28b}, T. Maurin ⁵⁸, A.J. Maury ⁶⁵, B. Maček ⁹³, C. Mavungu Tsava ¹⁰², A.E. May ¹⁰¹, E. Mayer ⁴⁰, R. Mazini ^{34j}, S.M. Mazza ¹³⁷, E. Mazzeo ³⁷, J.P. Mc Gowan ¹⁶⁷, S.P. Mc Kee ¹⁰⁶, C.C. McCracken ¹⁶⁶, E.F. McDonald ¹⁰⁵, L.F. Mcelhinney ⁹¹, J.A. Mcfayden ¹⁴⁹, R.P. McGovern ¹²⁹, R.P. Mckenzie ^{34j}, D.J. Mclaughlin ⁹⁶, S.J. McMahan ¹³⁵, C.M. Mcpartland ⁹², R.A. McPherson ^{167,ab}, S. Mehlhase ¹⁰⁹, A. Mehta ⁹², D. Melini ¹⁶⁵, B.R. Mellado Garcia ^{14,ah}, A.H. Melo ⁵⁴, F. Meloni ⁴⁷, A.M. Mendes Jacques Da Costa ¹⁰¹, L. Meng ⁹¹, S. Menke ¹¹⁰, M. Mentink ³⁷, E. Meoni ^{43b,43a}, G. Mercado ¹¹⁷, S. Merianos ¹⁵⁵, C. Merlassino ^{68a,68c}, C. Meroni ^{70a,70b}, J. Metcalfe ⁶, A.S. Mete ⁶, E. Meuser ¹⁰⁰, C. Meyer ⁶⁷, J-P. Meyer ¹³⁶, Y. Miao ^{112a}, R.P. Middleton ¹³⁵, M. Mihovilovic ⁶⁵, L. Mijović ⁵¹, G. Mikenberg ¹⁷¹, M. Mikestikova ¹³², M. Mikuž ⁹³, H. Mildner ¹⁰⁰, A. Milic ³⁷, D.W. Miller ³⁹, E.H. Miller ¹⁴⁶, A. Milov ¹⁷¹, D.A. Milstead ^{46a,46b}, T. Min ^{112a}, I.A. Minashvili ^{152b}, A.I. Mincer ¹¹⁸, B. Mindur ^{85a}, M. Mineev ³⁸, Y. Mino ⁸⁷, L.M. Mir ¹³, M. Miralles Lopez ⁵⁸, M. Mironova ^{18a}, M. Missio ⁴⁰, A. Mitra ¹⁶⁹, V.A. Mitsou ¹⁶⁵, Y. Mitsumori ¹¹¹, P.S. Miyagawa ⁹⁴, R. Mizuhiki ⁸⁴, T. Mkrtychyan ³⁷, M. Mlinarevic ⁹⁶, T. Mlinarevic ⁹⁶, M. Mlynarikova ¹³⁴, L. Mlynarska ^{85a}, C. Mo ^{141a}, H. Mobius ⁴⁷, S. Mobius ²⁰, M.H. Mohamed Farook ¹¹⁴, S. Mohapatra ⁴¹, M.F. Mohd Soberi ⁵¹, S. Mohiuddin ¹²², G. Mokgatitswane ^{34j}, R. Mole ²¹, L. Moleri ¹⁷¹, U. Molinatti ¹²⁷, L.G. Mollier ²⁰, L. Monaco ^{37,58}, B. Mondal ¹³², S. Mondal ¹³⁴, K. Mönig ⁴⁷, E. Monnier ¹⁰², L. Monsonis Romero ¹⁶⁵, A. Montella ^{46a,46b}, M. Montella ¹²⁰, F. Montereali ^{76a,76b}, F. Monticelli ⁹⁰, S. Monzani ^{68a,68c}, M.E.E. Moors ²⁵, A. Morancho Tarda ⁴², N. Morange ⁶⁵, M. Moreno Llácer ¹⁶⁵, C. Moreno Martinez ⁵⁵, J.M. Moreno Perez ^{23b}, P. Morettini ^{56b}, S. Morgenstern ^{62a}, M. Morii ⁶⁰, M. Morinaga ¹⁵⁶, F. Morodei ^{74a,74b}, P. Moschovakos ³⁷, B. Moser ⁵³, M. Mosidze ^{152b}, T. Moskalets ⁴⁴, P. Moskvitina ¹¹⁵, C.J. Mosomane ^{34b}, J. Moss ³², T. Motta Quirino ^{81d}, A. Moussa ^{36d}, Y. Moyal ^{171,k}, H. Moyano Gomez ¹³, E.J.W. Moyses ¹⁰³, T.G. Mroz ⁸⁶, S. Muanza ¹⁰², M. Mucha ²⁵, J. Mueller ¹³⁰, D. Muller ¹⁴⁴, G.A. Mullier ¹⁶³, A.J. Mullin ³³, J.J. Mullin ⁵⁰, A.C. Mullins ⁴⁴, A.E. Mulski ⁶⁰, D.P. Mungo ¹⁵⁸, D. Munoz Perez ¹²², F.J. Munoz Sanchez ¹⁰¹,

W.J. Murray ^{169,135}, E. Musajan ⁶¹, M. Muškinja ⁹³, C. Mwewa ⁴⁷, A.J. Myers ⁸, G. Myers ¹⁰⁶,
 M. Myska ¹³³, B.P. Nachman ¹⁴⁶, K. Nagai ¹²⁷, K. Nagano ⁸², R. Nagasaka ¹⁵⁶, J.L. Nagle ^{30,ao},
 E. Nagy ¹⁰², A.M. Nairz ³⁷, T. Nakagawa ⁸⁷, Y. Nakahama ⁸², K. Nakamura ⁸², K. Nakkalil ⁵,
 A. Nandi ^{62b}, H. Nanjo ¹²⁵, E.A. Narayanan ⁴⁴, Y. Narukawa ¹⁵⁶, L. Nasella ^{70a,70b}, S. Nasri ^{83c},
 C. Nass ²⁵, G. Navarro ^{23a}, A. Nayaz ¹⁹, S. Nechaeva ^{24b,24a}, F. Nechansky ¹³², L. Nedic ¹²⁷,
 A. Negri ^{72a,72b}, M. Negrini ^{24b}, C. Nellist ¹¹⁶, C. Nelson ¹⁰⁴, K. Nelson ¹⁰⁶, S. Nemecek ¹³²,
 M. Nessi ^{37,g}, M.S. Neubauer ¹⁶⁴, J. Newell ⁹², P.R. Newman ²¹, Y.W.Y. Ng ¹⁶⁴, B. Ngair ^{83b},
 H.D.N. Nguyen ¹⁰⁸, J.D. Nichols ¹²¹, R. Nicolaidou ¹³⁶, J. Nielsen ¹³⁷, M. Niemeyer ⁵⁴,
 J. Niermann ³⁷, N. Nikiforou ³⁷, I. Nikolic-Audit ¹²⁸, P. Nilsson ³⁰, G. Ninio ¹⁵⁴, A. Nisati ^{74a},
 R. Nisius ¹¹⁰, N. Nitika ¹⁷¹, E.K. Nkadimeng ^{34b}, T. Nobe ¹⁵⁶, D. Noll ¹⁴⁶, T. Nommensen ¹⁵⁰,
 M.B. Norfolk ¹⁴², B.J. Norman ³⁵, L.C. Nosler ^{18a}, M. Noury ^{36a}, J. Novak ⁹³, T. Novak ⁹³,
 P. Novotny ¹⁷¹, R. Novotny ¹³³, L. Nozka ¹²³, K. Ntekas ³⁷, D. Ntounis ¹⁴⁶,
 N.M.J. Nunes De Moura Junior ^{81b}, J. Ocariz ¹²⁸, I. Ochoa ^{131a}, A. Odella Rodriguez ¹³,
 S. Oerdek ⁴⁷, J.T. Offermann ³⁹, A. Ogrodnik ⁸⁶, A. Oh ¹⁰¹, C.C. Ohm ¹⁴⁷, H. Oide ⁸²,
 M.L. Ojeda ³⁷, Y. Okumura ¹⁵⁶, L.F. Oleiro Seabra ^{131a}, I. Oleksiyuk ⁵⁵, G. Oliveira Correa ¹³,
 D. Oliveira Damazio ³⁰, J.L. Oliver ¹, R. Omar ⁶⁷, A.P. O'Neill ²⁰, Y. Onoda ¹³⁹,
 A. Onofre ^{131a,131e,e}, P.U.E. Onyisi ¹¹, M.J. Oreglia ³⁹, D. Orestano ^{76a,76b}, R. Orlandini ^{76a,76b},
 R.S. Orr ¹⁵⁸, L.M. Osojnak ⁴¹, Y. Osumi ¹¹¹, G. Otero y Garzón ³¹, H. Otono ⁸⁸,
 M. Ouchrif ^{36d}, F. Ould-Saada ¹²⁶, T. Ovsiannikova ¹⁴⁰, M. Owen ⁵⁸, R.E. Owen ¹³⁵,
 S.A. Oyeniran ¹¹⁴, V.E. Ozcan ^{22a}, F. Ozturk ⁸⁶, N. Ozturk ⁸, S. Ozturk ⁸⁰, H.A. Pacey ¹²⁷,
 K. Pachal ^{159a}, A. Pacheco Pages ¹³, C. Padilla Aranda ¹³, G. Padovano ^{74a,74b},
 S. Pagan Griso ^{18a}, L. Pagani ^{75a,75b}, J. Pampel ²⁵, D.K. Panchal ¹¹, C.E. Pandini ⁵⁹,
 J.G. Panduro Vazquez ¹³⁵, H.D. Pandya ¹, H. Pang ¹³⁶, P. Pani ⁴⁷, G. Panizzo ^{68a,68c},
 L. Panwar ^{128,w}, L. Paolozzi ²¹, S. Parajuli ¹⁶⁴, A. Paramonov ⁶, C. Paraskevopoulos ⁵²,
 D. Paredes Hernandez ^{63b}, S.R. Paredes Saenz ⁵¹, A. Pareti ^{72a,72b}, K.R. Park ⁴¹, T.H. Park ¹¹⁰,
 F. Parodi ^{56b,56a}, J.A. Parsons ⁴¹, U. Parzefall ⁵³, B.A. Paschen ^{18a}, B. Pascual Dias ⁴⁰,
 L. Pascual Dominguez ⁹⁹, E. Pasqualucci ^{74a}, S. Passaggio ^{56b}, F. Pastore ⁹⁵, P. Patel ⁸⁶,
 U.M. Patel ⁵⁰, J.R. Pater ¹⁰¹, T. Pauly ³⁷, A. Paunovic ¹⁶, F. Pauwels ¹³⁴, C.I. Pazos ¹⁶¹,
 M. Pedersen ¹²⁶, R. Pedro ^{131a}, O. Penc ¹³², C.C. Penelaud ¹²⁸, S. Peng ¹⁵, G.D. Penn ¹⁷⁴,
 B.S. Peralva ^{81d}, A.P. Pereira Peixoto ¹⁴⁰, L. Pereira Sanchez ¹⁴⁶, D.V. Perpelitsa ^{30,ao},
 G. Perera ¹⁰³, E. Perez Codina ³⁷, M. Perganti ¹⁰, H. Pernegger ³⁷, S. Perrella ^{74a,74b},
 K. Peters ⁴⁷, R.F.Y. Peters ¹⁰¹, B.A. Petersen ³⁷, T.C. Petersen ⁴², E. Petit ¹⁰², V. Petousis ¹³³,
 A.R. Petri ^{70a,70b}, T. Petru ¹³⁴, M. Pettee ^{18a}, A. Petukhov ⁸⁰, K. Petukhova ³⁷, R. Pezoa ^{138g},
 L. Pezzotti ^{24b,24a}, G. Pezzullo ¹⁷⁴, L. Pfaffenbichler ³⁷, A.J. Pflieger ⁷⁸, T.M. Pham ¹⁷²,
 T. Pham ¹⁰⁵, P.W. Phillips ¹³⁵, G. Piacquadio ¹⁴⁸, E. Pianori ^{18a}, F. Piazza ¹²⁴, R. Piegai ³¹,
 D. Pietreanu ^{28b}, A.D. Pilkington ¹⁰¹, T. Pilusa ^{34j}, M. Pinamonti ^{68a,68c}, J.L. Pinfeld ²,
 G. Pinheiro Matos ⁴¹, B.C. Pinheiro Pereira ^{131a}, J. Pinol Bel ¹³, A.E. Pinto Pinoargote ¹²⁸,
 L. Pintucci ^{68a,68c}, K.M. Piper ¹⁴⁹, A. Pirttikoski ⁵⁵, D.A. Pizzi ³⁵, L. Pizzimento ^{63b},
 A. Plebani ³³, M.-A. Pleier ³⁰, V. Pleskot ¹³⁴, E. Plotnikova ³⁸, G. Poddar ⁹⁴, R. Poettgen ⁹⁸,
 L. Poggioli ¹²⁸, S. Polacek ¹³⁴, G. Polesello ^{72a}, A. Poley ¹⁴⁵, A. Polini ^{24b}, C.S. Pollard ¹⁶⁹,
 Z.B. Pollock ¹²⁰, E. Pompa Pacchi ¹²¹, N.I. Pond ⁹⁶, D. Ponomarenko ⁶⁷, L. Pontecorvo ³⁷,
 S. Popa ^{28a}, G.A. Popeneciu ^{28d}, A. Poreba ³⁷, D.M. Portillo Quintero ^{159a}, S. Pospisil ¹³³,
 M.A. Postill ¹⁴², P. Postolache ^{28c}, K. Potamianos ¹⁶⁹, P.A. Potepa ^{85a}, I.N. Potrap ³⁸,
 C.J. Potter ³³, H. Potti ¹⁵⁰, J. Poveda ¹⁶⁵, M.E. Pozo Astigarraga ³⁷, R. Pozzi ³⁷,
 A. Prades Ibanez ^{75a,75b}, S.R. Pradhan ¹⁴², J. Pretel ¹⁶⁷, D. Price ¹⁰¹, M. Primavera ^{69a},
 L. Primomo ^{68a,68c}, M.A. Principe Martin ⁹⁹, R. Privara ¹²³, T. Procter ^{85b}, M.L. Proffitt ¹⁴⁰,
 N. Proklova ¹²⁹, K. Prokofiev ^{63c}, G. Proto ¹¹⁰, J. Proudfoot ⁶, M. Przybycien ^{85a},

W.W. Przygoda ^{id85b}, A. Psallidas ^{id45}, D. Pudzha ^{id52}, P. Puhl ^{id57}, H.I. Purnell ^{id1},
 D. Pyatizbyantseva ^{id115}, J. Qian ^{id106}, R. Qian ^{id107}, D. Qichen ^{id127}, Y. Qin ^{id13}, T. Qiu ^{id51},
 A. Quadt ^{id54}, M. Queitsch-Maitland ^{id101}, G. Quetant ^{id55}, R.P. Quinn ^{id166}, D. Rafanoharana ^{id110},
 J.L. Rainbolt ^{id39}, S. Rajagopalan ^{id30}, E. Ramakoti ^{id38}, L. Rambelli ^{id56b,56a}, I.A. Ramirez-Berend ^{id35},
 K. Ran ^{id106,112c}, S.D. Randles ^{id92}, D.S. Rankin ^{id129}, N.P. Rapheeha ^{id34j}, H. Rasheed ^{id28b},
 A. Rastogi ^{id18a}, S. Rave ^{id100}, S. Ravera ^{id56b,56a}, B. Ravina ^{id37}, I. Ravinovich ^{id171}, M. Raymond ^{id37},
 A.L. Read ^{id126}, N.P. Readioff ^{id142}, D.M. Rebutzi ^{id72a,72b}, A.S. Reed ^{id58}, K. Reeves ^{id27},
 D. Reikher ^{id37}, A. Rej ^{id48}, C. Rembser ^{id37}, H. Ren ^{id61}, M. Renda ^{id28b}, F. Renner ^{id47},
 A.G. Rennie ^{id58}, M. Repik ^{id55}, A.L. Rescia ^{id56b,56a}, S. Resconi ^{id70a}, M. Ressegotti ^{id56b},
 S. Rettie ^{id116}, W.F. Rettie ^{id35}, M.M. Revering ^{id33}, O.L. Rezanova ^{id38}, P. Reznicek ^{id134}, H. Riani ^{id36d},
 N. Ribaric ^{id50}, B. Ricci ^{id68a,68c}, E. Ricci ^{id77a,77b}, R. Richter ^{id110}, E. Richter-Was ^{id85b}, M. Ridel ^{id128},
 S. Ridouani ^{id36d}, P. Riedler ^{id37}, E.M. Riefel ^{id46a,46b}, J.O. Rieger ^{id116}, M. Rimoldi ^{id34c},
 L. Rinaldi ^{id24b,24a}, P. Rincke ^{id163,54}, G. Ripellino ^{id163}, I. Riu ^{id13}, J.C. Rivera Vergara ^{id167},
 F. Rizatdinova ^{id122}, E. Rizvi ^{id94}, B.R. Roberts ^{id39}, S.S. Roberts ^{id137}, D. Robinson ^{id33}, A. Robson ^{id58},
 A. Rocchi ^{id75a,75b}, C. Roda ^{id73a,73b}, F.A. Rodriguez ^{id117}, S. Rodriguez Bosca ^{id37},
 Y. Rodriguez Garcia ^{id23a}, A.M. Rodríguez Vera ^{id117}, S. Roe ^{id37}, J.T. Roemer ^{id37}, O. Røhne ^{id126},
 R.A. Rojas ^{id37}, Z. Rokavec ^{id93}, C.P.A. Roland ^{id128}, A. Romaniouk ^{id78}, E. Romano ^{id72a,72b},
 M. Romano ^{id24b}, N. Rompotis ^{id92}, L. Roos ^{id128}, S. Rosati ^{id74a}, L. Roscher ^{id47}, B.J. Rosser ^{id39},
 E. Rossi ^{id127}, E. Rossi ^{id71a,71b}, L.P. Rossi ^{id60}, L. Rossini ^{id53}, R. Rosten ^{id120}, M. Rotaru ^{id28b},
 R. Roth ^{id37}, D. Rousseau ^{id65}, D. Rousso ^{id47}, S. Roy-Garand ^{id55}, A. Rozanov ^{id102},
 Z.M.A. Rozario ^{id58}, Y. Rozen ^{id153}, A. Rubio Jimenez ^{id165}, V.H. Ruelas Rivera ^{id19}, T.A. Ruggeri ^{id1},
 A. Ruggiero ^{id127}, A. Ruiz-Martinez ^{id165}, A. Rummler ^{id37}, G.B. Rupnik Boero ^{id37},
 N.A. Rusakovich ^{id38}, S. Ruscelli ^{id48}, H.L. Russell ^{id167}, G. Russo ^{id137}, J.P. Rutherford ^{id7},
 S. Rutherford Colmenares ^{id118}, M. Rybar ^{id134}, P. Rybczynski ^{id85a}, A. Ryzhov ^{id44},
 F. Safai Tehrani ^{id74a}, S. Saha ^{id1}, B. Sahoo ^{id171}, B.T. Saifuddin ^{id121}, M. Saimpert ^{id136},
 I. Sainz Saenz Diez ^{id62a}, G.T. Saito ^{id81c}, M. Saito ^{id156}, T. Saito ^{id156}, A. Sala ^{id70a,70b}, O.T. Salin ^{id65},
 A. Salnikov ^{id146}, J. Salt ^{id165}, A. Salvador Salas ^{id154}, F. Salvatore ^{id149}, A. Salzburger ^{id37},
 D. Sammel ^{id53}, E. Sampson ^{id91}, D. Sampsonidis ^{id155,d}, D. Sampsonidou ^{id124}, M.A.A. Samy ^{id58},
 J. Sánchez ^{id165}, V. Sanchez Sebastian ^{id165}, H. Sandaker ^{id126}, C.O. Sander ^{id47}, J.A. Sandesara ^{id172},
 M. Sandhoff ^{id173}, C. Sandoval ^{id23b}, L. Sanfilippo ^{id62a}, D.P.C. Sankey ^{id135}, T. Sano ^{id87}, A. Sansar ^{id22c},
 A. Sansoni ^{id52}, M. Santana Queiroz ^{id18b}, L. Santi ^{id37}, C. Santoni ^{id40}, H. Santos ^{id131a,131b},
 L. Santos Pereira Trigo ^{id47}, E. Sanzani ^{id24b,24a}, K.A. Saoucha ^{id83d}, J.G. Saraiva ^{id131a,131d},
 J. Sardain ^{id7}, S. Sarkar ^{id50}, O. Sasaki ^{id82}, K. Sato ^{id160}, C. Sauer ^{id37}, E. Sauvan ^{id4}, P. Savard ^{id158,aj},
 R. Sawada ^{id156}, C. Sawyer ^{id135}, L. Sawyer ^{id97}, A.M. Sayed ^{id27}, C. Sbarra ^{id24b}, A. Sbrizzi ^{id24b,24a},
 R. Scaglioni ^{id72a,72b}, T. Scanlon ^{id96}, J. Schaarschmidt ^{id140}, U. Schäfer ^{id100}, A.C. Schaffer ^{id65,44},
 D. Schaile ^{id109}, R.D. Schamberger ^{id148}, C. Scharf ^{id19}, M.M. Schefer ^{id20}, D. Scheirich ^{id134},
 M. Schernau ^{id138f}, C. Scheulen ^{id55}, C. Schiavi ^{id56b,56a}, M. Schioppa ^{id43b,43a}, S. Schlenker ^{id37},
 T. Schlomer ^{id54}, J. Schmeing ^{id173}, C.R. Schmidt ^{id49}, E. Schmidt ^{id110}, M.A. Schmidt ^{id173},
 K. Schmieden ^{id25}, C. Schmitt ^{id100}, N. Schmitt ^{id100}, S. Schmitt ^{id47}, N.A. Schneider ^{id109},
 L. Schoeffel ^{id136}, A. Schoening ^{id62b}, P.G. Scholer ^{id35}, E. Schopf ^{id144}, M. Schott ^{id25}, S. Schramm ^{id55},
 T. Schroer ^{id55}, H-C. Schultz-Coulon ^{id62a}, M. Schumacher ^{id53}, B.A. Schumm ^{id137}, Ph. Schune ^{id136},
 H.R. Schwartz ^{id7}, A. Schwartzman ^{id146}, T.A. Schwarz ^{id106}, Ph. Schwemling ^{id136},
 R. Schwienhorst ^{id107}, F.G. Sciacca ^{id20}, A. Sciandra ^{id30}, G. Sciolla ^{id27}, S.A. Scoville ^{id130},
 F. Scuri ^{id73a}, C.D. Sebastiani ^{id37}, K. Sedlaczek ^{id117}, A. Sehwat ^{id138b}, S.C. Seidel ^{id114},
 B.D. Seidlitz ^{id41}, C. Seitz ^{id47}, J.M. Seixas ^{id81b}, G. Sekhniaidze ^{id71a}, L. Selem ^{id128},
 N. Semprini-Cesari ^{id24b,24a}, A. Semushin ^{id175}, V. Senthilkumar ^{id116}, L. Serin ^{id65}, M. Sessa ^{id71a,71b},
 H. Severini ^{id121}, F. Sforza ^{id56b,56a}, A. Sfyrla ^{id55}, Q. Sha ^{id14}, H. Shaddix ^{id117}, A.H. Shah ^{id33},

R. Shaheen [ID147](#), J.D. Shahinian [ID129](#), M. Shamim [ID37](#), L.Y. Shan [ID14](#), M. Shapiro [ID18a](#), A. Sharma [ID37](#),
 A.S. Sharma [ID166](#), P. Sharma [ID30](#), K. Shaw [ID149](#), S.M. Shaw [ID101](#), D. Shemyakin [ID171](#), Q. Shen [ID14](#),
 D.J. Sheppard [ID145](#), P. Sherwood [ID96](#), L. Shi [ID112b](#), X. Shi [ID14](#), S. Shimizu [ID82](#), S. Shirabe [ID88](#),
 M. Shiyakova [ID38,z](#), M.J. Shochet [ID39](#), D.R. Shope [ID126](#), B. Shrestha [ID121](#), S. Shrestha [ID120,aq](#),
 I. Shreyber [ID38](#), M.J. Shroff [ID104](#), P. Sicho [ID132](#), A.M. Sickles [ID164](#), E. Sideras Haddad [ID34j](#),
 A.C. Sidley [ID116](#), A. Sidoti [ID24b](#), F. Siegert [ID49](#), Dj. Sijacki [ID16](#), F. Sili [ID61](#), J.M. Silva [ID51](#),
 I. Silva Ferreira [ID81b](#), M.V. Silva Oliveira [ID30](#), S.B. Silverstein [ID46a](#), S. Simion [ID65](#), R. Simoniello [ID37](#),
 E.L. Simpson [ID101](#), H. Simpson [ID149](#), L.R. Simpson [ID6](#), S. Simsek [ID80](#), S. Sindhu [ID54](#), S.N. Singh [ID27](#),
 S. Singh [ID30](#), S. Sinha [ID47](#), S. Sinha [ID101](#), M. Sioli [ID24b,24a](#), K. Sioulas [ID9](#), I. Siral [ID37](#), E. Sitnikova [ID47](#),
 J. Sjölin [ID46a,46b](#), A. Skaf [ID54](#), E. Skorda [ID21](#), P. Skubic [ID121](#), M. Slawinska [ID86](#), I. Slazyk [ID17](#),
 I. Sliusar [ID126](#), V. Smakhtin [ID171](#), B.H. Smart [ID135](#), S.Yu. Smirnov [ID138b](#), Y. Smirnov [ID34c](#),
 O. Smirnova [ID98](#), J.L. Smith [ID101](#), M.B. Smith [ID35](#), R. Smith [ID146](#), H. Smitmanns [ID100](#), M. Smizanska [ID91](#),
 K. Smolek [ID133](#), P. Smolyanskiy [ID133](#), A.A. Snesarev [ID38](#), H.L. Snoek [ID116](#), R.M. Snyder [ID50](#),
 S. Snyder [ID30](#), R. Sobie [ID167,ab](#), A. Soffer [ID154](#), C.A. Solans Sanchez [ID37](#), E.Yu. Soldatov [ID38](#),
 U. Soldevila [ID165](#), A.A. Solodkov [ID34j](#), S. Solomon [ID27](#), A. Soloshenko [ID38](#), O.V. Solovyanov [ID40](#),
 P. Sommer [ID49](#), A. Sopczak [ID133](#), A.L. Soppio [ID51](#), F. Sopkova [ID29b](#), J.D. Sorenson [ID114](#),
 I.R. Sotarriva Alvarez [ID139](#), V. Sothilingam [ID62a](#), O.J. Soto Sandoval [ID138c,138b](#), S. Sottocornola [ID67](#),
 R. Soualah [ID83a](#), D. South [ID47](#), N. Soybelman [ID171](#), S. Spagnolo [ID69a,69b](#), A.S. Spellman [ID124](#),
 D. Sperlich [ID53](#), B. Spisso [ID71a,71b](#), L. Splendori [ID102](#), M. Spousta [ID134](#), E.J. Staats [ID35](#), R. Stamen [ID62a](#),
 E. Stanecka [ID86](#), W. Stanek-Maslouska [ID47](#), M.V. Stange [ID49](#), B. Stanislaus [ID18a](#), M.M. Stanitzki [ID47](#),
 G.H. Stark [ID137](#), J. Stark [ID89](#), P. Staroba [ID132](#), P. Starovoitov [ID83d](#), R. Staszewski [ID86](#), C. Stauch [ID109](#),
 G. Stavropoulos [ID45](#), A. Stefl [ID37](#), A. Stein [ID100](#), P. Steinberg [ID30](#), B. Stelzer [ID145,159a](#), H.J. Stelzer [ID130](#),
 O. Stelzer [ID159a](#), H. Stenzel [ID57](#), T.J. Stevenson [ID149](#), G.A. Stewart [ID47](#), G. Stoicea [ID28b](#),
 M. Stolarski [ID131a](#), S. Stonjek [ID110](#), A. Straessner [ID49](#), J. Strandberg [ID147](#), S. Strandberg [ID46a,46b](#),
 M. Stratmann [ID173](#), M. Strauss [ID121](#), T. Strebler [ID102](#), P. Strizenec [ID29b](#), R. Ströhmer [ID168](#),
 D.M. Strom [ID124](#), R. Stroynowski [ID44](#), A. Strubig [ID46a,46b](#), S.A. Stucci [ID30](#), B. Stugu [ID17](#), J. Stupak [ID121](#),
 N.A. Styles [ID47](#), D. Su [ID146](#), S. Su [ID61](#), X. Su [ID61](#), D. Suchy [ID29a](#), A.D. Sudhakar Ponnu [ID54](#),
 L. Sudit [ID171](#), Y. Sue [ID82](#), K. Sugizaki [ID129](#), D.M.S. Sultan [ID127](#), L. Sultanaliyeva [ID25](#), S. Sultansoy [ID3b](#),
 S. Sun [ID172](#), W. Sun [ID14](#), S. Sundar Raman [ID166](#), N. Sur [ID98](#), J.P. Surdutovich [ID120](#), N. Suri Jr [ID174](#),
 M.R. Sutton [ID149](#), M. Svatos [ID132](#), P.N. Swallow [ID33](#), S.N. Swatman [ID37](#), M. Swiatlowski [ID159a](#),
 A. Swoboda [ID37](#), I. Sykora [ID29a](#), M. Sykora [ID134](#), T. Sykora [ID134](#), D. Ta [ID100](#), K. Tackmann [ID47,y](#),
 A. Taffard [ID162](#), R. Tafirout [ID159a](#), Y. Takubo [ID82](#), M. Talby [ID102](#), N.M. Tamir [ID154](#), A. Tanaka [ID156](#),
 J. Tanaka [ID156](#), R. Tanaka [ID65](#), M. Tanasini [ID148](#), Z. Tao [ID166](#), S. Tapia Araya [ID138g](#), S. Tapprogge [ID100](#),
 A. Tarek Abouelfadl Mohamed [ID37](#), S. Tarem [ID153](#), K. Tariq [ID14](#), G. Tarna [ID37](#), G.F. Tartarelli [ID70a](#),
 M.J. Tartarin [ID141b](#), P. Tas [ID134](#), M. Tasevsky [ID132](#), E. Tassi [ID43b,43a](#), A.C. Tate [ID164](#), Y. Tayalati [ID36e,aa](#),
 G.N. Taylor [ID105](#), W. Taylor [ID159b](#), R.J. Taylor Vara [ID165](#), A.S. Tegetmeier [ID89](#), P. Teixeira-Dias [ID95](#),
 J.J. Teoh [ID158](#), K. Terashi [ID156](#), J. Terron [ID99](#), S. Terzo [ID13](#), M. Testa [ID52](#), R.J. Teuscher [ID158,ab](#),
 A. Thaler [ID78](#), T. Thevenaux-Pelzer [ID102](#), J.P. Thomas [ID21](#), E.A. Thompson [ID18a](#), P.D. Thompson [ID21](#),
 E. Thomson [ID129](#), R.E. Thornberry [ID30](#), T.M. Thory-Rao [ID21](#), C.N. Thotamuna Wijewardhana [ID148](#),
 C. Tian [ID61](#), Y. Tian [ID55](#), V. Tikhomirov [ID80](#), Yu.A. Tikhonov [ID38](#), D. Timoshyn [ID134](#), E.X.L. Ting [ID1](#),
 P. Tipton [ID174](#), A. Tishelman-Charny [ID30](#), K. Todome [ID139](#), S. Todorova-Nova [ID134](#), L. Toffolin [ID68a,68c](#),
 M. Togawa [ID82](#), J. Tojo [ID88](#), S. Tokár [ID29a](#), O. Toldaiev [ID67](#), G. Tolkachev [ID102](#), M. Tomoto [ID82](#),
 L. Tompkins [ID146](#), E. Torrence [ID124](#), H. Torres [ID89](#), D.I. Torres Arza [ID138g](#), E. Torres Reoyo [ID165](#),
 E. Torró Pastor [ID165](#), M. Toscani [ID31](#), C. Toscirri [ID39](#), M. Tost [ID11](#), D.R. Tovey [ID142](#), T. Trefzger [ID168](#),
 P.M. Tricarico [ID13](#), A. Tricoli [ID30](#), I.M. Trigger [ID159a](#), S. Trincaz-Duvoid [ID128](#), D.A. Trischuk [ID167](#),
 A. Tropina [ID38](#), D. Truncali [ID75a,75b](#), L. Truong [ID34c](#), M. Trzebinski [ID86](#), A. Trzupek [ID86](#), F. Tsai [ID148](#),
 A. Tsiamis [ID155](#), P.V. Tsiareshka [ID38](#), S. Tsigaridas [ID159a](#), A. Tsirigotis [ID155,t](#), V. Tsiskaridze [ID152a](#),

E.G. Tskhadadze [ID152a](#), H.F. Tsoi [ID129](#), Y. Tsujikawa [ID87](#), V. Tsulaia [ID18a](#), K. Tsuri [ID119](#),
 D. Tsybychev [ID148](#), Y. Tu [ID63b](#), A. Tudorache [ID28b](#), V. Tudorache [ID28b](#), S.B. Tuncay [ID127](#),
 S. Turchikhin [ID56b,56a](#), I. Turk Cakir [ID3a](#), R. Turra [ID70a](#), T. Turtuvshin [ID38,ac](#), P.M. Tuts [ID41](#),
 Y. Uematsu [ID82](#), F. Ukegawa [ID160](#), P.A. Ulloa Poblete [ID138c,138b](#), G. Unal [ID37](#), A. Undrus [ID30](#),
 J. Urban [ID29b](#), P. Urrejola [ID138e](#), G. Usai [ID8](#), R. Ushioda [ID157](#), M. Usman [ID108](#), F. Ustuner [ID51](#),
 Z. Uysal [ID80](#), V. Vacek [ID133](#), B. Vachon [ID104](#), T. Vafeiadis [ID37](#), A. Vaitkus [ID96](#), C. Valderanis [ID109](#),
 E. Valdes Santurio [ID46a,46b](#), M. Valente [ID37](#), S. Valentineti [ID24b,24a](#), A. Valero [ID165](#),
 E. Valiente Moreno [ID165](#), A. Vallier [ID89](#), J.A. Valls Ferrer [ID165](#), D.R. Van Arneman [ID116](#),
 R. Van Den Broucke [ID128](#), A. Van Der Graaf [ID48](#), H.Z. Van Der Schyf [ID34j](#), P. Van Gemmeren [ID6](#),
 M. Van Rijnbach [ID37](#), S. Van Stroud [ID96](#), I. Van Vulpen [ID116](#), P. Vana [ID134](#), M. Vanadia [ID75a,75b](#),
 U.M. Vande Voorde [ID147](#), W. Vandelli [ID37](#), E.R. Vandewall [ID146](#), D. Vannicola [ID154](#), R. Vari [ID74a](#),
 M. Varma [ID174](#), E.W. Varnes [ID7](#), C. Varni [ID85a](#), D. Varouchas [ID65](#), L. Varriale [ID165](#), K.E. Varvell [ID150](#),
 M.E. Vasile [ID28b](#), A. Vasileiadou⁹, L. Vaslin⁸², M.D. Vassilev [ID146](#), A. Vasyukov [ID38](#),
 L.M. Vaughan [ID122](#), R. Vavricka¹³⁴, T. Vazquez Schroeder [ID13](#), J. Veatch [ID32](#), V. Vecchio [ID101](#),
 M.J. Veen [ID103](#), I. Veliscek [ID30](#), I. Velkovska [ID93](#), L.M. Veloce [ID158](#), F. Veloso [ID131a,131c](#),
 A.G. Veltman [ID51](#), S.H. Venetianer [ID161](#), S. Veneziano [ID74a](#), A. Ventura [ID69a,69b](#), A. Verbitskiy [ID110](#),
 M. Verducci [ID73a,73b](#), C. Vergis [ID94](#), M. Verissimo De Araujo [ID81b](#), W. Verkerke [ID116](#),
 J.C. Vermeulen [ID116](#), C. Vernieri [ID146](#), M. Vessella [ID162](#), M.C. Vetterli [ID145,aj](#), A. Vgenopoulos [ID100](#),
 N. Viaux Maira [ID138g,af](#), L. Vicenik [ID133](#), T. Vickey [ID142](#), O.E. Vickey Boeriu [ID142](#),
 G.H.A. Viehhauser [ID127](#), L. Vigani [ID62b](#), M. Vigi [ID110](#), M. Villa [ID24b,24a](#), M. Villaplana Perez [ID165](#),
 E.M. Villhauer³⁹, E. Vilucchi [ID52](#), M. Vincent [ID165](#), M.G. Vincter [ID35](#), A. Visibile [ID116](#), A. Visive [ID116](#),
 C. Vittori [ID161](#), I. Vivarelli [ID24b,24a](#), M.I. Vivas Albornoz [ID47](#), E. Voevodina [ID110](#), F. Vogel [ID109](#),
 J.C. Voigt [ID49](#), P. Vokac [ID133](#), Yu. Volkotrub [ID85b](#), L. Vomberg [ID25](#), E. Von Toerne [ID25](#),
 B. Vormwald [ID37](#), K. Vorobev [ID50](#), M. Vos [ID165](#), K. Voss [ID144](#), M. Vozak [ID37](#), L. Vozdecky [ID121](#),
 N. Vranjes [ID16](#), M. Vranjes Milosavljevic [ID16](#), M. Vreeswijk [ID116](#), N.K. Vu [ID112a](#), R. Vuillermet [ID37](#),
 O. Vujinovic [ID100](#), I. Vukotic [ID39](#), I.K. Vyas [ID35](#), J.F. Wack [ID33](#), A. Wada [ID111](#), S. Wada [ID160](#),
 C. Wagner¹⁴⁶, J.M. Wagner [ID18a](#), W. Wagner [ID173](#), S. Wahdan [ID173](#), H. Wahlberg [ID90](#), C.H. Waits [ID121](#),
 J. Walder [ID135](#), R. Walker [ID109](#), K. Walkingshaw Pass [ID58](#), W. Walkowiak [ID144](#), A. Wall [ID129](#),
 E.J. Wallin [ID98](#), T. Wamorkar [ID146](#), K. Wandall-Christensen [ID165](#), A. Wang [ID61](#), A.Z. Wang [ID137](#),
 C. Wang [ID47](#), C. Wang [ID11](#), H. Wang [ID18a](#), J. Wang [ID63c](#), P. Wang [ID101](#), P. Wang [ID96](#), R. Wang [ID60](#),
 R. Wang [ID106](#), R. Wang [ID6](#), S.M. Wang [ID151](#), S. Wang [ID14,an](#), T. Wang [ID115](#), T. Wang [ID61](#),
 W.T. Wang [ID127](#), W. Wang [ID113c](#), X. Wang [ID164](#), X. Wang [ID141a](#), X. Wang [ID47](#), Y. Wang [ID148](#),
 Y. Wang [ID114](#), Z. Wang [ID106](#), Z. Wang [ID14](#), Z. Wang [ID63b](#), C. Wanotayaroj [ID82](#), A. Warburton [ID104](#),
 A.L. Warnerbring [ID144](#), S. Waterhouse [ID96](#), A.T. Watson [ID21](#), H. Watson [ID51](#), M.F. Watson [ID21](#),
 E. Watton [ID37](#), G. Watts [ID140](#), B.M. Waugh [ID96](#), J.M. Webb [ID53](#), C. Weber [ID30](#), M.S. Weber [ID20](#),
 C. Wei [ID61](#), Y. Wei [ID53](#), A.R. Weidberg [ID127](#), E.J. Weik [ID118](#), J. Weingarten [ID48](#), C. Weiser [ID53](#),
 C.J. Wells [ID47](#), T. Wenaus [ID30](#), T. Wengler [ID37](#), N.S. Wenke¹¹⁰, N. Wermes [ID25](#), D. Werner [ID47](#),
 M. Wessels [ID62a](#), A.M. Wharton [ID91](#), A.S. White [ID37](#), A. White [ID8](#), M.J. White [ID1](#), D. Whiteson [ID162](#),
 L. Wickremasinghe [ID125](#), W. Wiedenmann [ID172](#), M. Wielers [ID135](#), R. Wierda [ID147](#), C. Wiglesworth [ID42](#),
 H.G. Wilkens [ID37](#), J.J.H. Wilkinson [ID33](#), S. Williams [ID33](#), S. Willocq [ID103](#), D.J. Wilson [ID101](#),
 P.J. Windischhofer [ID39](#), F.I. Winkel [ID31](#), F. Winklmeier [ID124](#), B.T. Winter [ID53](#), M. Wittgen [ID146](#),
 M. Wobisch [ID97](#), T. Wojtkowski⁵⁹, Z. Wolffs [ID116](#), J. Wollrath³⁷, M.W. Wolter [ID86](#), H. Wolters [ID131a,131c](#),
 M.C. Wong¹³⁷, E.L. Woodward [ID41](#), S.D. Worm [ID47](#), B.K. Wosiek [ID86](#), K.A. Wozniak [ID55](#),
 K.W. Woźniak [ID86](#), S. Wozniewski [ID54](#), K. Wraight [ID58](#), C. Wu [ID158](#), C. Wu [ID21](#), J. Wu [ID156](#),
 M. Wu [ID112b](#), M. Wu [ID115](#), S.L. Wu [ID172](#), S. Wu [ID14,an](#), X. Wu [ID61](#), Y.Q. Wu [ID158](#), Y. Wu [ID61](#),
 Z. Wu [ID102](#), Z. Wu [ID112a](#), J. Wuerzinger [ID110](#), T.R. Wyatt [ID101](#), B.M. Wynne [ID51](#), S. Xella [ID42](#),
 L. Xia [ID112a](#), M. Xie [ID61](#), A. Xiong [ID124](#), I. Xiotidis [ID37](#), D. Xu [ID14](#), H. Xu [ID61](#), L. Xu [ID61](#), R. Xu [ID129](#),

T. Xu , W. Xu^{112a}, Y. Xu , Z. Xu , R. Xue , B. Yabsley , S. Yacoob , Y. Yamaguchi , E. Yamashita , H. Yamauchi , T. Yamazaki , Y. Yamazaki , S. Yan , Z. Yan , C. Yang , H.J. Yang , H.T. Yang , S. Yang , X. Yang , X. Yang , Y. Yang , Y. Yang⁶¹, W-M. Yao , C.L. Yardley , J. Ye , S. Ye , X. Ye , I. Yeletsikh , B. Yeo , M.R. Yexley , T.P. Yildirim , K. Yorita , C.J.S. Young , C. Young , I.N.L. Young , N.D. Young¹²⁴, Y. Yu , J. Yuan , M. Yuan , R. Yuan , L. Yue , M. Zaazoua , B. Zabinski , I. Zahir , Q.U.A. Zahoor , A. Zaio^{56b,56a}, Z.K. Zak , T. Zakareishvili , S. Zambito , J. Zang , R. Zanzottera , O. Zaplatilek , E. Zaya , C. Zeitnitz , H. Zeng , D.T. Zenger Jr , T. Ženiš , S. Zenz , D. Zerwas , W. Zhan , B. Zhang , D.F. Zhang , G. Zhang , J. Zhang , J. Zhang , L. Zhang , L. Zhang , P. Zhang , R. Zhang , S. Zhang , Y. Zhang , Y. Zhang , Y. Zhang , Y. Zhang , Z. Zhang¹⁰¹, Z. Zhang , Z. Zhang , Z. Zhang , Z. Zhang , H. Zhao , T. Zhao , Y. Zhao , Z. Zhao , Z. Zhao , A. Zhemchugov , J. Zheng , K. Zheng , L. Zheng , X. Zheng , Z. Zheng , D. Zhong , B. Zhou , B. Zhou , N. Zhou , Y. Zhou , Y. Zhou , Y. Zhou⁷, Z. Zhou , J. Zhu , X. Zhu^{141b}, Y. Zhu , X. Zhuang , K. Zhukov , P. Ziakas , N.I. Zimine , J. Zinsser , M. Ziolkowski , L. Živković , A. Zoccoli , K. Zoch , A. Zografos , T.G. Zorbas , L. Zwalinski .

¹Department of Physics, University of Adelaide, Adelaide; Australia.

²Department of Physics, University of Alberta, Edmonton AB; Canada.

³(^a)Department of Physics, Ankara University, Ankara; (^b)Division of Physics, TOBB University of Economics and Technology, Ankara; Türkiye.

⁴LAPP, Université Savoie Mont Blanc, CNRS/IN2P3, Annecy; France.

⁵APC, Université Paris Cité, CNRS/IN2P3, Paris; France.

⁶High Energy Physics Division, Argonne National Laboratory, Argonne IL; United States of America.

⁷Department of Physics, University of Arizona, Tucson AZ; United States of America.

⁸Department of Physics, University of Texas at Arlington, Arlington TX; United States of America.

⁹Physics Department, National and Kapodistrian University of Athens, Athens; Greece.

¹⁰Physics Department, National Technical University of Athens, Zografou; Greece.

¹¹Department of Physics, University of Texas at Austin, Austin TX; United States of America.

¹²Institute of Physics, Azerbaijan Academy of Sciences, Baku; Azerbaijan.

¹³Institut de Física d'Altes Energies (IFAE), Barcelona Institute of Science and Technology, Barcelona; Spain.

¹⁴Institute of High Energy Physics, Chinese Academy of Sciences, Beijing; China.

¹⁵Physics Department, Tsinghua University, Beijing; China.

¹⁶Institute of Physics, University of Belgrade, Belgrade; Serbia.

¹⁷Department for Physics and Technology, University of Bergen, Bergen; Norway.

¹⁸(^a)Physics Division, Lawrence Berkeley National Laboratory, Berkeley CA; (^b)University of California, Berkeley CA; United States of America.

¹⁹Institut für Physik, Humboldt Universität zu Berlin, Berlin; Germany.

²⁰Albert Einstein Center for Fundamental Physics and Laboratory for High Energy Physics, University of Bern, Bern; Switzerland.

²¹School of Physics and Astronomy, University of Birmingham, Birmingham; United Kingdom.

²²(^a)Department of Physics, Bogazici University, Istanbul; (^b)Department of Physics Engineering, Gaziantep University, Gaziantep; (^c)Department of Physics, Istanbul University, Istanbul; Türkiye.

- ^{23(a)}Facultad de Ciencias y Centro de Investigaciones, Universidad Antonio Nariño, Bogotá;^(b)Departamento de Física, Universidad Nacional de Colombia, Bogotá; Colombia.
- ^{24(a)}Dipartimento di Fisica e Astronomia A. Righi, Università di Bologna, Bologna;^(b)INFN Sezione di Bologna; Italy.
- ²⁵Physikalisches Institut, Universität Bonn, Bonn; Germany.
- ²⁶Department of Physics, Boston University, Boston MA; United States of America.
- ²⁷Department of Physics, Brandeis University, Waltham MA; United States of America.
- ^{28(a)}Transilvania University of Brasov, Brasov;^(b)Horia Hulubei National Institute of Physics and Nuclear Engineering, Bucharest;^(c)Department of Physics, Alexandru Ioan Cuza University of Iasi, Iasi;^(d)National Institute for Research and Development of Isotopic and Molecular Technologies, Physics Department, Cluj-Napoca;^(e)National University of Science and Technology Politehnica, Bucharest;^(f)West University in Timisoara, Timisoara;^(g)Faculty of Physics, University of Bucharest, Bucharest; Romania.
- ^{29(a)}Faculty of Mathematics, Physics and Informatics, Comenius University, Bratislava;^(b)Department of Subnuclear Physics, Institute of Experimental Physics of the Slovak Academy of Sciences, Kosice; Slovak Republic.
- ³⁰Physics Department, Brookhaven National Laboratory, Upton NY; United States of America.
- ³¹Universidad de Buenos Aires, Facultad de Ciencias Exactas y Naturales, Departamento de Física, y CONICET, Instituto de Física de Buenos Aires (IFIBA), Buenos Aires; Argentina.
- ³²California State University, CA; United States of America.
- ³³Cavendish Laboratory, University of Cambridge, Cambridge; United Kingdom.
- ^{34(a)}Department of Physics, University of Cape Town, Cape Town;^(b)iThemba Labs, Western Cape;^(c)Department of Mechanical Engineering Science, University of Johannesburg, Johannesburg;^(d)National Institute of Physics, University of the Philippines Diliman (Philippines);^(e)Department of Physics, Stellenbosch University, Matieland;^(f)University of KwaZulu-Natal, School of Agriculture and Science, Mathematics, Westville;^(g)University of South Africa, Department of Physics, Pretoria;^(h)University of Pretoria, Department of Mechanical and Aeronautical Engineering, Pretoria;⁽ⁱ⁾University of Zululand, KwaDlangezwa;^(j)School of Physics, University of the Witwatersrand, Johannesburg; South Africa.
- ³⁵Department of Physics, Carleton University, Ottawa ON; Canada.
- ^{36(a)}Faculté des Sciences Ain Chock, Université Hassan II de Casablanca;^(b)Faculté des Sciences, Université Ibn-Tofail, Kénitra;^(c)Faculté des Sciences Semlalia, Université Cadi Ayyad, LPHEA-Marrakech;^(d)LPMR, Faculté des Sciences, Université Mohamed Premier, Oujda;^(e)Faculté des sciences, Université Mohammed V, Rabat;^(f)Institute of Applied Physics, Mohammed VI Polytechnic University, Ben Guerir; Morocco.
- ³⁷CERN, Geneva; Switzerland.
- ³⁸Affiliated with an international laboratory covered by a cooperation agreement with CERN.
- ³⁹Enrico Fermi Institute, University of Chicago, Chicago IL; United States of America.
- ⁴⁰LPC, Université Clermont Auvergne, CNRS/IN2P3, Clermont-Ferrand; France.
- ⁴¹Nevis Laboratory, Columbia University, Irvington NY; United States of America.
- ⁴²Niels Bohr Institute, University of Copenhagen, Copenhagen; Denmark.
- ^{43(a)}Dipartimento di Fisica, Università della Calabria, Rende;^(b)INFN Gruppo Collegato di Cosenza, Laboratori Nazionali di Frascati; Italy.
- ⁴⁴Physics Department, Southern Methodist University, Dallas TX; United States of America.
- ⁴⁵National Centre for Scientific Research "Demokritos", Agia Paraskevi; Greece.
- ^{46(a)}Department of Physics, Stockholm University;^(b)Oskar Klein Centre, Stockholm; Sweden.
- ⁴⁷Deutsches Elektronen-Synchrotron DESY, Hamburg and Zeuthen; Germany.
- ⁴⁸Fakultät Physik, Technische Universität Dortmund, Dortmund; Germany.

- ⁴⁹Institut für Kern- und Teilchenphysik, Technische Universität Dresden, Dresden; Germany.
- ⁵⁰Department of Physics, Duke University, Durham NC; United States of America.
- ⁵¹SUPA - School of Physics and Astronomy, University of Edinburgh, Edinburgh; United Kingdom.
- ⁵²INFN e Laboratori Nazionali di Frascati, Frascati; Italy.
- ⁵³Physikalisches Institut, Albert-Ludwigs-Universität Freiburg, Freiburg; Germany.
- ⁵⁴II. Physikalisches Institut, Georg-August-Universität Göttingen, Göttingen; Germany.
- ⁵⁵Département de Physique Nucléaire et Corpusculaire, Université de Genève, Genève; Switzerland.
- ⁵⁶(^a) Dipartimento di Fisica, Università di Genova, Genova; (^b) INFN Sezione di Genova; Italy.
- ⁵⁷II. Physikalisches Institut, Justus-Liebig-Universität Giessen, Giessen; Germany.
- ⁵⁸SUPA - School of Physics and Astronomy, University of Glasgow, Glasgow; United Kingdom.
- ⁵⁹LPSC, Université Grenoble Alpes, CNRS/IN2P3, Grenoble INP, Grenoble; France.
- ⁶⁰Laboratory for Particle Physics and Cosmology, Harvard University, Cambridge MA; United States of America.
- ⁶¹Department of Modern Physics and State Key Laboratory of Particle Detection and Electronics, University of Science and Technology of China, Hefei; China.
- ⁶²(^a) Kirchhoff-Institut für Physik, Ruprecht-Karls-Universität Heidelberg, Heidelberg; (^b) Physikalisches Institut, Ruprecht-Karls-Universität Heidelberg, Heidelberg; Germany.
- ⁶³(^a) Department of Physics, Chinese University of Hong Kong, Shatin, N.T., Hong Kong; (^b) Department of Physics, University of Hong Kong, Hong Kong; (^c) Department of Physics and Institute for Advanced Study, Hong Kong University of Science and Technology, Clear Water Bay, Kowloon, Hong Kong; China.
- ⁶⁴Department of Physics, National Tsing Hua University, Hsinchu; Taiwan.
- ⁶⁵IJCLab, Université Paris-Saclay, CNRS/IN2P3, 91405, Orsay; France.
- ⁶⁶Centro Nacional de Microelectrónica (IMB-CNM-CSIC), Barcelona; Spain.
- ⁶⁷Department of Physics, Indiana University, Bloomington IN; United States of America.
- ⁶⁸(^a) INFN Gruppo Collegato di Udine, Sezione di Trieste, Udine; (^b) ICTP, Trieste; (^c) Dipartimento Politecnico di Ingegneria e Architettura, Università di Udine, Udine; Italy.
- ⁶⁹(^a) INFN Sezione di Lecce; (^b) Dipartimento di Matematica e Fisica, Università del Salento, Lecce; Italy.
- ⁷⁰(^a) INFN Sezione di Milano; (^b) Dipartimento di Fisica, Università di Milano, Milano; Italy.
- ⁷¹(^a) INFN Sezione di Napoli; (^b) Dipartimento di Fisica, Università di Napoli, Napoli; Italy.
- ⁷²(^a) INFN Sezione di Pavia; (^b) Dipartimento di Fisica, Università di Pavia, Pavia; Italy.
- ⁷³(^a) INFN Sezione di Pisa; (^b) Dipartimento di Fisica E. Fermi, Università di Pisa, Pisa; Italy.
- ⁷⁴(^a) INFN Sezione di Roma; (^b) Dipartimento di Fisica, Sapienza Università di Roma, Roma; Italy.
- ⁷⁵(^a) INFN Sezione di Roma Tor Vergata; (^b) Dipartimento di Fisica, Università di Roma Tor Vergata, Roma; Italy.
- ⁷⁶(^a) INFN Sezione di Roma Tre; (^b) Dipartimento di Matematica e Fisica, Università Roma Tre, Roma; Italy.
- ⁷⁷(^a) INFN-TIFPA; (^b) Università degli Studi di Trento, Trento; Italy.
- ⁷⁸Universität Innsbruck, Department of Astro and Particle Physics, Innsbruck; Austria.
- ⁷⁹Department of Physics and Astronomy, Iowa State University, Ames IA; United States of America.
- ⁸⁰Istinye University, Sariyer, Istanbul; Türkiye.
- ⁸¹(^a) Departamento de Engenharia Elétrica, Universidade Federal de Juiz de Fora (UFJF), Juiz de Fora; (^b) Universidade Federal do Rio De Janeiro COPPE/EE/IF, Rio de Janeiro; (^c) Instituto de Física, Universidade de São Paulo, São Paulo; (^d) Rio de Janeiro State University, Rio de Janeiro; (^e) Federal University of Bahia, Bahia; Brazil.
- ⁸²KEK, High Energy Accelerator Research Organization, Tsukuba; Japan.
- ⁸³(^a) Khalifa University of Science and Technology, Abu Dhabi; (^b) New York University Abu Dhabi, Abu Dhabi; (^c) United Arab Emirates University, Al Ain; (^d) University of Sharjah, Sharjah; United Arab

Emirates.

⁸⁴Graduate School of Science, Kobe University, Kobe; Japan.

⁸⁵(^a) AGH University of Krakow, Faculty of Physics and Applied Computer Science, Krakow; (^b) Marian Smoluchowski Institute of Physics, Jagiellonian University, Krakow; Poland.

⁸⁶Institute of Nuclear Physics Polish Academy of Sciences, Krakow; Poland.

⁸⁷Faculty of Science, Kyoto University, Kyoto; Japan.

⁸⁸Research Center for Advanced Particle Physics and Department of Physics, Kyushu University, Fukuoka ; Japan.

⁸⁹L2IT, Université de Toulouse, CNRS/IN2P3, UPS, Toulouse; France.

⁹⁰Instituto de Física La Plata, Universidad Nacional de La Plata and CONICET, La Plata; Argentina.

⁹¹Physics Department, Lancaster University, Lancaster; United Kingdom.

⁹²Oliver Lodge Laboratory, University of Liverpool, Liverpool; United Kingdom.

⁹³Department of Experimental Particle Physics, Jožef Stefan Institute and Department of Physics, University of Ljubljana, Ljubljana; Slovenia.

⁹⁴Department of Physics and Astronomy, Queen Mary University of London, London; United Kingdom.

⁹⁵Department of Physics, Royal Holloway University of London, Egham; United Kingdom.

⁹⁶Department of Physics and Astronomy, University College London, London; United Kingdom.

⁹⁷Louisiana Tech University, Ruston LA; United States of America.

⁹⁸Fysiska institutionen, Lunds universitet, Lund; Sweden.

⁹⁹Departamento de Física Teórica C-15 and CIAFF, Universidad Autónoma de Madrid, Madrid; Spain.

¹⁰⁰Institut für Physik, Universität Mainz, Mainz; Germany.

¹⁰¹School of Physics and Astronomy, University of Manchester, Manchester; United Kingdom.

¹⁰²CPPM, Aix-Marseille Université, CNRS/IN2P3, Marseille; France.

¹⁰³Department of Physics, University of Massachusetts, Amherst MA; United States of America.

¹⁰⁴Department of Physics, McGill University, Montreal QC; Canada.

¹⁰⁵School of Physics, University of Melbourne, Victoria; Australia.

¹⁰⁶Department of Physics, University of Michigan, Ann Arbor MI; United States of America.

¹⁰⁷Department of Physics and Astronomy, Michigan State University, East Lansing MI; United States of America.

¹⁰⁸Group of Particle Physics, University of Montreal, Montreal QC; Canada.

¹⁰⁹Fakultät für Physik, Ludwig-Maximilians-Universität München, München; Germany.

¹¹⁰Max-Planck-Institut für Physik (Werner-Heisenberg-Institut), München; Germany.

¹¹¹Graduate School of Science and Kobayashi-Maskawa Institute, Nagoya University, Nagoya; Japan.

¹¹²(^a) Department of Physics, Nanjing University, Nanjing; (^b) School of Science, Shenzhen Campus of Sun Yat-sen University; (^c) University of Chinese Academy of Science (UCAS), Beijing; China.

¹¹³(^a) School of Physics, Nankai University, Tianjin; (^b) Institute of Frontier and Interdisciplinary Science and Key Laboratory of Particle Physics and Particle Irradiation (MOE), Shandong University, Qingdao; (^c) School of Physics, Zhengzhou University; China.

¹¹⁴Department of Physics and Astronomy, University of New Mexico, Albuquerque NM; United States of America.

¹¹⁵Institute for Mathematics, Astrophysics and Particle Physics, Radboud University/Nikhef, Nijmegen; Netherlands.

¹¹⁶Nikhef National Institute for Subatomic Physics and University of Amsterdam, Amsterdam; Netherlands.

¹¹⁷Department of Physics, Northern Illinois University, DeKalb IL; United States of America.

¹¹⁸Department of Physics, New York University, New York NY; United States of America.

¹¹⁹Ochanomizu University, Otsuka, Bunkyo-ku, Tokyo; Japan.

- ¹²⁰Ohio State University, Columbus OH; United States of America.
- ¹²¹Homer L. Dodge Department of Physics and Astronomy, University of Oklahoma, Norman OK; United States of America.
- ¹²²Department of Physics, Oklahoma State University, Stillwater OK; United States of America.
- ¹²³Palacký University, Joint Laboratory of Optics, Olomouc; Czech Republic.
- ¹²⁴Institute for Fundamental Science, University of Oregon, Eugene, OR; United States of America.
- ¹²⁵Graduate School of Science, University of Osaka, Osaka; Japan.
- ¹²⁶Department of Physics, University of Oslo, Oslo; Norway.
- ¹²⁷Department of Physics, Oxford University, Oxford; United Kingdom.
- ¹²⁸LPNHE, Sorbonne Université, Université Paris Cité, CNRS/IN2P3, Paris; France.
- ¹²⁹Department of Physics, University of Pennsylvania, Philadelphia PA; United States of America.
- ¹³⁰Department of Physics and Astronomy, University of Pittsburgh, Pittsburgh PA; United States of America.
- ¹³¹(^a) Laboratório de Instrumentação e Física Experimental de Partículas - LIP, Lisboa; (^b) Departamento de Física, Faculdade de Ciências, Universidade de Lisboa, Lisboa; (^c) Departamento de Física, Universidade de Coimbra, Coimbra; (^d) Centro de Física Nuclear da Universidade de Lisboa, Lisboa; (^e) Departamento de Física, Escola de Ciências, Universidade do Minho, Braga; (^f) Departamento de Física Teórica y del Cosmos, Universidad de Granada, Granada (Spain); (^g) Departamento de Física, Instituto Superior Técnico, Universidade de Lisboa, Lisboa; Portugal.
- ¹³²Institute of Physics of the Czech Academy of Sciences, Prague; Czech Republic.
- ¹³³Czech Technical University in Prague, Prague; Czech Republic.
- ¹³⁴Charles University, Faculty of Mathematics and Physics, Prague; Czech Republic.
- ¹³⁵Particle Physics Department, Rutherford Appleton Laboratory, Didcot; United Kingdom.
- ¹³⁶IRFU, CEA, Université Paris-Saclay, Gif-sur-Yvette; France.
- ¹³⁷Santa Cruz Institute for Particle Physics, University of California Santa Cruz, Santa Cruz CA; United States of America.
- ¹³⁸(^a) Departamento de Física, Pontificia Universidad Católica de Chile, Santiago; (^b) Millennium Institute for Subatomic physics at high energy frontier (SAPHIR), Santiago; (^c) Instituto de Investigación Multidisciplinario en Ciencia y Tecnología, y Departamento de Física, Universidad de La Serena; (^d) Universidad Andres Bello, Department of Physics, Santiago; (^e) Universidad San Sebastian, Recoleta; (^f) Instituto de Alta Investigación, Universidad de Tarapacá, Arica; (^g) Departamento de Física, Universidad Técnica Federico Santa María, Valparaíso; Chile.
- ¹³⁹Department of Physics, Institute of Science, Tokyo; Japan.
- ¹⁴⁰Department of Physics, University of Washington, Seattle WA; United States of America.
- ¹⁴¹(^a) State Key Laboratory of Dark Matter Physics, School of Physics and Astronomy, Shanghai Jiao Tong University, Key Laboratory for Particle Astrophysics and Cosmology (MOE), SKLPPC, Shanghai; (^b) State Key Laboratory of Dark Matter Physics, Tsung-Dao Lee Institute, Shanghai Jiao Tong University, Shanghai; China.
- ¹⁴²Department of Physics and Astronomy, University of Sheffield, Sheffield; United Kingdom.
- ¹⁴³Department of Physics, Shinshu University, Nagano; Japan.
- ¹⁴⁴Department Physik, Universität Siegen, Siegen; Germany.
- ¹⁴⁵Department of Physics, Simon Fraser University, Burnaby BC; Canada.
- ¹⁴⁶SLAC National Accelerator Laboratory, Stanford CA; United States of America.
- ¹⁴⁷Department of Physics, Royal Institute of Technology, Stockholm; Sweden.
- ¹⁴⁸Departments of Physics and Astronomy, Stony Brook University, Stony Brook NY; United States of America.
- ¹⁴⁹Department of Physics and Astronomy, University of Sussex, Brighton; United Kingdom.

- ¹⁵⁰School of Physics, University of Sydney, Sydney; Australia.
- ¹⁵¹Institute of Physics, Academia Sinica, Taipei; Taiwan.
- ¹⁵²(^a) E. Andronikashvili Institute of Physics, Iv. Javakhishvili Tbilisi State University, Tbilisi; (^b) High Energy Physics Institute, Tbilisi State University, Tbilisi; (^c) University of Georgia, Tbilisi; Georgia.
- ¹⁵³Department of Physics, Technion, Israel Institute of Technology, Haifa; Israel.
- ¹⁵⁴Raymond and Beverly Sackler School of Physics and Astronomy, Tel Aviv University, Tel Aviv; Israel.
- ¹⁵⁵Department of Physics, Aristotle University of Thessaloniki, Thessaloniki; Greece.
- ¹⁵⁶International Center for Elementary Particle Physics and Department of Physics, University of Tokyo, Tokyo; Japan.
- ¹⁵⁷Graduate School of Science and Technology, Tokyo Metropolitan University, Tokyo; Japan.
- ¹⁵⁸Department of Physics, University of Toronto, Toronto ON; Canada.
- ¹⁵⁹(^a) TRIUMF, Vancouver BC; (^b) Department of Physics and Astronomy, York University, Toronto ON; Canada.
- ¹⁶⁰Division of Physics and Tomonaga Center for the History of the Universe, Faculty of Pure and Applied Sciences, University of Tsukuba, Tsukuba; Japan.
- ¹⁶¹Department of Physics and Astronomy, Tufts University, Medford MA; United States of America.
- ¹⁶²Department of Physics and Astronomy, University of California Irvine, Irvine CA; United States of America.
- ¹⁶³Department of Physics and Astronomy, University of Uppsala, Uppsala; Sweden.
- ¹⁶⁴Department of Physics, University of Illinois, Urbana IL; United States of America.
- ¹⁶⁵Instituto de Física Corpuscular (IFIC), Centro Mixto Universidad de Valencia - CSIC, Valencia; Spain.
- ¹⁶⁶Department of Physics, University of British Columbia, Vancouver BC; Canada.
- ¹⁶⁷Department of Physics and Astronomy, University of Victoria, Victoria BC; Canada.
- ¹⁶⁸Fakultät für Physik und Astronomie, Julius-Maximilians-Universität Würzburg, Würzburg; Germany.
- ¹⁶⁹Department of Physics, University of Warwick, Coventry; United Kingdom.
- ¹⁷⁰Waseda University, Tokyo; Japan.
- ¹⁷¹Department of Particle Physics and Astrophysics, Weizmann Institute of Science, Rehovot; Israel.
- ¹⁷²Department of Physics, University of Wisconsin, Madison WI; United States of America.
- ¹⁷³Fakultät für Mathematik und Naturwissenschaften, Fachgruppe Physik, Bergische Universität Wuppertal, Wuppertal; Germany.
- ¹⁷⁴Department of Physics, Yale University, New Haven CT; United States of America.
- ¹⁷⁵Yerevan Physics Institute, Yerevan; Armenia.
- ^a Also at Affiliated with an institute formerly covered by a cooperation agreement with CERN.
- ^b Also at An-Najah National University, Nablus; Palestine.
- ^c Also at Borough of Manhattan Community College, City University of New York, New York NY; United States of America.
- ^d Also at Center for Interdisciplinary Research and Innovation (CIRI-AUTH), Thessaloniki; Greece.
- ^e Also at Centre of Physics of the Universities of Minho and Porto (CF-UM-UP); Portugal.
- ^f Also at CERN, Geneva; Switzerland.
- ^g Also at Département de Physique Nucléaire et Corpusculaire, Université de Genève, Genève; Switzerland.
- ^h Also at Departament de Física de la Universitat Autònoma de Barcelona, Barcelona; Spain.
- ⁱ Also at Department of Financial and Management Engineering, University of the Aegean, Chios; Greece.
- ^j Also at Department of Modern Physics and State Key Laboratory of Particle Detection and Electronics, University of Science and Technology of China, Hefei; China.
- ^k Also at Department of Physics, Ben Gurion University of the Negev, Beer Sheva; Israel.
- ^l Also at Department of Physics, Bolu Abant İzzet Baysal University, Bolu; Türkiye.

- m* Also at Department of Physics, King's College London, London; United Kingdom.
- n* Also at Department of Physics, Stellenbosch University; South Africa.
- o* Also at Department of Physics, University of Fribourg, Fribourg; Switzerland.
- p* Also at Department of Physics, University of Thessaly; Greece.
- q* Also at Department of Physics, Westmont College, Santa Barbara; United States of America.
- r* Also at Faculty of Physics, Sofia University, 'St. Kliment Ohridski', Sofia; Bulgaria.
- s* Also at Faculty of Physics, University of Bucharest; Romania.
- t* Also at Hellenic Open University, Patras; Greece.
- u* Also at Henan University; China.
- v* Also at Imam Mohammad Ibn Saud Islamic University; Saudi Arabia.
- w* Also at Indian Institute of Technology (IIT), Jodhpur; India.
- x* Also at Institutio Catalana de Recerca i Estudis Avancats, ICREA, Barcelona; Spain.
- y* Also at Institut für Experimentalphysik, Universität Hamburg, Hamburg; Germany.
- z* Also at Institute for Nuclear Research and Nuclear Energy (INRNE) of the Bulgarian Academy of Sciences, Sofia; Bulgaria.
- aa* Also at Institute of Applied Physics, Mohammed VI Polytechnic University, Ben Guerir; Morocco.
- ab* Also at Institute of Particle Physics (IPP); Canada.
- ac* Also at Institute of Physics and Technology, Mongolian Academy of Sciences, Ulaanbaatar; Mongolia.
- ad* Also at Institute of Physics, Azerbaijan Academy of Sciences, Baku; Azerbaijan.
- ae* Also at Institute of Theoretical Physics, Iliia State University, Tbilisi; Georgia.
- af* Also at Millennium Institute for Subatomic physics at high energy frontier (SAPHIR), Santiago; Chile.
- ag* Also at National Institute of Physics, University of the Philippines Diliman (Philippines); Philippines.
- ah* Also at School of Physics, University of the Witwatersrand, Johannesburg; South Africa.
- ai* Also at The Collaborative Innovation Center of Quantum Matter (CICQM), Beijing; China.
- aj* Also at TRIUMF, Vancouver BC; Canada.
- ak* Also at Università di Napoli Parthenope, Napoli; Italy.
- al* Also at Università degli Studi Link; Italy.
- am* Also at University and INFN Torino, Torino; Italy.
- an* Also at University of Chinese Academy of Sciences (UCAS), Beijing; China.
- ao* Also at University of Colorado Boulder, Department of Physics, Colorado; United States of America.
- ap* Also at University of Siena; Italy.
- aq* Also at Washington College, Chestertown, MD; United States of America.
- ar* Also at Yeditepe University, Physics Department, Istanbul; Türkiye.
- * Deceased